LUND UNIVERSITY

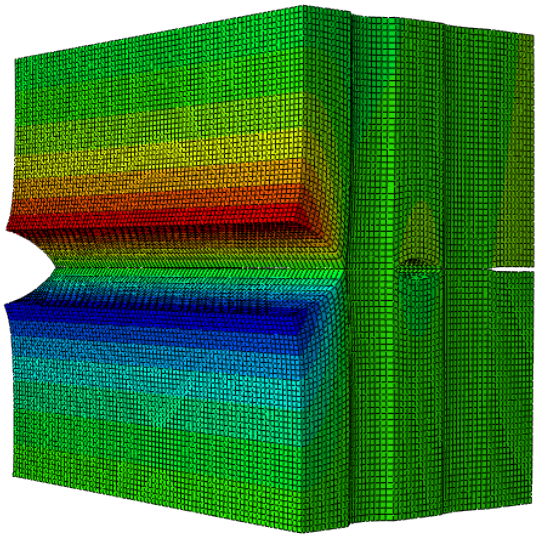

MODELING OF MOISTURE-INDUCED DEFORMATIONS AND STRESSES IN CROSS-LAMINATED TIMBER AND TIMBER-CONCRETE COMPOSITE FLOORS

MARCUS JOHANSSON

Structural Mechanics

Master's Dissertation

DEPARTMENT OF CONSTRUCTION SCIENCES

DIVISION OF STRUCTURAL MECHANICS

ISRN LUTVDG/TVSM--21/5249--SE (1-83) | ISSN 0281-6679

MASTER'S DISSERTATION

MODELING OF MOISTURE-INDUCED DEFORMATIONS AND STRESSES IN CROSS-LAMINATED TIMBER AND TIMBER-CONCRETE COMPOSITE FLOORS

MARCUS JOHANSSON

Supervisor: Professor **ERIK SERRANO**, Division of Structural Mechanics, LTH.

Examiner: Dr **HENRIK DANIELSSON**, Division of Structural Mechanics, LTH.

Printed by V-husets tryckeri LTH, Lund, Sweden, July 2021 *(PI)*.

For information, address:
Division of Structural Mechanics,
Faculty of Engineering LTH, Lund University, Box 118, SE-221 00 Lund, Sweden.
Homepage: www.byggmek.lth.se

Abstract

Cross-laminated timber is a fairly new material, composed of layers of timber boards cross-placed. The product allows for new construction techniques and can be seen as a more sustainable alternative to steel and concrete. Its structure makes it more robust and less dependent on the variation in properties of wood for different geometrical dimensions. As a new material, the CLT is not well studied, and its behavior not as well known. As it is composed of timber, moisture becomes a factor important to consider. Deformations, and resulting stresses, are largely affected by change in moisture content and relative humidity. The gaps that appear between the boards from drying leads to disadvantages, mainly concerning a higher burning rate.

In this master thesis, CLT elements of different configurations are investigated as regards uniform and non-uniform moisture loading. By non-uniform drying is meant a drying of the CLT resulting in a moisture gradient over the thickness of the CLT. The deformed shape and the width of the opening of the gaps that results from the moisture loading are examined, assuming no edge bonding.

Parametric studies were conducted for the drying of CLT elements, varying the board thickness, board width, number of layers and relation of thickness between layers. A timber-concrete composite structure is also studied, looking at a CLT slab with newly poured wet concrete on top of the CLT element and the resulting increased humidity of the timber that follows.

The study is performed by the use of a commercial finite element software, Abaqus. An important part of the work is to investigate different modeling approaches.

A main result regarding the gap openings that moisture induced deformations lead to is that to minimize their width, the boards should have as small dimensions as possible, both considering their thickness and width. The number of layers and a varying thickness between the layers had no significant effect on the gap widths apart from the varying thickness each board received. Another conclusion is that the gap openings that appear on the outer face of the CLT become twice as wide as those in the inner parts of the CLT. The gap widths are larger for the case of uniform drying than for non-uniform. Even though the gaps are smaller for smaller widths, the number of gaps are higher, and the exposed area is larger. The gap width for one percent change in moisture content were commonly around 0.3 mm. The element would displace 0.18 mm/m when subjected to non-uniform loading, corresponding to a difference of one percent MC between both sides.

The TCC structures keep a RH above 75 percent for the two top layers, even a year after casting. It is mostly the top half of the CLT element that reaches a higher humidity. The orientation of the board layers relative to the concrete notch has a slight effect on the top layer's maximal value for the RH and when that value peaks. Stresses of more than 1 MPa are expected at the top layer interface. Between the layers, the rolling shear stress is likely to reach half of its maximum strength.

Sammanfattning

Korslimmat trä är ett tämligen nytt material, bestående av korslagda lager av brädor. Produkten tillåter nya byggmetoder och kan ses som ett grönare alternativ till stål och betong. Dess uppbyggnad gör det mer robust och mindre beroende av träets varierande egenskaper för olika geometriska dimensioner. Som ett nytt byggnadsmaterial är dess beteende och karaktär inte lika välstuderat. Med trä som ingående material blir fukt en viktig faktor att beakta. Deformationer och påföljande spänningar är i högsta grad ett resultat av förändrad fuktkvot och relativ fuktighet. De glipor som uppstår mellan bräderna vid uttorkning är missgynnsamma och leder till bland annat ett påskyndat brandförlopp.

I detta examensarbete utsätts olika uppsättningar av KL-träelement för ensidig och dubbelsidig fuktbelastning. Elementets deformerade form och glipbredder som uppstår som ett resultat av uttorkning studeras. I samtliga fall studeras KL-trä utan kantlimning.

Uttorkningen av elementen studeras med hjälp av parameterstudier. Här varieras brädernas tjocklek, brädernas bredd, antalet skikt och varierande tjocklek mellan de ingående skikten. Samverkansbjälklag studeras också: KL-träelement med nygjuten betong ovanpå och den ökade fuktighet i träet som följer.

Studien utförs med ett kommersiellt finita element-program (Abaqus). En viktig del av arbetet syftar till att bredda kunskapen om hur sådana modeller kan sättas upp.

En huvudslutsats kopplad till de glipor som fuktdeformationer ger upphov till är att en minsta glipbredd erhålls när de ingående bräderna är av minsta möjliga storlek, både sett till dess tjocklek och bredd. Att variera antalet lager eller att ge olika tjocklek mellan de ingående skikten ger ingen märkbar effekt på glipbredden, bortsett från vad som kan förväntas av att brädernas enskilda tjocklek ändras. En annan slutsats är att gliporna för elementens yttre skikt blir dubbelt så stora som för de inre. Gliporna är större för tvåsidig uttorkning än för ensidig. Trots att gliporna blir mindre för smalare brädor så blir antalet glipor desto fler, vilket leder till att en större total area exponeras. Vid en procents ändring av fuktkvoten blir glipornas bredd vanligen kring 0,3 mm. Elementet böjs 0,18 mm/m när det utsätts för en ensidig fuktbelastning motsvarande en procent skillnad i fuktkvot mellan över- och underkant.

Samverkansbjälklagen behåller en RF över 75 procent för de två övre skikten, även ett år efter pågjutningen. Det är främst den övre halvan av KL-träelementet som når en högre RF. Skiktens geometriska riktning i förhållande till urtaget för betongen påverkar maxvärdet för RF och när kulmen inträffar. Spänningar större än 1 MPa förväntas för det översta skiktets gränsyta. Mellan skikten förväntas rullskjuvningen nå hälften av det maximalt tillåtna värdet.

Acknowledgement

This report is a master dissertation for the master's degree in civil engineering at Lund University, faculty of engineering. It is performed at the division of Structural mechanics.

I want to thank my supervisor Prof. Erik Serrano and examiner Dr. Henrik Danielsson, for their assistance and their patience. Their experience and former works have allowed me to get a deeper understanding of the subject.

I am thankful for the help of choosing the topic, a topic that has allowed me to broaden my understanding for mechanics, modeling and CLT.

I also want to thank my classmates and my family who have kept me motivated to complete the work and my studies.

This report is the last segment of my time as a student in Lund. The university has given me knowledge in the subjects I have the greatest interest in by people being experts in their field, while also being a setting for many personal encounters.

Lund, May 2021

Marcus Johansson

Nomenclature

Abbreviations

BC	Boundary condition
CLT	Cross-laminated timber
CO2	Carbon dioxide
FSP	Fibre saturation point
MC	Moisture Content
MPa	Megapascal
RH	Relative Humidity
TCC	Timber-Concrete Composite

Variables

c	Specific heat
D	Diffusion coefficient (MC)
g	Moisture flow
h	Film coefficient
k_w	Diffusion coefficient (RH)
l	Length
m	Mass
q_n	Flow across boundary
S_u	Surface emission
T	Temperature
u	Moisture content
w	Relative humidity
λ	Thermal conductivity
ρ	Density

FEM

$\boldsymbol{a}$	Nodal temperatures
$\boldsymbol{B}$	Derivative of **N**
$\boldsymbol{D}$	Constitutive matrix
$\boldsymbol{f}$	Force vector
G	Time function
$\boldsymbol{q}$	Flux vector
$\boldsymbol{K}$	Stiffness matrix
k	Conductivity
$\boldsymbol{N}$	Shape function
$\boldsymbol{n}$	Normal vector
Q	Heat supply
S	Surface
V	Volume
v	Arbitrary weight function
div	Divergence
∇	Gradient
τ	Time coordinate
$\int$	Integral
$\oint$	Contour integral

Table of Contents

Abstract I
Sammanfattning III
Acknowledgement V
Nomenclature VII
Abbreviations VII
Variables VII
FEM VIII
Introduction 1
Background and overview 1
Aims and objectives 2
Scope 3
Approach and software 3
Limitations 4
Usage of timber 5
Timber in construction 5
Environmental impact 6
Material 7
Wood 7
Structure 7
Orthotropy 8
Moisture parameter 9
Fibre Saturation Point 10
Sorption 10
Moisture content of concrete 12
Surface convection 13
CLT 15
CLT 15
Timber-concrete composite floor 15
Benefits with CLT 16
Limiting the gap width 16
Finite element method 17
Defining the finite element method 17
Temperature 17
Constitutive relation 17

Strong formulation 18
Weak formulation 18
FE formulation 19
Transient 20
Approximation in time 21
Analogy between heat and moisture transfer 24
Stiffness matrix 24
Validation of numerical simulation 25
Convergence criteria 25
Convergence study 25
One-dimensional calculation 27
Modeling 29
Building the models 29
Scripting 31
Models 33
Reference case 33
Uniform drying 34
Non-uniform drying 35
Bending 36
Timber-concrete composite (TCC) 37
Elements 40
Evaluation criteria 41
Bending, gap width, mold growth 41
Rolling shear 41
Input data 43
Results 47
Uniform drying 47
Thickness 48
Width 51
Factor 53
Number of layers 55
Elongation 58
Non-uniform drying 58
Bending 59
2D Composite 60

Relative humidity 60
Displacement 65
Bending 67
Stresses 67
Discussion 71
Uniform loading 71
Non-uniform loading 72
2D Composite 72
Modeling 74
Conclusion 77
Future work 79
References 81

Introduction

Background and overview

Cross-laminated timber (CLT) can be seen as an upscaled plywood: an uneven number of layers each built up of multiple boards (*laminates*), with each layer oriented perpendicular to the adjacent layers. This tackles the problem of timber being an orthotropic material, with different properties in each direction. By having multiple layers cross-placed the properties in two perpendicular directions are kept similar and the CLT element becomes relatively dimensional stable. More layers and boards also mean a more reliable material since defects in a single board will have a smaller effect for the entirety of the element.

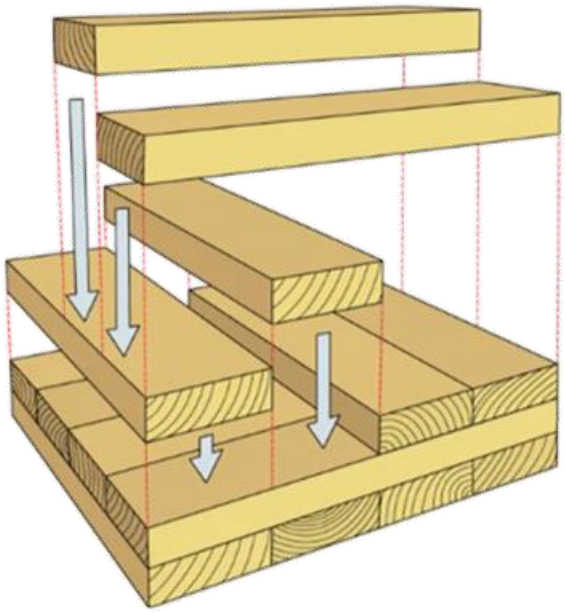

Figure 1. The configuration of a CLT element. (Nock n.d.)

Cross-laminated timber is a fairly new material, being developed in the 1990s in Austria and Switzerland. The question was how the wood found locally could replace the more common concrete. As it is a new building material, the knowledge of its behavior is not as well-known as for the more traditionally used materials, such as concrete. (Borgström & Fröbel 2019)

Moisture is crucial to consider when designing timber constructions. Not only does a high moisture content risk mold growth, but it also affects the mechanical properties. A change of *moisture content* (MC) leads to shrinkage and swelling which in turn leads to undesirable deformations and stresses. Wood is orthotropic, meaning that its behavior differs for three principal directions of the material. The CLT is designed in a way that makes the orthotropy less prominent at a global scale, for properties such as moisture-induced expansion. At a local scale, this can lead to stresses at the interfaces between the crossed laminates. As the boards dry and shrink, the gaps between the boards get wider, if the edges are not glued together. With a non-uniform distribution of the moisture content across the cross-section, leading to a difference in deformation between each side, the element could curve.

To make CLT floor slabs with greater spans, concrete can be casted on top to withstand a greater bending moment (Swedish wood 2017c). This being known as a *timber-concrete composite* (TCC) structure. Newly casted concrete is associated with high moisture content. As the concrete is in direct contact with the timber of the CLT, the moisture content of the timber is likely to increase greatly.

The structural behavior of CLT subjected to moisture loading is to be examined in this master thesis. A CLT element will be examined for uniform and non-uniform drying. The drying of a timber-concrete composite model will also be studied, as the moisture in the newly casted concrete dries through the timber. The study is done by modeling in a *finite element* software. Models are made to mimic a real CLT element at a reasonable level of detail. No experimental work is done.

Good knowledge of the behavior of the material in different environments and loading cases gives more reliable and accurate designs. In the long term, such increased knowledge could be incorporated in structural codes e.g. in terms of relaxing partial coefficients or modification factors, without jeopardizing safety.

The thesis also addresses questions relating to modeling techniques and the interpretation of the results. It is of interest to expand the knowledge on how to make models of CLT elements, timber, and moisture load as realistic as possible, yet small and simple.

The behavior will be analyzed in the finite element software *Abaqus*. Along with the interest to broaden the understanding of modeling in Abaqus, other research have been presented in which the software has been seen as a suitable option. For example, Fortino, Mirianon and Toratti (2009) who states in their work that "Recent literature shows a growing interest in modeling 3D orthotropic wood structures by Abaqus."

Aims and objectives

The main aim of this master thesis is to systematically analyze the behavior of CLT for several situations involving moistening and drying. The report can be divided into two parts: drying of CLT and drying of a timber-concrete composite structure. For the drying of a CLT element, multiple configurations will be compared against one another, varying for example the thickness of the boards. For such a variation, a parametric study will be made. The study will mainly focus on uniform drying, but non-uniform drying will also be examined. The resulting output data will be presented with a main focus on the gap width between the laminates. The parametric study will show how large influence each studied parameter has on the results. The overall behavior of the slab will be checked, among it the elongation of the element as a whole and how it deforms in other ways. The other part of the thesis investigates the drying of a composite structure; a CLT slab with casted concrete on top. When the composite structure is drying, the concrete will be modeled as being fully wet and the timber having a slightly higher moisture content than the surroundings, mimicking a realistic situation. Recommendations on design will be given if suitable. Another aim of this work is to answer questions related to modeling techniques. All cases will be set up in a modeling environment based on scripting.

The specific objectives are to:

1. Study the deformation behavior of CLT using FE-analyses
    a. Drying/moistening effect on gap width in CLT
    b. Influence of non-uniform moisture content on deformations
2. Study the influence of high moisture content from concrete on deformations in TCC structures

The study is followed by discussion concerning the results and the different modeling approaches. The expected outcomes are increased knowledge on the moisture deformations in general and on the influence of the CLT-layout on the width of the gaps after drying. In addition, the work is expected to expand the knowledge on how modeling of variations in moisture content can be done.

Doing an experimental study takes a large amount of time and can be technically troublesome. The usage of a finite element computer model saves time and makes it possible to study a variety of configurations and at many different locations of the model. Additionally, a computer model can replicate the same calculations multiple times with the same result, not being subjected to discrepancies.

Scope

In this thesis a variety of configurations concerning CLT elements are examined for drying. The main cases are listed as follows:

- Uniform drying (two-sided)
- Non-uniform drying (one-sided)
- Curvature from non-uniform MC-distribution
- Drying of composite structure

All models consider drying of one percent in moisture content, except the model for the timber-concrete composite element. Here, initial values of relative humidity are assumed, simulating how a real case of drying might look like. These TCC structures will be analyzed using a two-dimensional model unlike the other models, which will be three-dimensional.

For the first two cases, the widening of the gaps between the boards, mainly as a result of the shrinkage, is the factor of greatest interest. Those widths between the boards of a layer will mainly be referred to as gaps (or crack widths). The third case will look at the curvature occurring as a result for the non-uniform drying. The composite structure will be modeled without any gaps, as they are assumed to be glued together. Here the deformations and stresses are of larger interest as well as the moisture distribution over time, and consequently, the composite structure will be more interesting to study for different time steps.

Approach and software

All studies are made in a modeling environment. The commercial FE-software used is Abaqus (version 6.19-1). As Abaqus models are saved as Python scripts, they can simply be altered for a parametric study. The composite structure will be modeled as a two-dimensional model. The

other three-dimensional models will still differ for each case, as different sets of boundary conditions will be needed. The timber material used for CLT will be Norway Spruce.

The software does not support calculations on moisture content. However, the ability to calculate temperature distribution can be used for moisture content as well since the governing differential equations for both these physical quantities (temperature and moisture) are similar. The parametric studies are done with the help of Python scripting. With every Abaqus model, a script is saved which can be altered and rerun. Another alternative is to run the macro manager while modeling to save concurrent actions as a script.

Limitations

One limitation relates to the scope of the investigations. The number of possible investigations are immense, and the number of cases must be kept rather limited for practical reasons. The modeling only focuses on the direct effect of moisture, and not mechanical loading nor effects from a combination of both.

The anisotropic behavior of wood will be simplified to being perfectly homogeneous and orthotropic, with the radial direction in the same direction as the thickness of the CLT element. In other words, the curvature of the annual rings will not be considered. This could disregard deformations such as cuping for a uniform drying case.

Temperature will be assumed to be constant and MC not temperature dependent. The relation between deformation and MC-change are assumed to be linear, meaning that e.g. a two percent MC change gives twice as large deformations as one percent. The timber is defined as a linear-elastic material.

No experimental work will be made, and the project's focus is on the modeling. Adhesives will not be modeled and are therefore seen as infinitely thin with no effect on moisture diffusion and, in addition, full interaction between the layers is assumed. Note that in the CLT models it is assumed that edges are not glued, but for the TCC-models, edge glued laminations are assumed.

Usage of timber

Timber in construction

Timber has a long history and tradition as a building material in Sweden, being the prominent choice where wood is available in large volumes (Näringsdepartementet 2018). During the 20th century, timber gave way for other materials such as steel and concrete. Now the interest of building more in timber has once again increased (Näringsdepartementet 2004). One reason is that timber is a more environmentally friendly material. The construction industry stands for a large part of the global CO2-emissions (EOS 2017). As the industry strives towards being more environmentally friendly, new building methods and materials are sought for. As timber has a low carbon footprint and is one of few renewable materials, timber construction is being viewed as a sustainable option.

The Swedish government has initiated strategies towards a more circular and bio economy in which timber construction is identified as a key factor in this transition. At a local government level, the municipalities of Växjö and Skellefteå are examples where local strategies towards more timber construction have been established. (Näringsdepartementet 2018)

Up until 1995, timber buildings higher than two stories were banned in urban planning areas. The regulation was set as early as 1874 to hinder the spread of fires, which had devastated many Swedish cities during the 19th century and earlier. The ban was lifted as the new building regulations were implemented. Now, Boverkets byggregler (BBR) were performance based rather than prescriptive, meaning that multistory buildings were allowed for any material, given that the performance requirements, such as the fire resistance, were met. (Näringsdepartementet 2004)

Since then, many new ways to use timber in construction have been developed, for which many earlier downsides of timber have been less prominent. New building techniques allowing for massive timber elements make timber a good option for a robust and fire-resistant framework (Borgström & Fröbel 2019). Massive timber elements, such as CLT, burn at a slow rate. The outer surface will eventually turn into char which has insulating properties such that the material in the interior will still be structurally stable (Greenspec 2020). Massive timber is generally a better choice than unprotected steel, as it can keep its structural integrity even when subjected to high temperatures (Borgström & Fröbel 2019).

Concrete and steel have been by far the most common building materials of the last century. This means that the industry is not as used to timber in construction and the knowledge of how to use the material is limited. Turning to new building techniques for larger projects is associated with high risk, being one reason for why a transition towards more timber construction takes time. The design of CLT structures is still not a part of Eurocode, but it is under development (Borgström & Fröbel 2019). Today, about 90 percent of single-family houses in Sweden are built with a timber frame. The corresponding percentage for apartment buildings is considerably lower, at around 10 percent. (Näringsdepartementet 2018)

Environmental impact

The building sector stands for a monumental part of the negative environmental impact. It is for example responsible for 36 percent, or more than a third, of all greenhouse gas emissions in the EU (EOS 2017). 40 percent of the energy demand goes into the building sector. It is therefore crucial for the building sector to change if environmental goals are to be met. According to the European initiative Roadmap 2050 (EOS 2017), the greenhouse gas emissions should be cut by 80-95 percent below the 1990s level until year 2050. While a decrease in CO2-emissions can be seen in the EU, the global emissions have kept increasing (European commission, 2020).

The major energy consumption during a buildings lifespan used to be under its usage (Swedish wood 2017b). However, this is now shifting to the building phase due to harsher regulations as regards energy use, leading to a lower energy consumption during the operational phase of the building's life.

The steel and cement industry are among the largest Swedish emitters of carbon dioxide. Steel and iron production stands for six percent and cement three percent of Sweden's total CO2-emissions (Naturvårdsverket 2019). In the chemical process of making cement clinker, the mass of carbon dioxide emitted roughly equals to the mass cement produced, not accounting for the energy usage of the manufacturing itself and the heating of the furnaces (Fagerlund 1999). Cement does however bind carbon dioxide during its lifetime and would eventually return to calcium hydroxide as before the calcination, although being a slow process.

In contrast, timber structures act as carbon sinks, storing CO2 in the material during its lifetime. In other words, building with timber makes it possible to have negative green-house gas emissions, reducing the amount of carbon dioxide in the atmosphere instead of adding to it. (Scalet 2015)

Timber is one of few, if not the only largely available, renewable building material. Alongside the crisis of climate change, many non-renewable resources are overused, and demand keeps rising. One example is sand, by which most of the extracted is used in concrete (UNEP 2019). Sand is currently the second most used extracted resource after water, with water also being an important component in concrete. The high demand for sand has led to illegal extractions, causing strand erosion and floods when removed. Those protesting the illegal activities does so with their life at risk. It is therefore desirable to replace those with renewable materials such as timber for a more sustainable building sector.

Material

Wood

Timber is an organic and renewable material with the oldest heritage in Sweden (Swedish wood 2017a). In Sweden, the most commonly used wood-types are Norway spruce (Picea Abies) and Scots pine (Pinus Sylvestris), both being examples of softwood (Säll 2002). Norway spruce is also the more common alternative for structural timber. Norway spruce will therefore be the material chosen for the calculations and modeling.

Wood, being a natural material, has a structure that gives varying properties across its extent and in different directions. Since the material is naturally formed and not engineered, its properties might also vary drastically from each specimen and even within the specimen itself (Swedish wood 2017a, Säll 2002).

Structure

The wood consists of tracheids, ray tracheids and parenchymatous (Swedish wood 2017d). The tracheids make up more than 90 percent of the wood volume (Borgström 2016). The tracheids are long and hollow cells, generally called *fibres*. The fibres and their orientation have a large impact on the mechanical properties. The strength of timber is larger in its longitudinal direction, i.e., along the fibre direction. (Säll 2002)

Figure 2. Cross-section of a spruce log. The pith extents through the middle with the wood, cambium and bark surrounding it. The figure is not to scale and the extensions of the respective zones are purely schematic.

The pith runs through the middle of the tree (Borgström 2016). This is enclosed by the wood, which can be separated to heartwood and sapwood. The heartwood is closest to the pith and is formed from sapwood at a certain age (Säll H. 2002). The heartwood has a higher strength and will make the timber stronger against shear stresses where the shear plane cuts through both heart- and sapwood. *Rolling shear* will choose its way through the weaker sapwood, being one reason for why rolling shear stress is of greatest significance, see further chapter *Rolling shear* under *Evaluation criteria*.

In the formation of heartwood, free water is expelled from the cell lumen, or cell cavities (Säll 2002). The cells dies from the lack of water. Extractives are being secreted and stored in the

cell walls. The moisture content in the heartwood is therefore much lower than in the sapwood, with a MC of 30-50 percent, compared to the sapwoods 120-160 percent, according to Swedish wood (2017a).

Outside the wood is the cambium. The cambium produces new cells: bark cells outwards and wood cells inwards. The fibre cells formed in the cambium dies soon after they are formed.

The annual rings can be divided into earlywood and latewood, formed during spring and summer, respectively (Swedish wood 2017e). Latewood is denser with fibres being longer and with thicker cell walls. This makes latewood stronger than earlywood. One can also link a higher density to a stronger and more durable material. Wood from southern Sweden is denser than the one from the north (Swedish wood 2017a). This is because the latewood part is wider in southern Sweden. Latewood is about three times denser than earlywood and can generally be distinguished by its darker color.

Orthotropy

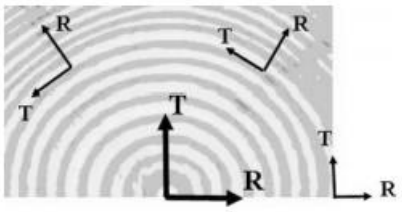

Figure 3. Tangential and radial direction of wood. (Fortino, Mirianon & Toratti 2009)

Wood has different properties in different directions. The shrinkage might therefore be different in different parts of each board, leading to irregular deformations even for a uniform drying.

Wooden materials can more easily be described as homogeneous materials with in each point rectangular orthotropy (Fortino, Mirianon & Toratti 2009). *Orthotropy* means that the material has different properties in different geometrical directions and with three main directions existing that are perpendicular to one another (Ottosen & Petersson 1992). As described for the structure of trees, the tree growths from the inner pith and outwards in a circular manner. Therefore, the direction tangential to the growth rings will follow the curvature of the annual rings, see Figure 3. Modeling the material as being rectilinear and orthogonal will thereby be a simplification, ignoring the varying orientation of a cylindrical coordinate system.

The material directions to consider are therefore:

- Longitudinal: following the direction of the fibres, along the length of the stem.
- Tangential: Tangential to the growth rings.
- Radial: lateral to the growth rings, outwards from the pith.

A cylindrical coordinate system is not used in the models. The boards are modeled as rectilinearly orthotropic with the radial direction along the boards thickness.

The longitudinal direction has by far the highest stiffness and strength (Säll 2002). The stiffness in the longitudinal direction is 20 times larger than in the radial direction, which by itself is twice as large as for the tangential direction.

The relations between the moisture expansion coefficients in the various directions are similar. The shrinkage and swelling are 20 times larger in radial direction than in longitudinal direction, and expansion in tangential direction is twice as large as compared to radial direction. (Swedish wood 2017f)

The relation between the values for each direction used in the modeling might differ from the just mentioned ones, which are approximate. For the precise values used in the modeling, see chapter *Input data*.

The longitudinal direction for a board is not always as ideal as it has been assumed. In reality, it is common that there is an angle between the fibre direction and the length of the board. The fibres also tend to twist around the mid of the stem. (Säll 2002)

Moisture parameter

Moisture is a factor of great importance to consider for wood. A change in moisture will lead to swelling and shrinkage and will also affect the mechanical performance. One way of measuring the amount of moisture in the material is the *moisture content*.

The moisture content (MC) is defined as the mass of the water within the material divided by the mass of the dried material (Burström 2014).

$$Moisture\ content = \frac{mass\ of\ water}{mass\ of\ dry\ material}$$

The moisture content is expressed in percent. The value can however be larger than 100 percent. While this could be the case right at a conjoining concrete surface, it will not be considered nor possible to achieve in the models made.

Relative humidity (RH) is defined as *vapor pressure* divided by *saturation vapor pressure*. The saturation vapor pressure is the maximal vapor pressure for air at a given temperature. (Nevander & Elmarsson 1981)

$$Relative\ humidity\ RH = \frac{vapor\ pressure\ v}{saturation\ vapor\ pressure\ v_s}$$

The modeling of the moisture transport can be made with either moisture content or relative humidity as parameter/potential. For the drying of CLT elements, the moisture content will be used as parameter. The results will in those cases be expressed per one percent change in moisture content.

For the TCC model, the use of moisture content is problematic. Two different materials in contact, such as timber and concrete, will strive for similar vapor pressure. The structure will be in equilibrium when the relative humidity is the same for both materials at the given temperature. Expressing this in terms of moisture content is difficult. Relative humidity will therefore be used for the composite model.

The relative humidity for concrete will be preset from results from experimental studies of membrane curing. It is then assumed that no drying takes place from the top surface of the concrete and that the drying through the timber will be low. The moisture load on the timber part of the TCC is described by prescribing the relative humidity in the concrete part. The drying of concrete does not only depend on moisture flow. Presetting values of the humidity of the concrete for every time step will also account for the hydration and chemical binding of water to the cement. Drying of two different water-cement ratios (kg water per kg cement) will be compared, 0.6 and 0.38. It is assumed that RH will not vary across the thickness of the concrete slab and, consequently, the diffusion coefficient of concrete will not be needed for calculations.

Fibre Saturation Point

Timber expands as the moisture content increases. The elongation matches well a linear relation. The rate of expansion decreases rapidly after the *fibre saturation point* FPS is reached. Up until then, water has accumulated in the cell walls. Above the fibre saturation point, capillary condensation occurs in the cavities (lumen). This breaking point occurs at somewhere between 25-30 percent. (Chiniforush, A.A. Akbarnezhad, A. Valipour, H. Malekmohammadi, S. 2019)

In the calculations, relative humidity above 100 percent will never be reached, which will correspond to a MC of roughly 27 percent, or more. It is assumed that the FSP will never be exceeded. In a study by Autengruber, M. Lukacevic, M. and Füssl, J. (2020), a similar study of a TCC element was conducted. The results show a moisture content reaching above the FSP for the timber closest to the concrete, but not for the larger part of the timber element.

Sorption

If relative humidity is to be used, as for the model of the timber-concrete composite floor, a different value needs to be set for the diffusion coefficient of the materials than the one used if the moisture content is used as primary variable. The relation is stated via the *sorption isotherm*, see Figure 4. Values are taken from Alsayegh (2012) as the figure is easy to read and obtain values from. As the sorption isotherm shows, the relation between moisture content and relative humidity is not linear.

The moisture flow g depends on the gradient of moisture content and the diffusion coefficient according to *Fick's law*, see equation (1). (Nevander & Elmarsson 1981)

$$g = -D\frac{du}{dx} \tag{1}$$

$$\begin{cases} g = moisture\ flow \\ u = moisture\ content \\ D = diffusion\ coefficient \end{cases}$$

The gradient of the moisture content can be viewed as a gradient dependent on the relative humidity which in turn is dependent on location *dx*. The relation is set according to equation (2) below. (Nevander & Elmarsson 1981)

$$g = -D\frac{du}{dw}\frac{dw}{dx} \tag{2}$$

$$w = relative\ humidity$$

The equation shows the moisture flow as a function of the change in relative humidity. This relation is not linear; it varies according to the sorption isotherm. The term k_w can be expressed from the relation above. This term will be the relation between the relative humidity and the moisture flow as expressed in the absorption isotherm.

$$k_w = D\frac{du}{dw} \tag{3}$$

The sorption isotherm specifies the relation between moisture content and relative humidity for a given material. The isotherm for absorption and desorption differs, a phenomenon known as hysteresis. The curve for absorption always gives a moisture content lower than for desorption. As the moisture in the concrete of the TCC structure will dry out through the timber, absorption in the timber is expected for the most part.

The coefficient set for concrete will not affect the results, as the relative humidity of the entirety of the slab will be predefined throughout the entire time period.

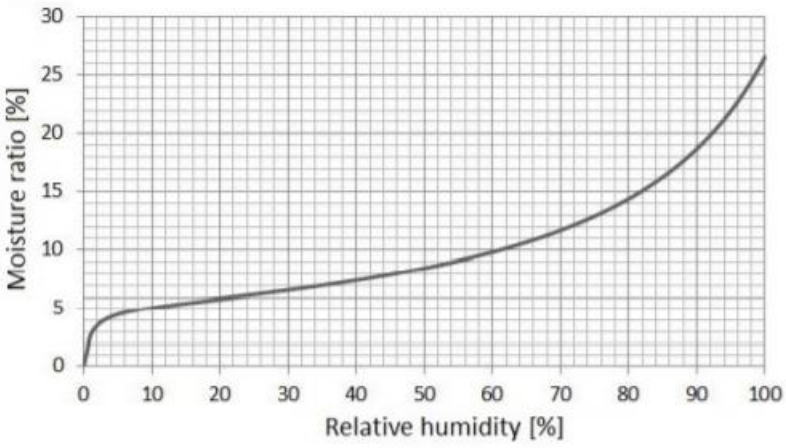

Figure 4. Absorption isotherm used for Norway Spruce (Alsayegh 2012).

Three parts of the sorption isotherm can be distinguished, in which the slope differs. These parts relate to different mechanisms; Monomolecular adsorption, polymolecular adsorption and capillary condensation. For absorption at a low relative humidity, moisture binds by monomolecular adsorption, adding water molecules at the pores surfaces in a layer with a

thickness of one molecule. More layers are added as the relative humidity increases. These layers have a lower attraction. Therefore, a higher relative humidity is needed for each addition in moisture content, hence why the sorption isotherm curve flattens. At even higher relative humidity, the slope gets steeper again as capillary condensation now dominates the moisture addition. (Nevander & Elmarsson 1981)

The name isotherm is used to emphasize that the relation holds true for constant temperature (Burström 2014). Temperature is however considered to have a marginal effect on the sorption. Although the temperature is expected to increase during the hardening of the concrete, this is not considered. The isotherm is chosen for a temperature of 20 degrees.

Moisture content of concrete

Assessing the amount of moisture in the concrete could be done in different ways, using either moisture content or relative humidity as potential. The initial amount of moisture depends on the concrete recipe. For the drying of the concrete layer, one has to account for the hydration and the fact that most of the water in the concrete mixture will bind chemically to the cement and will thereafter no longer count as moisture. This needs to be accounted for in the modeling as the reduced humidity of concrete cannot solely be described by drying. A few different options were considered. The listed examples below give an idea on how this could be done and how to take the hydration into consideration. For the listed examples, a water/cement (w/c) ratio of 0.6 is assumed. The w/c ratio is the weight of water in relation to the weight of cement.

The moisture content for the concrete could be set by dividing the amount of water by the dry density of cement. The amount of water should then be the amount that would be added according to the concrete mixture of interest. The amount of ballast used should also be accounted for. The values are given by Göran Fagerlund (1999).

For vct=0.6:

$$MC_{concrete} = \frac{m_{water}}{m_{cement} + m_{ballast}} = \frac{180}{300 + 1865} = 0.083$$

A value of 8.3 % MC is too low for the model. Dividing the mass of water by the density of timber gives a guess for the moisture content of the timber, giving 36 percent, a more reasonable value.

$$\frac{180}{500} = 0.36 = 36\%\, MC$$

Another option is to check the amount of moisture that needs to dry out from a cured concrete mixture. By assuming a high hydration, the amount of water can be calculated according to (Fagerlund 1999); Hydration represents the amount of curing done for the cement.

$$W_e = W - C\alpha 0.25 = 180 - 300 \cdot 0.8 \cdot 0.25 = 120\ kg/m^3$$

$$\begin{cases} W_e = free\ water \\ W = all\ added\ water \\ C = cement \\ \alpha = hydration\ (after\ \approx 1000\ h\ fig\ 2{:}11) \end{cases}$$

120 kg of moisture per cubic meter needs to dry out according to formula 2:12 chapter 6 Concrete folder. Dividing the value by the density for timber gives a value for a moisture content. That moisture content is in addition to the initial moisture content of timber.

$$MC = \frac{m_{moisture}}{m_{timber}} = \frac{120}{500} = 0{,}24 = 24\%$$

$$24 + 12 = 36\%\ MC\ (adding\ starting\ condition\ for\ the\ wood)$$

The above shows the uncertainties involved if MC is to be used as primary variable. Therefore, it was determined that the most suitable potential to use for the TCC model is the relative humidity. It is assumed that the RH is 100 % initially. This value will decrease with time according to experimental results taken from a study by Mjörnell (2003). One mayor advantage of using RH as a potential is that two different materials, such as wood and concrete, will strive for equilibrium for vapor pressure, not moisture content.

Surface convection

For the drying of the TCC model, the resistance for the surface convection (on the surface without concrete) is accounted for.

The moisture flow leaving the surface is given by equation (4) (Fortino, Mirianon & Toratti 2009).

$$q_n = \rho S_u\left(u_{air} - u_{surf}\right) \qquad (4)$$

In Abaqus, temperature is instead used as analogous variable. The flow is according to equation (5). (Dassault Systèmes 2015)

$$q_n = h\left(T_{air} - T_{surf}\right) \qquad (5)$$

The film coefficient *h* can then be replaced by the corresponding values for moisture flow. The value must also change to make use of relative humidity instead of moisture content.

$$\rho S_u \frac{u}{w} = h \qquad (6)$$

According to the sorption isotherm, 65 percent RH corresponds to 11 percent MC. The density ρ for spruce is 440 kg/m^3 (Swedish Wood 2017a). Lastly, the coefficient of surface emission S_u is defined (Fortino, Mirianon & Toratti 2009). A value for moisture content *u* of 0.11 is used.

$$S_u = 3.2 \cdot 10^{-8} e^{4u} = 5.0 \cdot 10^{-8}\ m/s$$

This gives the value of the film coefficient that should be used in Abaqus.

$$h = \rho S_u \frac{11}{65} = 440 \cdot 5.0 \cdot 10^{-8} \cdot \frac{11}{65} = 3.7 \cdot 10^{-6}$$

Note that the formula for the film coefficient in reality is dependent on the moisture content and not a constant value.

CLT

CLT

Cross-laminated timber, CLT for short, consists of layers of wooden boards glued together with each layer oriented perpendicular to the adjacent layers. Since the material properties vary for different directions, placing each board in different directions makes the element as a whole more homogeneous and dimensional stable.

As multiple layers are put together, the properties of a single board are of less importance. Therefore, imperfections and varying parameters have less of an impact. The properties of each element will vary less and as a result a more reliable design and a lower safety margin is needed. CLT elements consists of an uneven number of layers to make the cross-section symmetrical and avoid uneven deformation.

CLT is a relatively new material, developed in the 90s in Austria to replace concrete with the locally available timber (Borgström & Fröbel 2019). At that time, the former regulation limiting wooden structures in Sweden to no more than two stories, was lifted (Näringsdepartementet 2004). This gives new possibilities for timber as a structural material. This advancement in timber building comes at a time of environmental awareness. CLT comes at a time when its potential might be the greatest.

The boards are glued together between layers. The edges can be glued together as well, but not necessarily. Gluing the edges should be done for elements with a ratio between board width and thickness lower than four to protect from rolling shear stresses (Borgström & Fröbel 2019). The quality of the wood is often set as higher for the outer layers where tension and compression are the largest.

Timber-concrete composite floor

Timber-concrete composite (TCC) structure consists of a CLT element with concrete casted on top of it. The reason is a higher bending stiffness with the concrete layer being strong against compression stresses and timber being better to withstand tensile stresses. The timber-concrete composite floor gives a higher bending strength than a single CLT element with the same thickness, making it preferable for longer spans. The composite floor also has better dynamic and acoustic properties as well as a higher stiffness, making it easier to redistribute horizontal forces.

To make the most out of a composite floor, full interaction between the concrete and the timber is required. When no interaction occurs, the two layers can displace independently of each other. The interaction is needed for the concrete to take the entirety of the compressive stresses.

Ways of achieving interaction is to place connectors between concrete and timber or to make notches in the timber and fill with the concrete. The latter is used for the model, as it is expected to lead to a higher moisture flow, and full interaction is assumed. When using notches, it is common to also connect with screws to take the tensile stresses that might act between the elements. (Swedish wood 2017c)

Benefits with CLT

The main benefit of the CLT structure is its ability to carry load in two directions. Crossing the laminates makes the properties in the two lateral directions similar. The loading can be carried in multiple directions and notches and overhangs can be cut out more easily and reshaped to a desirable form. Since one element consists of multiple boards, each board has a smaller impact on the entirety of the structure, making it more reliable and less affected by imperfections and knots. This is referred to as the system effect. (Borgström & Fröbel 2019)

The manufacturing has a high degree of prefabrication (Stora Enso n.d., Näringsdepartementet 2018). Prefabrication makes for higher precision. It also means shorter construction time on site as well as less noise and disturbance around the site (Stora Enso n.d.). Another advantage is that of the light weight, giving the ability to build additional stories to an already existing structure without the need to strengthen it (EOS 2017). Timber also shows good performance against fire.

Massive timber elements make for easy and creative building, as the elements can be cut into almost any size. Timber elements are good isolators in themselves and has, just as concrete, the ability to store heat in the material and even out the temperature difference of day and night. (Borgström & Fröbel 2019)

Limiting the gap width

One essential reason to look at the shrinkage of wood and CLT is the emergence of gaps between the boards. The necessity of limiting the width of those gaps are several.

One mayor reason for limiting the size of the gap width is fire safety. A larger crack width has a higher burning rate as more timber is exposed. Massive timber elements, such as CLT, perform well against fire as the charring of the surface caused by the fire isolates the remaining inside of the timber element (Falk, Dietsch, Schmid 2016). However, a crack would open for the fire to reach further into the element and speed up the fire progression. Borgström & Frödel (2019) also points out that a higher burning rate is expected for CLT around its gaps as well as its corners.

Another problem with a large gap width is the aesthetics. Larger gaps also hinder air tightness and therefore has an effect on both heat and moisture transport (Falk, Philipp, Schmid 2016).

A study presented by Falk, Dietsch and Schmid (2016) shows how the width of the gap affects the charring depth. A gap width up to two millimeters gives a negligible change while a larger gap width shows an effect. Above two millimeters, the charring rate should be increased by a factor of 1.2.

Finite element method

The modeling will be made using the finite element method. The modeling will consist of two separate finite element calculations: one for the moisture content and a second for the deformations and stresses.

Below, the FEM formulation will first be derived for stationary calculations with the analogy for heat transfer, followed by the derivation of the transient formulation with linear approximation. Lastly, the constitutive relations for heat transfer and moisture diffusion are compared and their corresponding differential equations and finite element formulations. All following derivations will be made for three-dimensional models. A derivation for a two-dimensional case would however be similar and consist of the same steps.

The equations and derivations are taken from *Introduction to the finite element method* (Ottosen & Petersson 1992). The descriptions for the transient case follow the description given in *Transient heat flow* (Persson n.d.).

Defining the finite element method

With the finite element method, a larger structure is split into smaller, finite elements. By knowing the values at the nodes of the element, the variation within the element and along its boundaries are approximated by the shape functions (interpolating functions) which apply for that element and geometrical dimension. The values between nodes are approximated, often using linear or quadratic functions. By using smaller element sizes more accurate results can be obtained (accurate in the sense of solving the underlying differential equations).

Temperature

Constitutive relation

The *constitutive equation* for heat flow used in this work describes its linear dependence on temperature. Since heat flows from higher temperature to lower, a minus sign is added.

$$\boldsymbol{q} = -\boldsymbol{D}\nabla T \;\Leftrightarrow\; -\begin{bmatrix} k_{xx} & k_{xy} & k_{xz} \\ k_{yx} & k_{yy} & k_{yz} \\ k_{zx} & k_{zy} & k_{zz} \end{bmatrix} \begin{bmatrix} \delta T/\delta x \\ \delta T/\delta y \\ \delta T/\delta z \end{bmatrix} \; [J/m^2 s] \qquad (7)$$

The matrix $\boldsymbol{D}$ is called the *constitutive matrix* and k is the *thermal conductivity*. The matrix appearance differs depending on the type of material. Wood is orthotropic. For an orthotropic material, the thermal conductivity differs in all three directions. However, the thermal gradient ∇T in x-direction is assumed to affect only the heat flow in x-direction and so on, resulting in one coefficient for each gradient.

$$\boldsymbol{D} = \begin{bmatrix} k_{xx} & 0 & 0 \\ 0 & k_{yy} & 0 \\ 0 & 0 & k_{zz} \end{bmatrix} \qquad (8)$$

Strong formulation

The equation for the strong form is formulated as the equilibrium condition for an infinitely small part, starting from the balance principle for a volume V with a boundary surface S.

$$\int_V Q dV = \oint_S \boldsymbol{q_n} dS \tag{9}$$

The variable *Q* is the amount of heat supplied to the body per unit of time. *S* denotes the surface from which heat flow leaves the body. The flow $\boldsymbol{q}_n$ is the *scalar product* of the flow in that region and the vector normal to the surface, giving the flow out from the body.

$$\boldsymbol{q}_n = \boldsymbol{q}^T \boldsymbol{n} \tag{10}$$

The Gauss divergence theorem is stated as:

$$\int_V div(\boldsymbol{q}) dV = \int_S \boldsymbol{q}^T \boldsymbol{n} dS \tag{11}$$

The equation (9) is rewritten with the Gauss' divergence theorem to get equation *(12*).

$$\int_V Q dV = \oint_S \boldsymbol{q^T n} dS = \int_V div(\boldsymbol{q}) dV \tag{12}$$

Since the equation holds true for an arbitrary volume, the relation can be expressed without the integration.

$$Q = div(\boldsymbol{q}) \tag{13}$$

The divergence of $\boldsymbol{q}$ is as stated below.

$$div(\boldsymbol{q}) = \frac{\delta q_x}{\delta x} + \frac{\delta q_y}{\delta y} + \frac{\delta q_z}{\delta z} \tag{14}$$

The term $\boldsymbol{q}$ is replaced in equation (13) with the constitutive relation according to equation (7).

$$div(\boldsymbol{D}\nabla T) + Q = 0 \tag{15}$$

The boundary conditions *h* and *g* are set for heat flow and temperature, respectively, at the boundary, surfaces S_h and S_g. This gives the strong form.

$$div(\boldsymbol{D}\nabla T) + Q = 0$$
$$q_n = \boldsymbol{q}^T \boldsymbol{n} = h \text{ on surface } S_h$$
$$T = g \text{ on surface } S_g$$

Weak formulation

From the strong form, the weak form is derived. Firstly, the strong form is multiplied by an arbitrary weight function *v* and integrated over the volume.

$$\int_V v div(\boldsymbol{q}) dV - \int_V v Q dV = 0 \tag{16}$$

The first term in (16) is integrated by part using the Green-Gauss theorem, formulated according to equation (17).

$$\int_V v div(\boldsymbol{q}) dV = \int_S v \boldsymbol{q}^T \boldsymbol{n} dS - \int_V (\nabla v)^T \boldsymbol{q} dV \tag{17}$$

This in used in equation (16), which can be rewritten as equation (18).

$$\int_V (\nabla v)^T \boldsymbol{q} dV = \int_S v \boldsymbol{q}^T \boldsymbol{n} dS - \int_V v Q dV \tag{18}$$

The boundary conditions from the strong form are inserted into the equation. The boundary heat flow across surface S_h is expressed as h. Along surface S_g the temperature g is known. The variable $\boldsymbol{q}$ is also replaced with the constitutive relation. The weak form can then be formulated.

$$\int_V (\nabla v)^T \boldsymbol{D} \nabla T dV = -\int_{S_h} v h dS - \int_{S_g} v \boldsymbol{q}_n dS + \int_V v Q dV$$
$$T = g \text{ on surface } S_g$$

The boundary condition stating the heat flow is used explicitly in the weak formulation and is therefore called a natural boundary condition. The temperature boundary condition still must be prescribed. It is therefore called an essential boundary condition. It is essential to have a known temperature somewhere in the model for the calculations to be possible.

FE formulation

In the finite element formulation of heat flow, the temperatures are the primary unknowns at the elements nodes. The values in between nodes are interpolated by

$$T = \boldsymbol{N}\boldsymbol{a} \tag{19}$$

where $\boldsymbol{N}$ is the global *shape function matrix* and $\boldsymbol{a}$ is a vector containing the temperatures at the nodal points of the entire body. The shape functions are functions of each node, making an approximation for an arbitrary part of the element based on those nodes. The gradient of T can be set.

$$\nabla T = \nabla \boldsymbol{N}\boldsymbol{a} = \boldsymbol{B}\boldsymbol{a} \tag{20}$$

The arbitrary weight function is set as a function of the global shape function $\boldsymbol{N}$ and an arbitrary matrix $\boldsymbol{c}$, in accordance with the Galerkin method.

$$v = \boldsymbol{N}\boldsymbol{c} \tag{21}$$

Since both the weight function $\boldsymbol{v}$ and the matrix $\boldsymbol{c}$ are arbitrary, the gradient can be expressed as below.

$$\nabla v = \boldsymbol{B}\boldsymbol{c} \tag{22}$$

With the weight function being scalar and the matrices single dimensional, the value equals its transpose.

$$v = \boldsymbol{c}^T \boldsymbol{N}^T \tag{23}$$

All the reformulations in equations (19)-(23) are inserted in the weak formulation.

$$\boldsymbol{c}^T\left(\int_V \boldsymbol{B^T D B} dV \boldsymbol{a}\right) = \boldsymbol{c}^T\left(-\int_{S_h} \boldsymbol{N}^T h dS - \int_{S_g} \boldsymbol{N}^T \boldsymbol{q_n} dS + \int_V \boldsymbol{N}^T Q dV\right) \quad (24)$$

Since $\boldsymbol{c}^T$ is a factor of each term and arbitrary, it can be neglected.

The finite element formulation is rewritten in a compact form, with new matrixes as below. $\boldsymbol{K}$ is the stiffness matrix and $\boldsymbol{f_b}$ and $\boldsymbol{f_l}$ are the boundary load vector and the element load vector, respectively.

$$\boldsymbol{K} = \int_V \boldsymbol{B^T D B} dV$$
$$\boldsymbol{f_b} = -\int_{S_h} \boldsymbol{N}^T h dS - \int_{S_g} \boldsymbol{N}^T \boldsymbol{q_n} dS$$
$$\boldsymbol{f_l} = \int_V \boldsymbol{N}^T Q dV$$

The FE-formulation is then expressed as:

$$\boldsymbol{K a} = \boldsymbol{f_b} + \boldsymbol{f_l} = \boldsymbol{f}$$

Solving the equation gives the nodal temperatures in $\boldsymbol{a}$. By using the global shape function matrix, the approximate temperature can then be obtained for an arbitrary point within an element and the flow by the constitutive equation.

Transient

For the TCC model, a transient analysis is made. In a transient calculation the calculation is done over time. This means that it is necessary to also consider the change in temperature that happens as a result of the heat flow over time. When the influx and outflux of heat differ, it means that the difference will accumulate in the material and change its temperature. How much heat that can be stored for each degree depends on the material's density ρ and the specific heat c. The governing differential equation for the transient problem is found by adding an extra term to the strong form equation *(15*).

$$-div(\boldsymbol{D}\nabla T) + Q = \rho c \frac{dT}{dt} \quad (25)$$

As for steady-state, the terms are multiplied by an arbitrary weight function v and integrated. With Green-gauss theorem the weak form is achieved similarly to before but now containing an additional term, which in turn depends on the time derivative of the temperature field.

$$\int_V (\nabla v)^T \boldsymbol{D}\nabla T dV + \int_V v\rho c \frac{dT}{dt} dV = -\int_{S_h} v h dS - \int_{S_g} v \boldsymbol{q_n} dS + \int_V v Q dV \quad (26)$$

The temperature is approximated by the global shape function matrix according to (19). The time derivative of the temperature field can then be expressed as:

$$\frac{dT}{dt} = \boldsymbol{N}\frac{d\boldsymbol{a}}{dt} = \boldsymbol{N}\dot{\boldsymbol{a}} \tag{27}$$

since it is assumed that the shape functions do not depend on time. With the Galerkin method, the scalar weight function *v* is chosen as before, (21) and (22).

$$v = \boldsymbol{N}\boldsymbol{c} = \boldsymbol{c}^T\boldsymbol{N}^T \tag{28}$$

$$\nabla v = \boldsymbol{B}\boldsymbol{c} = \boldsymbol{c}^T\boldsymbol{B}^T \tag{29}$$

∇T is given as in (20).

$$\nabla T = \nabla \boldsymbol{N}\boldsymbol{a} = \boldsymbol{B}\boldsymbol{a} \tag{30}$$

The finite element formulation for transient heat flow can thus be written as follows.

$$\begin{aligned}\boldsymbol{c}^T\left(\int_V \boldsymbol{B}^T\boldsymbol{D}\mathbf{B}dV\boldsymbol{a} + \int_V \boldsymbol{N}^T\rho c\boldsymbol{N}dV\dot{\boldsymbol{a}}\right)\\ = \boldsymbol{c}^T\left(-\int_{S_h}\boldsymbol{N}^T h dS - \int_{S_g}\boldsymbol{N}^T\boldsymbol{q_n}dS + \int_V \boldsymbol{N}^T Q dV\right)\end{aligned} \tag{31}$$

With $\boldsymbol{K}$ and $\boldsymbol{f}$ as defined previously, the finite element formulation can be stated along with the capacity matrix $\boldsymbol{C}$.

$$\boldsymbol{K} = \int_V \boldsymbol{B}^T\boldsymbol{D}\boldsymbol{B}dV$$

$$\boldsymbol{f_b} = -\int_{S_h}\boldsymbol{N}^T h dS - \int_{S_g}\boldsymbol{N}^T\boldsymbol{q_n}dS$$

$$\boldsymbol{f_l} = \int_V \boldsymbol{N}^T Q dV$$

$$\boldsymbol{C} = \int_V \boldsymbol{N}^T\rho c\boldsymbol{N}dV$$

$$\boldsymbol{K}\boldsymbol{a} + \boldsymbol{C}\dot{\boldsymbol{a}} = \boldsymbol{f}$$

Approximation in time

Since the governing equation to be solved is time dependent, it is essential to find a suitable time integration scheme. Here, the derivation assuming a linear time approximation is given.

The time is divided into time steps Δt. τ is the *time coordinate* within such a step, starting at $\tau = 0$ and ending at $\tau = \Delta t$. The approximation for the temperature between two values can be calculated as a linear approximation as follows in equation (32). The approximation goes from index *i* to *i+1*.

$$\boldsymbol{a}(\tau) = \frac{\boldsymbol{a}_{i+1} - \boldsymbol{a}_i}{\Delta t}\tau + \boldsymbol{a}_i \tag{32}$$

This is rewritten with time functions *G*, similarly to shape functions.

$$\boldsymbol{a}(\tau) = G_i \boldsymbol{a}_i + G_{i+1} \boldsymbol{a}_{i+1} \tag{33}$$

$$\begin{cases} G_i = 1 - \dfrac{\tau}{\Delta t} \\ G_{i+1} = \dfrac{\tau}{\Delta t} \end{cases}$$

When the time coordinate equals zero, the starting temperature would equal to $\boldsymbol{a}_i$ and the temperature after time Δt equals to $\boldsymbol{a}_{i+1}$. The change in temperature is obtained by derivation.

$$\dot{\boldsymbol{a}}(\tau) = \frac{\boldsymbol{a}_{i+1} - \boldsymbol{a}_i}{\Delta t} \tag{34}$$

$\boldsymbol{a_i}$ is assumed to be known, $\boldsymbol{a}_{i+1}$ at time t_{i+1} is to be determined. To introduce this choice of the time approximation, the FE-formulation is once again multiplied with a weight function in time $w(\tau)$ and integrated over the time step.

$$\int_0^{\Delta t} w\boldsymbol{K}\boldsymbol{a} d\tau + \int_0^{\Delta t} w\boldsymbol{C}\dot{\boldsymbol{a}} d\tau = \int_0^{\Delta t} w\boldsymbol{f} d\tau \tag{35}$$

The time approximation is inserted.

$$\int_0^{\Delta t} w\boldsymbol{K}\left[\frac{\boldsymbol{a}_{i+1} - \boldsymbol{a}_i}{\Delta t}\tau + \boldsymbol{a}_i\right] d\tau + \int_0^{\Delta t} w\boldsymbol{C}\frac{\boldsymbol{a}_{i+1} - \boldsymbol{a}_i}{\Delta t} d\tau = \int_0^{\Delta t} w\boldsymbol{f} d\tau \tag{36}$$

C, ***K***, $\boldsymbol{a_i}$ and $\boldsymbol{a_{i+1}}$ are independent of time and can be placed outside of the integrals.

$$\boldsymbol{K}\frac{\boldsymbol{a}_{i+1} - \boldsymbol{a}_i}{\Delta t}\int_0^{\Delta t} w\tau d\tau + \boldsymbol{K}\boldsymbol{a}_i \int_0^{\Delta t} w d\tau + \boldsymbol{C}\frac{\boldsymbol{a}_{i+1} - \boldsymbol{a}_i}{\Delta t}\int_0^{\Delta t} w d\tau = \int_0^{\Delta t} w\boldsymbol{f} d\tau \tag{37}$$

Divide by $\int_0^{\Delta t} w d\tau$ to obtain

$$\boldsymbol{K}\frac{\boldsymbol{a}_{i+1} - \boldsymbol{a}_i}{\Delta t}\frac{\int_0^{\Delta t} w\tau d\tau}{\int_0^{\Delta t} w d\tau} + \boldsymbol{K}\boldsymbol{a}_i + \boldsymbol{C}\frac{\boldsymbol{a}_{i+1} - \boldsymbol{a}_i}{\Delta t} = \frac{\int_0^{\Delta t} w\boldsymbol{f} d\tau}{\int_0^{\Delta t} w d\tau} \tag{38}$$

Introducing a weighting parameter θ

$$\theta = \frac{1}{\Delta t}\frac{\int_0^{\Delta t} w\tau d\tau}{\int_0^{\Delta t} w d\tau} \tag{39}$$

we obtain

$$\boldsymbol{K}[\boldsymbol{a}_i + \theta(\boldsymbol{a}_{i+1} - \boldsymbol{a}_i)] + \boldsymbol{C}\frac{\boldsymbol{a}_{i+1} - \boldsymbol{a}_i}{\Delta t} = \frac{\int_0^{\Delta t} w\boldsymbol{f} d\tau}{\int_0^{\Delta t} w d\tau} = \bar{\boldsymbol{f}} \tag{40}$$

If the load vector also is assumed to vary linearly, the equation will correspond to the approximated time functions for the temperature according to (33).

$$\boldsymbol{f}(\tau) = G_i \boldsymbol{f}_i + G_{i+1} \boldsymbol{f}_{i+1} = \left(1 - \frac{\tau}{\Delta t}\right) \boldsymbol{f}_i + \frac{\tau}{\Delta t} \boldsymbol{f}_{i+1} \tag{41}$$

Final form of the force vector is given by adding equation (41) to the formulation for $\bar{\boldsymbol{f}}$.

$$\boldsymbol{f}(\tau) = \left(1 - \frac{\tau}{\Delta t}\right) \boldsymbol{f}_i + \frac{\tau}{\Delta t} \boldsymbol{f}_{i+1} = \boldsymbol{f}_i + \frac{\tau}{\Delta t} (\boldsymbol{f}_{i+1} - \boldsymbol{f}_i) \tag{42}$$

$$\bar{\boldsymbol{f}} = \frac{\int_0^{\Delta t} w \boldsymbol{f} d\tau}{\int_0^{\Delta t} w d\tau} = \frac{\int_0^{\Delta t} w \left(\boldsymbol{f}_i + \frac{\tau}{\Delta t} (\boldsymbol{f}_{i+1} - \boldsymbol{f}_i)\right) d\tau}{\int_0^{\Delta t} w d\tau} \tag{43}$$

The integral can be separated and the terms $\boldsymbol{f}$ and Δt placed outside of the integrals.

$$\bar{\boldsymbol{f}} = \boldsymbol{f}_i \frac{\int_0^{\Delta t} w d\tau}{\int_0^{\Delta t} w d\tau} + \frac{1}{\Delta t} (\boldsymbol{f}_{i+1} - \boldsymbol{f}_i) \frac{\int_0^{\Delta t} w \tau d\tau}{\int_0^{\Delta t} w d\tau} \tag{44}$$

The first integral is cancelled out and the second is replaced by the weighting parameter θ.

$$\boldsymbol{f}_i + \theta (\boldsymbol{f}_{i+1} - \boldsymbol{f}_i) = \bar{\boldsymbol{f}} \tag{45}$$

Equation (40) can now be solved for the temperature for the next time step $\boldsymbol{a}_{i+1}$.

$$\boldsymbol{C} \frac{\boldsymbol{a}_{i+1} - \boldsymbol{a}_i}{\Delta t} + \boldsymbol{K}[\boldsymbol{a}_i + \theta (\boldsymbol{a}_{i+1} - \boldsymbol{a}_i)] = \bar{\boldsymbol{f}} \tag{46}$$

The terms are separated and multiplied by Δt.

$$\boldsymbol{C}\boldsymbol{a}_{i+1} - \boldsymbol{C}\boldsymbol{a}_i + \Delta t \boldsymbol{K}\boldsymbol{a}_i + \Delta t \boldsymbol{K}\theta \boldsymbol{a}_{i+1} - \Delta t \boldsymbol{K}\theta \boldsymbol{a}_i = \Delta t \bar{\boldsymbol{f}} \tag{47}$$

Re-arranged for each temperature $\boldsymbol{a}$.

$$\boldsymbol{a}_{i+1}(\boldsymbol{C} + \Delta t \boldsymbol{K}\theta) - \boldsymbol{a}_i\big(\boldsymbol{C} - \Delta t \boldsymbol{K}(1 - \theta)\big) - \Delta t \bar{\boldsymbol{f}} = 0 \tag{48}$$

Solved for $\boldsymbol{a}_{i+1}$.

$$\boldsymbol{a}_{i+1} = (\boldsymbol{C} + \Delta t \theta \boldsymbol{K})^{-1}\big[\big(\boldsymbol{C} - \Delta t \boldsymbol{K}(1 - \theta)\big)\boldsymbol{a}_i + \Delta t \bar{\boldsymbol{f}}\big] \tag{49}$$

Lastly, the resulting equation is expressed in a simplified manner.

$$\hat{\boldsymbol{K}} \boldsymbol{a}_{i+1} = \hat{\boldsymbol{f}}$$

$$\hat{\boldsymbol{K}} = (\boldsymbol{C} + \Delta t \theta \boldsymbol{K})$$
$$\hat{\boldsymbol{f}} = \big[\big(\boldsymbol{C} - \Delta t \boldsymbol{K}(1 - \theta)\big)\boldsymbol{a}_i + \Delta t \bar{\boldsymbol{f}}\big]$$

Analogy between heat and moisture transfer

Abaqus does not have a built-in function for modeling moisture content. However, the program is able to model heat flow problems, solving for flow and temperature. The differential equation for heat flow, *Fourier's law*, that is used in Abaqus is shown in equation (50).

$$\frac{dT}{dt} = \frac{d}{dx}\left(\frac{\lambda}{c\rho}\frac{dT}{dx}\right) \tag{50}$$

This differential equation is similar to *Fick's law* which describes moisture transport by diffusion. Thus, assuming that the temperature T is analogous to the moisture content u, we can write:

$$\frac{du}{dt} = \frac{d}{dx}\left(D\frac{du}{dx}\right) \tag{51}$$

The difference lies in the definition of the coefficient D. Setting both the density ρ and the specific heat c to a value of 1 gives a thermal conductivity λ that is equivalent to the diffusivity D.

Stiffness matrix

The stiffness matrix $\boldsymbol{K}$ is a symmetric matrix, as a consequence following from the assumption of a linear elastic material and making use of the Galerkin method. In the below expressions, the first, second and third dimensions correspond to the longitudinal, tangential and radial directions, respectively. An orthotropic material is assumed for the wood used and the stiffness matrix $\boldsymbol{K}$ is defined by its inverse $\boldsymbol{K}^{-1}$.

$$\boldsymbol{K}^{-1} = \begin{bmatrix} \frac{1}{E_R} & -\frac{v_{TR}}{E_T} & -\frac{v_{LR}}{E_L} & 0 & 0 & 0 \\ -\frac{v_{RT}}{E_R} & \frac{1}{E_T} & -\frac{v_{LT}}{E_L} & 0 & 0 & 0 \\ -\frac{v_{RL}}{E_R} & -\frac{v_{TL}}{E_T} & \frac{1}{E_L} & 0 & 0 & 0 \\ 0 & 0 & 0 & \frac{1}{G_{RT}} & 0 & 0 \\ 0 & 0 & 0 & 0 & \frac{1}{G_{RL}} & 0 \\ 0 & 0 & 0 & 0 & 0 & \frac{1}{G_{TL}} \end{bmatrix}$$

The stiffness matrix is defined in Abaqus by using the option *engineering constants*: defining the modulus of elasticity, Poisson's ratio, and shear modulus. (Dassault Systèmes 2015)

Validation of numerical simulation

Convergence criteria

The *convergence criteria* mean that for infinitely smaller elements the solution should be infinitely close to the correct solution. This is achieved by attaining *completeness requirement* and *compatibility requirement*. (Ottosen & Petersson 1992)

Completeness: The approximation must be able to represent an arbitrary constant moisture gradient. It must also be able to represent an arbitrary constant moisture content. This basically means that the approximation must be able to describe a change in MC for each geometrical dimension. For a three-dimensional case, the equation must look like the following.

$$u_{MC} = \alpha_1 + \alpha_2 x + \alpha_3 y + \alpha_4 z + possibly\ other\ terms$$

Compatibility/conforming requirement: The approximation of the moisture content over element boundaries must be continuous. This means that the values for each element must be the same at the boundaries where the elements meet.

The convergence criteria are met if both the completeness and compatibility requirements are met.

$$Convergence = completeness + compatibility$$

Convergence study

A simpler convergence study was made to check the viability of a certain mesh size. The width of the gap between the boards of the outer most layer, at the CLT plates surface, for the reference case was measured and compared for different mesh sizes.

With the thickness of the boards being as low as 20 mm for some cases, it is reasonable to set a mesh size no more than 10 mm.

The results for a few different mesh sizes are shown in Table 1.

Table 1. Gap width for different mesh sizes. For every halving, the difference in gap width in percent are shown.

Mesh size	0.01	0.005	0.003	0.0025	0.002
Gap [mm]	0.3157	0.3302	0.3351	0.3362	0.3371
Diff [%]	-	4.61	-	1.80	-

One problem with the student version of Abaqus is that the number of nodes for a model is limited to 250,000. The model made for the convergence study allowed for a mesh size of 2 millimeters per element. To give some margin for eventually larger models for other modeling cases, a mesh size of 2.5 millimeters were set. However, an even finer mesh would take longer time to compute. The chosen mesh gives an acceptable computing time.

One-dimensional calculation

When calculating the elongation, as a result of changing moisture content, in a simpler manner without a finite element-software, a one-dimensional approach can be used. Multiplying the expansion coefficient by the original length and change in moisture content gives change in length (δl).

$$\alpha \cdot MC \cdot l = \delta l$$

$$\begin{cases} \alpha = expansion\ coefficient \\ MC = change\ in\ moisture\ content \\ l = length \end{cases}$$

For the gap width in the outer most layer of the CLT plate, with a relatively thick lamination, one can expect this calculation to agree with the actual value, as the expansion would occur rather freely with a low influence from the rest of the structure. Thus, assuming the coefficient of expansion in the tangential direction is of relevance, one obtains:

$$0.0026 \cdot 1 \cdot 0.2 = 52 \cdot 10^{-5}\ m$$

The elongation of a representative part as the one used in the FE-models would depend on the coefficient of expansion in the longitudinal direction, independent of the number of boards.

$$0.0001 \cdot 1 \cdot 0.2 = 2.0 \cdot 10^{-5}\ m$$

This value can be compared to the elongation of the model. The value from the model ought to be similar. However, as the CLT differs in its directions, the result for both directions might differ.

Modeling

Building the models

For each configuration, two models were built: One for calculating the moisture distribution and another for the deformation. Both models will have the same geometry. The model giving the moisture-induced deformations have the moisture distribution from a previous calculation loaded as a predefined field. One reason for this simplified, one-way coupling approach is that it is assumed that the displacements depend on the change in moisture content, but not the other way around.

The drying of CLT elements is assigned a change in moisture content of one percent and all results from such an analysis are assumed to vary linearly with the change in moisture content. The initial gap width is assumed to be zero.

The idea is to make a simplified model that as realistically as possible mimics the real behavior of a CLT element. This is done by modeling a small representative part of an infinitely large CLT plate. Such a model represents an arbitrary part of the plate, set apart from the boundaries and mechanical supports. Since the element is arranged in a repetitive manner, a smaller model can be achieved by the use of symmetry planes and constraints. It is assumed that the complete CLT plate is simply supported at the ends, infinitely far away from the modeled part. This means that the studied representative volume is free to expand.

With an infinitely large element, it is assumed that each laminate's cross-section remains leveled and perpendicular to its longitudinal direction. Such an assumption of symmetry can be achieved by the *constraint equation*, see Figure 5. In general, constraint equation makes it possible to define dependencies, such as that of the displacement, of different nodes. By forcing all the nodes on a surface to have equal displacement, a surface can be kept plane during deformation. However, this type of constraint has only been set for a uniform load case and for a steady-state calculation with only the start and end values being of interest. A non-uniform distribution of the moisture content would in reality lead to a non-uniform distribution of displacements.

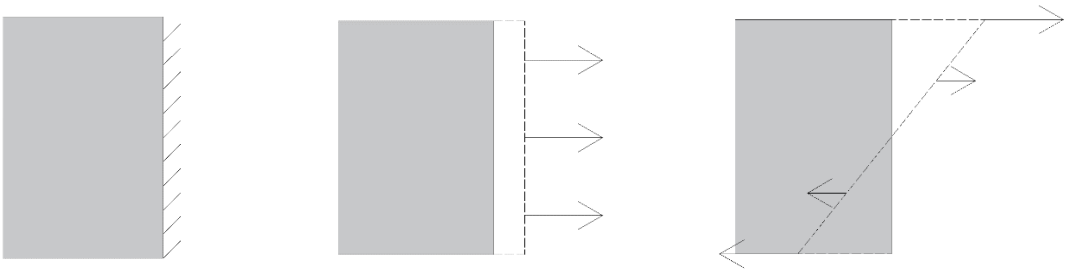

Figure 5. Symmetry plane (left), Constraint equation (middle), constraint coupling (right). Illustration of how the restricted surface will behave after expansion.

As one side is restricted by constraint equation, the other side is set as a symmetry plane, restricting any displacement apart from the planes normal as well as restricting any rotation. For symmetry planes located right at the gaps, the symmetry plane is set for the boards crossing the section and the edges for the gaps left free. In other words, the gaps' edges are never given any constraints. The displacement for the edges after simulation is thereby meant to correspond

to the opening width of the gaps. For the uniform model, only one gap edge is present and will correspond to half the gap width.

With all the assumptions, a smaller model can be set to represent the entirety of the infinitely large element. An example of this is shown in Figure 6, showing the geometry of the model for the uniform load case. The models are further described in the following chapter.

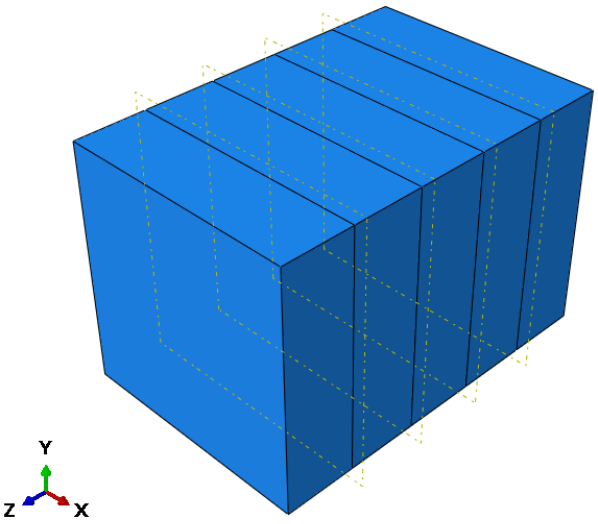

Figure 6. Model of CLT element for uniform drying. Z-coordinate follows across the thickness of the element. The distance of x and y for the part is half the width of a board. This example has five layers.

For a non-uniform drying the element is expected to bend. Here, the constraint equation is replaced with *constraint coupling*. The constraint coupling is a special case of the constraint equations, making a group of nodes, e.g. on a surface, act in accordance with the existence of a stiff coupling to a reference node. Placing the reference node in the middle of such a surface, at its neutral axis, makes the surface act accordingly. The constraint coupling accounts for the distance from that node, keeping the constrained surface plane, mimicking a cross-section for a beam under bending. A node cannot be assigned to two coupling constraints at the same time, which in the current project means that the constraint will only be set at the surfaces crossing the direction of the largest bending.

The coupling constraint is also used when checking the bending. The difference between the non-uniform and bending models are the location of the symmetry plane, as the displacement ought to be measured for different locations.

When two parts are joined together, as for the bending model, *tie constraint* is used. The nodes of a slave surface will act according to its master nodes of the matching surface.

When looking at the gap width, the nodes with the largest displacements for a gap are compared. The largest displacement are expected at the middle of the gap, furthest from its ends. One cannot guarantee that a node will appear at a mid-point as the thickness of a layer might not correspond to the thickness of the mesh element.

For the gap width, the interesting case to look at is when the model has fully reached its new moisture content, or when the model has reached an even steady-state distribution. Therefore,

a transient analysis is not of interest. The transient calculation will however be used for the 2D TCC model.

The TCC model is made two-dimensional. The left end is set as a symmetry plane, fixing the surface but allowing for the thickness of the slab to expand. The right end has a coupling constraint. The set-up allows for the slab to bend. Both ends will be seen as plane even though the deformation will occur unevenly across the cross-section. The TCC model will also have a film coefficient added for the surface convection at the lower surface between the timber and the room below. The slab will only dry through that surface.

The time-period is divided in days. This is only of interest for the composite model as the other models are calculated as steady-state: only steady-state condition is looked at and the time for the model to reach it is irrelevant.

Scripting

Scripting is a good way to perform a parameter study in Abaqus. Along with the model file .cae, Abaqus also store every action done as a Python script in a .jnl-file. Altering this file is one approach for making a script. Therefore, it is desirable to keep the number of steps taken at a minimum, or to clear out some of the lines later on, to keep the script simple and easy to overview. A script can also be made using the Macro manager. With Macro manager one can choose what actions to record. With the finalized code, one can alter the desired parameters. The main purpose of the script is the possibility to enclose the code with a for-loop, making a parameter study easier to make. One should also make sure that the name of the model and job changes for every iteration. By saving the new script as a .py-file, it can be run as a script directly in Abaqus.

Models

Different models will be used when studying different load cases and applications. All models are considered representations of a small part, cut from an infinitely large element. By the use of symmetry planes and constraints, the infinitely large element can be represented by a smaller model. Figure 7 shows where symmetry planes can be found in the case of a CLT element of five layers. Note that symmetries can be found where these planes cut through the boards, and that the gaps between the boards are treated as free surfaces.

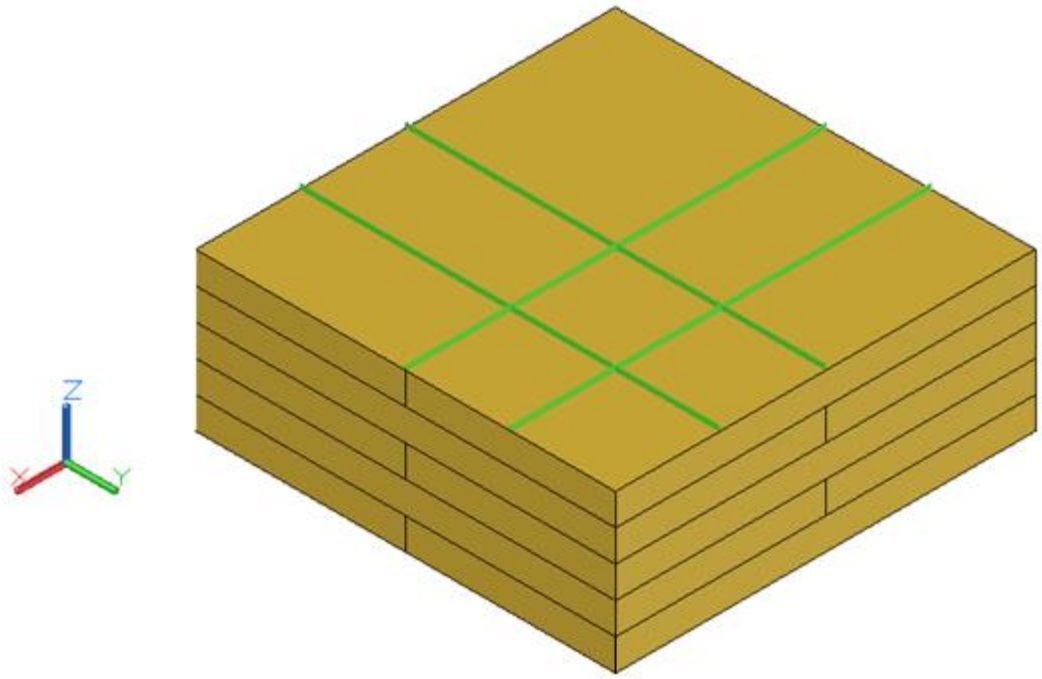

Figure 7. Five layered CLT element. The green lines shows where symmetries can be found: between boards and through the middle of each board. The element extends infinitely in X- and Y-directions.

Reference case

To make results from different calculations comparable, the dimensions of the modeled elements should be similar. When making a parametric study, only one parameter value will be varied, and the others kept constant. The model with standard values is referred to as the reference case. The reference model has five boards, each with a thickness of 30 mm and a width of 200 mm, see Table 2. The reference case will also define the dimensions for the models used when evaluating the behavior for non-uniform drying. Note that for the reference case, the board thickness is the same for every board, which will later be referred to as a factor of 1:1. The thickness of the entire CLT element will be 150 mm. The total thickness will be kept constant except for the cases with changed board thicknesses.

The following parameters will be varied: board thickness, board width, layer thickness factor, and number of layers. The *layer thickness factor* (factor) is defined as the ratio of board thicknesses, where they change for every second layer. As an example, a factor of 1:2 means that the outer and middle layers (layer 1, 3, 5) have a thickness twice as large as the two others.

Table 2. Dimensions for the reference case. Note that every board has the same thickness.

Dimensions for the reference case	
Board thickness	$30\ mm$
Board width	$200\ mm$
Number of layers	5

Uniform drying

The element is assumed to be in a state of uniform moisture content and is subjected to uniform drying. The model is exposed to a lowering of its moisture content percentage by one, for example from 12% to 11% moisture content and assuming that this takes place in the complete specimen.

The study of the uniform drying will mostly focus on the width of the gaps between the boards. The idea is to keep the thickness of the entirety of the element constant for every case for a fair comparison between configurations. This means that changing the factor or number of layers will change the board thickness in a way that still gives the same total thickness of 150 mm. The total thickness of the element will however change when modeling for different board thicknesses, for example giving a total thickness of 100 millimeters when having boards of 20 millimeters.

Starting with a uniform moisture distribution and assuming a uniform decrease of moisture content, one can expect that the cross-sections of the CLT along the symmetry planes will remain plane and perpendicular to the boards direction. The model can then be reduced to only include the CLT part between those symmetry planes, see Figure 8.

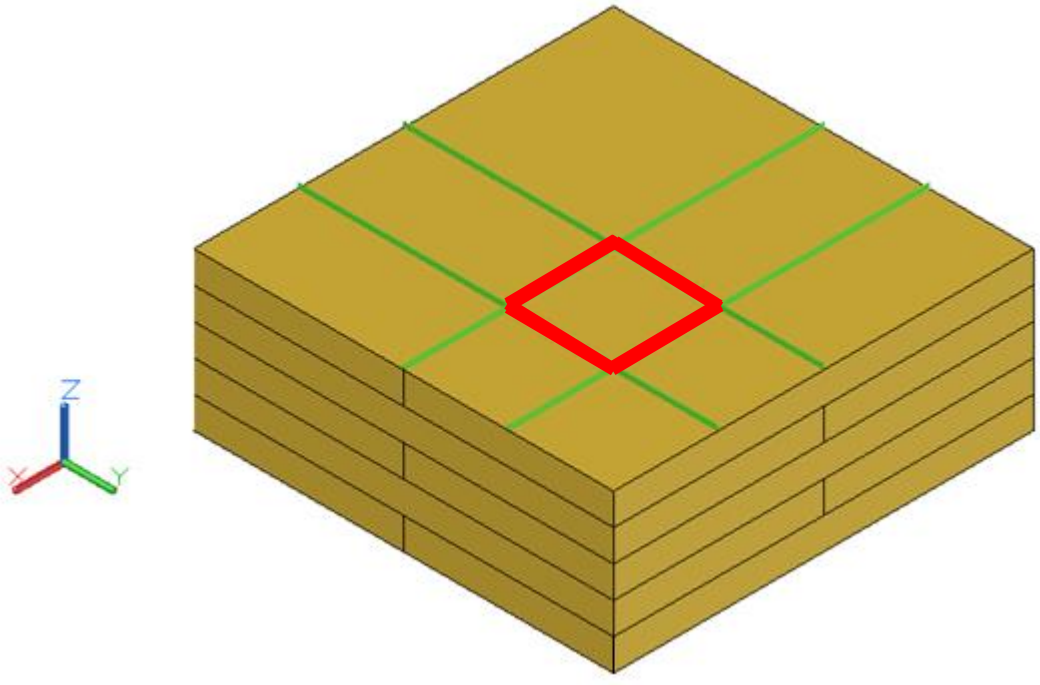

Figure 8. Five layered CLT element with indication of smallest representative volume, taking into account symmetries. The sides of the square are 100 mm long, half the board width.

Symmetry planes are located along every board edge, as well as along the middle of each board. The size of the studied part of the CLT-plate can therefore be shortened down to half the width of each board, making the model's top surface be a perfect square of 100 mm for the reference case. The depth is still set to 150 mm. The symmetry is accounted for by a combination of boundary conditions and constraint equations, to allow the element as a whole to contract, but with the symmetry planes keeping their perpendicular orientation with respect to the boards.

Non-uniform drying

The moisture distribution is here set to a linearly varying distribution across the thickness of the CLT plate, with one side having a moisture content of one percent lower value. For this model, the entirety of the thickness needs consideration.

In each transverse layer two half boards are modeled, see Figure 9 and Figure 10. The surface along which the gaps are located is assumed to be a symmetry plane. As bending is expected to occur for non-uniform drying, this new model will be needed.

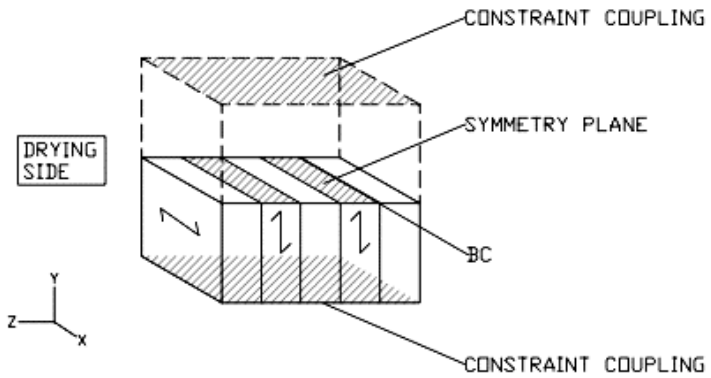

Figure 9. One of the two parts that builds up the model for the non-uniform loading are shown, with the dashed line showing the silhouette of the second part. The two parts are joined at a symmetry plane attached only to the surfaces of the two boards that cross the symmetry plane. The three surfaces left free are edges of the gaps. Boundary condition BC is set along a line and will restrict the model from moving in the xz-plane.

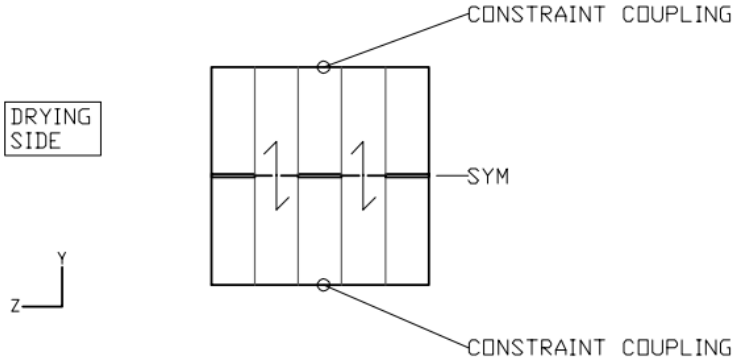

Figure 10. The non-uniform loading model from the side. The figure shows how boards cross the symmetry line.

The outer ends (the surfaces coinciding with the xz-plane, see Figure 9) are set as coupling constraints. The bending is expected to be larger for the elements weaker two-board direction i.e. corresponding to rotation about the x-axis, see Figure 9. Bending will occur in the other direction as well i.e. rotation about the y-axis. This could have been modeled assuming a constraint coupling on the surfaces parallel to the yz-planes. However, constraints cannot be set for two surfaces sharing nodes. On the symmetry plane, the nodes closest to the end that does not dry are restricted from movement in any direction.

Only one case of non-uniform loading has been studied, with the configuration according to the reference case. This is then compared with the uniform drying for the same configuration.

Bending

An additional model has been made in order to facilitate the evaluation of the bending of the CLT element, see Figure 11. This one differs from the non-uniform drying as the fixed nodes, those restricted from any displacement, are set at another location.

Two parts are stacked together as for the non-uniform drying. One end will be entirely fixed, which can be done if that surface is in the middle if a board, assuming the cross-section to be perpendicular to the slab direction. The other end will also be located in the middle of the next board. Constraint coupling has been set at that end.

By this model, the value of the bending will not be affected by local displacement because of the gaps. To get the value of the bending, the displacement at both ends are compared. The difference gives the displacement in lateral direction. The deformations are measured in the middle of the model along its neutral axis. As two measurements are taken at the neutral axis and in the middle of the boards, the deformation measured should not be affected by neither the gaps nor shrinking.

The edges of the gaps are left free, just as for the non-uniform model. No boundary conditions are set between the two parts, which are just joined together with a tie constraint.

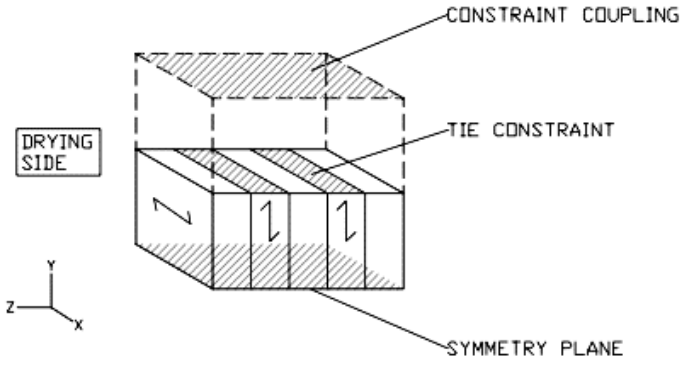

Figure 11. One of the two parts that builds up the bending model are shown, with the dashed line showing the silhouette of the second part. The two parts are joined together by a tie constraint attached only to the surfaces of the two boards that crosses the symmetry plane. One end is fixed by a symmetry plane, the other a coupling constraint. The surfaces are kept plane even as the part bends.

Timber-concrete composite (TCC)

For the TCC model, the calculations are performed using relative humidity as primary variable, instead of using moisture content. The RH time history for the concrete layer is predefined by prescribing a single value for every node belonging to the concrete part, at each instant in time. The relation between MC and RH is given by the sorption isotherm. That nonlinear relation is in turn used to define the expansion and diffusion coefficients as nonlinearly dependent on RH. This is done by using tabular input data in Abaqus, see chapter *Input data*.

For the TCC structure, it is relevant to study the time-dependent moisture distribution. This could tell, for example, what maximal relative humidity within the CLT can be expected and at what depth. Therefore, unlike for the other models, a transient analysis is made. For a transient analysis, the structure is studied over time. The bending of the TCC due to the moisture-induced deformations will also be checked, as well as the maximal stress values.

The timber-concrete composite structure is modeled as a 2D model. Full interaction is assumed between concrete and timber. The dimensions of the TCC structure is shown in Figure 12. The dimensions of the CLT element are set as for the reference case with five layers of 30 millimeters each. All edges are assumed to be glued together, giving no gaps between boards. Two different situations are considered by alternating the material directions of the layers. The two corresponding models are named model A and B. Model A has layer 1, 3 and 5 oriented perpendicular to the concrete notch. Model B has the layers oriented at 90 degrees compared to model A, see Figure 12.

The dimensions used for the notch are based on a similar study by Autengruber, M. Lukacevic, M. and Füssl, J. (2020). As stated by Swedish wood (2017c), the concrete slab usually has a thickness of 40 percent of the entire TCC structure. This gives the concrete slab a thickness of 100 millimeters for a CLT element of 150 millimeters.

Moisture induced expansion is assumed to be zero for concrete. However, as full interaction is assumed between the wood and the concrete, displacement will occur for the concrete because of the expansion occurring in the timber. It is furthermore assumed that the vertical cross sections, left and right edges of the models in Figure 12, remain plane during deformation. This is accomplished by the use of constraint equations, where a single control node is used for one such edge.

The concrete layer is given a relative humidity in accordance with a drying process for concrete hydration under membrane curing. Drying is assumed to only occur through the CLT element and out to the room below, as could be the case if a non-permeable layer is placed above the concrete slab.

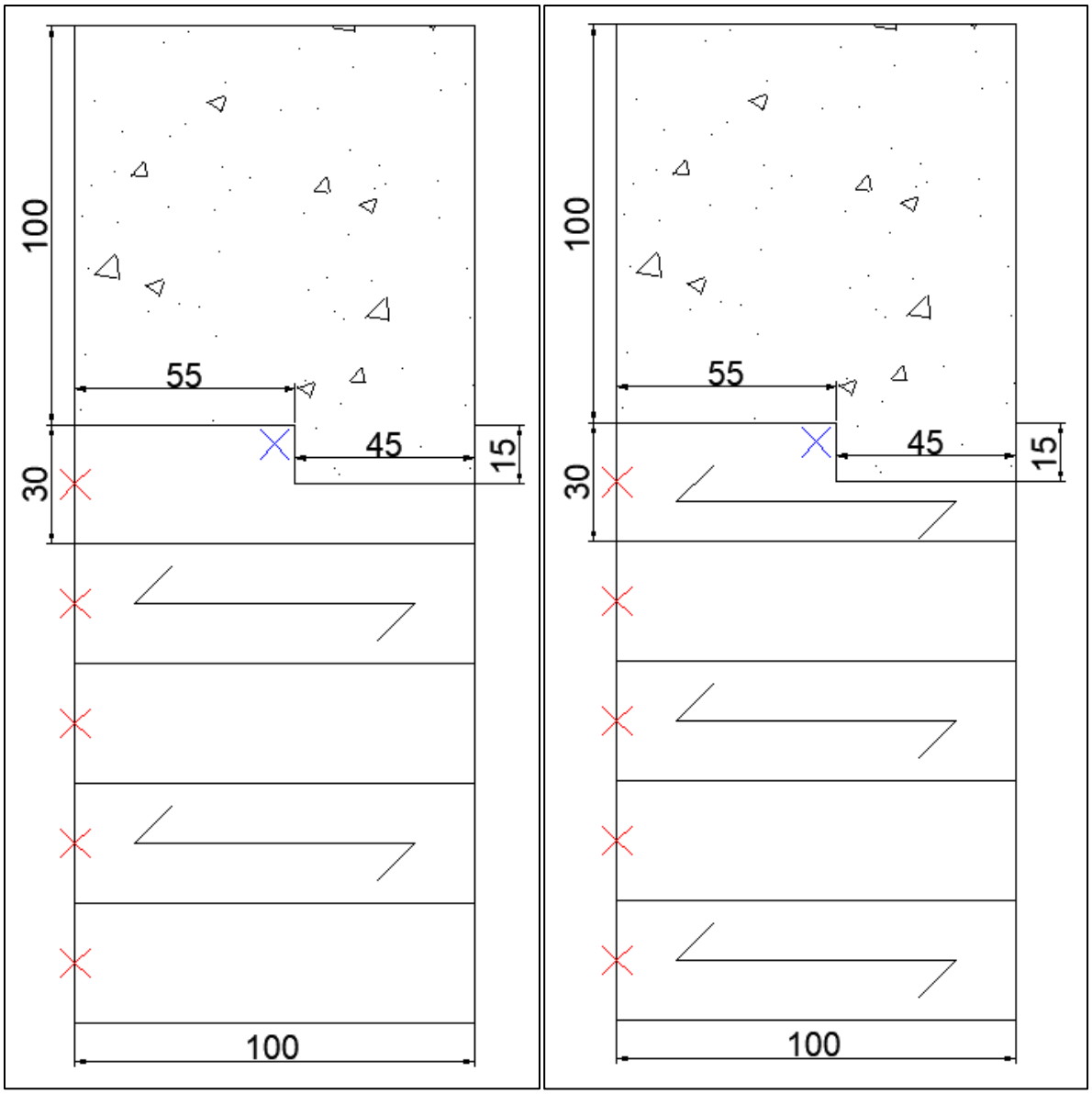

Figure 12. Layout of the two TCC models. Model A (left) and B (right). Crosses shows nodes where relative humidity is checked.

As the element is modeled as infinitely large, it is seen as reasonable to simplify the models both sides as staying perpendicular. The left side is set as a symmetry boundary and the other as a coupling constraint. The top left node is set as fixed. Every other node is allowed to displace along the elements thickness. A higher moisture content in the timber will lead to the TCC element increasing its thickness. The element is expected to get its largest expansion for the timber closest to the concrete, in other words, in the middle of the TCC element. Therefore, even though the model allows the element to curve, the effect from bending might be small.

To evaluate the results from the simulations, the relative humidity at the midpoint of each layer at the left-most location furthest from the notch, see red crosses in Figure 12, are measured. Another point is checked, close to where the highest humidity is expected. This point is located 5 millimeters in each direction from the inner corner of the notch, see blue cross. Humidity at the surface will be checked, as well as the elongation and bending of the representative part being modeled. Elongation and bending are defined based on the displacement at the corners

of the model, see Figure 13. The displacements are named X1, X2, Y1 and Y2, based on the direction of the displacement and based on the position of the monitoring point. The outer most positions are used, as those are expected to be the positions with largest displacement.

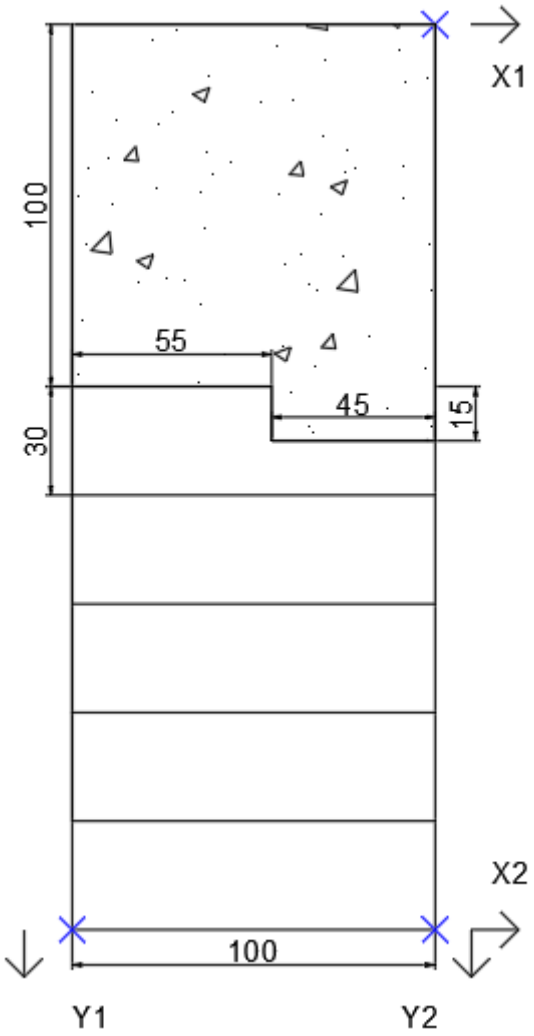

Figure 13. Model of the TCC floor, showing what nodes will be studied for displacement.

By obtaining the displacement at both upper and lower part of the model, the bending can be given, comparable to the ordinary CLT element. It is calculated as the difference in x-displacement divided by the structure's height, see (52). It is assumed that the plane surface boundary rotates so that the value would be the same in y-direction, thereby making it comparable to the displacement for the 3D-models.

$$v = \frac{X2 - X1}{h} \tag{52}$$

Elements

An element size of 0.0025 meters are set for every model, see *Convergence study*. Linear elements are used for models of the CLT and quadratic elements for the TCC model.

Two types of elements are used; continuum stress/displacement elements and mass diffusion elements for the two models, denoted by a C and DC. The CLT elements are modeled with 3D elements of 8 nodes. The TCC model has two-dimensional four node plane strain elements. The elements notations are therefore C3D8 for CLT element and CPE4 for TCC structure. Full integration is set, not reduced. (Dassault Systèmes 2015)

Evaluation criteria

Bending, gap width, mold growth

The values for bending, gap width and relative humidity should be kept as low as possible. A value can be given for each parameter as a maximal value that should not be surpassed.

The maximal accepted bending is listed in Eurocode (SS-EN 95-1-1:2004).

$$w_{fin} = \frac{l}{150} = 6.\bar{6}\ mm/m$$

The European product standard for CLT applies to CLT made from boards that have a maximum gap width of 6 millimeters (SS-EN 16351:2015). For a low charring rate, the gap width should be lower than 2 millimeters.

To assure minimal risk for mold growth, the critical relative humidity should be set to 75 percent. (Nevander & Elmarsson 1981)

Rolling shear

The type of stress that is usually of greatest importance is the rolling shear. The shear strength in the radial-tangential plane, rolling shear, is lower than the strength in other directions. The strength is higher as the shear plane cuts through the fibres, unlike for the rolling shear. For rolling shear, the fibres roll against one another at cracking. The crack will also go through the weaker earlywood, unlike for the other shear planes where the cracking has to go through both early- and latewood. The design value considering rolling shear is set to 1.2 MPa. (Borgström 2016)

Table 3. List of limits considering performance of timber element.

Max bending	6.67 mm/m
Max gap width	6 mm (or 2 mm)
Max relative humidity	75 percent (for longer period of time)
Max rolling shear	1.2 MPa

Input data

The material used is Norway Spruce and the modeling is made in meters. The material is linear elastic with parameters defined as engineering constants, giving modulus of elasticity, Poisson's ratio, and shear modulus. The material is orthogonal and different values are set for each geometrical direction.

As stated in chapter *Material*, the stiffness in the longitudinal direction is about 20 times greater than that of the radial direction, which in turn will have a value about twice as high as for the tangential direction. The opposite is true for thermal expansion, where the radial is 20 times larger than for longitudinal, and tangential twice as large as for radial. Also, the G_{TR} is way smaller than the shear modulus for other planes.

Multiple in-parameters has been taken directly from Swedish wood. Those values are seen as likely to be used by others in other research and building designs, hence why those values seems reasonable to use here as well. As the relation between moisture content and relative humidity is not linear, different values for the diffusion and expansion are set for different relative humidities, see Table 6 and Table 7.

The values for diffusion are taken from Sjödin & Serrano (2006), expressed per second. The values are multiplied by 3600 to give time steps in hours and by 24 to get the values per day. The values are then changed for relative humidity instead of moisture content according to the relation given by the sorption isotherm, see Figure 4. Abaqus software does not consider any units and the user therefore needs to keep track of them. Thus, the time period will be measured in unit of days. The diffusion coefficients are irrelevant for the drying of CLT elements as steady-state analyses are made. The values are relevant for the transient modeling of the composite model. The diffusion coefficient D is set equal for the tangential and the radial directions.

The values for the shear modulus are taken from Dahl (2009), giving a mean value from multiple sources. Here, the order for which the indexes of the Poisson's ratio is presented is important to keep track of. The relation is stated in equation (53).

$$\frac{v_{ij}}{E_{ii}} = \frac{v_{ji}}{E_{jj}} \tag{53}$$

The modulus of elasticity in length direction is 12,000 MPa, equal for C30 (Borgström 2016). 400 MPa equals the value for tangential direction. The value for the radial direction is set as 50 percent larger.

Table 4. Input data for 3D model.

Variable	Symbol	Value
Young's modulus	E_L	$12{,}000\ MPa$
	E_T	$400\ MPa$
	E_R	$600\ MPa$
Shear modulus[1]	G_{LT}	$700\ MPa$
	G_{LR}	$700\ MPa$
	G_{RT}	$50\ MPa$
Poisson's ratio[1]	ν_{LT}	0.5
	ν_{LR}	0.5
	ν_{RT}	0.33
	ν_{TL}	$0.01\overline{6}$
	ν_{RL}	0.025
	ν_{TR}	0.22
Film coefficient[2]	h	$3.7 \cdot 10^{-6}$
Expansion[3] (swelling/shrinking)	α_L	$1 \cdot 10^{-4}\ m/m$
	α_T	$2.6 \cdot 10^{-3}\ m/m$
	α_R	$1.2 \cdot 10^{-3}\ m/m$
Diffusion[4] (for MC)	D_L	$1.123 \cdot 10^{-4}\ m/m$
	$D_{R/T}$	$3.456 \cdot 10^{-5}\ m/m$

1 – (Dahl K. 2009)

2 – (Fortino, Mirianon & Toratti 2009)

3 – (Swedish wood 2017f)

4 – (Sjödin, J. & Serrano, E. 2016)

In Abaqus, non-linear relations, such as the diffusion and expansion coefficient, are given tabular data, meaning that the software will interpolate linearly between each value set. The values are picked arbitrary. It is made sure that the curvature gets smaller over time. Abaqus cannot define the relation as a function and one has to rely on a simplified multi-linear relation between preset nodes (Dassault Systèmes 2015). An alternative would be to implement a user-defined material, which is however outside the scope of this work.

Values for moisture content MC at different relative humidities RH are taken from sorption isotherm, resulting in the values in Table 5. For 100 percent RH, the isotherm shows a value of 27 percent moisture content. At such high levels, the values are hard to estimate exactly.

Table 5. Relative humidity at different values of moisture content.

RH	65	75	85	95	100
MC	11	13	16	22	27

The humidity-dependency need to be set for the diffusion coefficient *D* and the expansion coefficient *α*. The chosen values are presented in Table 6 and Table 7 below.

Table 6. Expansion coefficient for different RH.

Expansion coefficient					
RH	65	75	85	95	100
Factor	11/65	13/75	16/85	22/95	27/100
α_L	$1.69 \cdot 10^{-5}$	$1.73 \cdot 10^{-5}$	$1.88 \cdot 10^{-5}$	$2.32 \cdot 10^{-5}$	$2.70 \cdot 10^{-5}$
α_T	$4.40 \cdot 10^{-4}$	$4.51 \cdot 10^{-4}$	$4.89 \cdot 10^{-4}$	$6.02 \cdot 10^{-4}$	$7.02 \cdot 10^{-4}$
α_R	$2.03 \cdot 10^{-4}$	$2.08 \cdot 10^{-4}$	$2.26 \cdot 10^{-4}$	$2.78 \cdot 10^{-4}$	$3.24 \cdot 10^{-4}$

Table 7. Diffusion coefficient for different RH.

Diffusion					
RH	65	75	85	95	100
Factor	11/65	13/75	16/85	22/95	27/100
D_L	$1.90 \cdot 10^{-5}$	$1.95 \cdot 10^{-5}$	$2.11 \cdot 10^{-5}$	$2.60 \cdot 10^{-5}$	$3.03 \cdot 10^{-5}$
D_T, D_R	$5.85 \cdot 10^{-6}$	$5.99 \cdot 10^{-6}$	$6.51 \cdot 10^{-6}$	$8.00 \cdot 10^{-6}$	$9.33 \cdot 10^{-6}$

The material parameters for concrete are set as isotropic. Expansion of the concrete slab is assumed to not occur by change in humidity by itself, setting expansion coefficient α to zero. The slab will however expand as the timber expands.

Table 8. Input data for concrete in the TCC model

Variable	**Symbol**	**Value**
Young's modulus	E	33,000 MPa
Poisson's ratio	ν	0.2

1 – (SS:EN 1992-1-1, 3.1), for C30

2 – (Burström 2014)

For the composite structure, a two-dimensional model is used with plane strain elements. The material parameters are still set as engineering constants. The timber needs two materials to be defined: one for each direction. For a two-dimensional Abaqus model, the orientation could not by set in three-dimensions. The two materials defined will be the same material, but for different orientations.

The timber is assumed to have an initial moisture content of 65 percent, in accordance with the upper limit for service class 1 at 20° C (Borgström & Fröbel 2019), and the concrete is set to 100 percent, assuming it to be completely soaked. The relative humidity of the concrete will change over time according to experimental results, see Figure 14.

As stated in *Projektering av VVS-installationer* (Warfvinge & Dahlblom 2015), the relative humidity in a room should be kept between 40 and 60 percent. The higher limit is unpreferable for the drying process and will give a slower procedure. Therefore, 60 percent will be the RH set for the room.

Table 9. Initial RH for the materials in the TCC model.

Relative humidity initial values	
Concrete	100 %
Timber	65 %
Room	60 %

Approximate values for the relative humidity of the concrete for different time steps are taken from the graph in Figure 14. The values are taken from Mjörnell (2003) and are experimental values for membrane curing. Assuming that no drying occurs through the top surface and that the flow through the CLT is relatively small, membrane curing seems like a reasonable approximation. The values for the concrete's relative humidity as function of time are added into Abaqus as tabular, in the same way as for the diffusion and expansion coefficient.

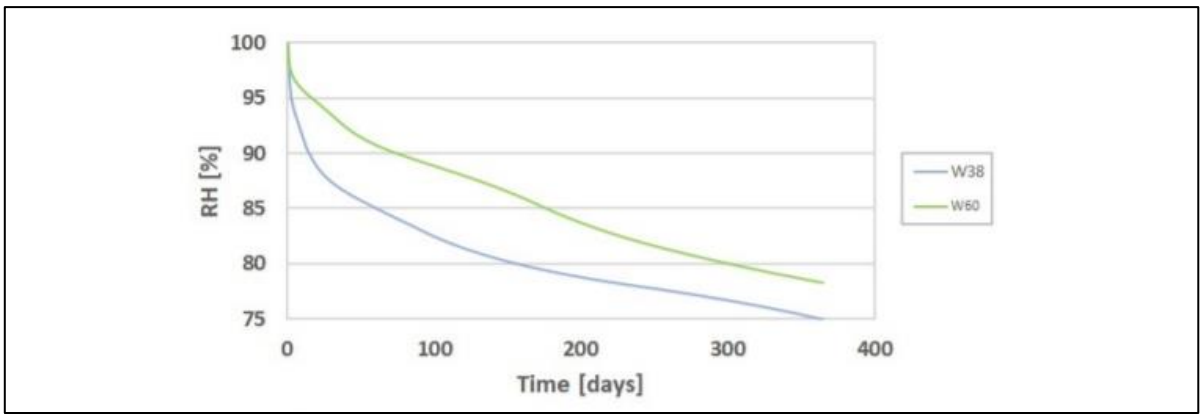

Figure 14. Experimental values of relative humidity for drying of concrete with w/c 0.6 and 0.38. (Mjörnell 2003)

Values are picked from Figure 14 for both w/c 0.6 and 0.38 concrete, listed in Table 10 and Table 11.

Table 10. Relative humidity at different time steps for concrete w/c 0.6. Values used as input data.

Time [Days]	0	5	25	50	100	200	300	400
Relative Humidity	100	97	94	91	88	83	80	77

Table 11. Relative humidity at different time steps for concrete w/c 0.38. Values used as input data.

Time [Days]	0	5	25	50	100	200	300	400
Relative Humidity	100	94	88	86	83	79	76	73

The total time period set for the TCC modeling is 400 days. The time-period seemed reasonable for drying of concrete. Also being the time period for which the RH for the experimental drying processes where read.

Results

In the following text, gaps are named according to Figure 15, with the first gap referring to the gap between the board of the outermost layer. The second gap is located at the second layer and so on. For uniform drying the model is symmetric, hence why measurements are only needed for one side of the model as the values for the other side will be the same. In other words, three gaps will be studied for a model of five layers. The values are rounded to a value of three significant figures and presented in millimeters.

The largest displacement for a node in a gap is chosen. This value is subtracted by the value for the node at the linked end of the gap to account for the elongation of the element. The resulting value is doubled to get the true width of the gap.

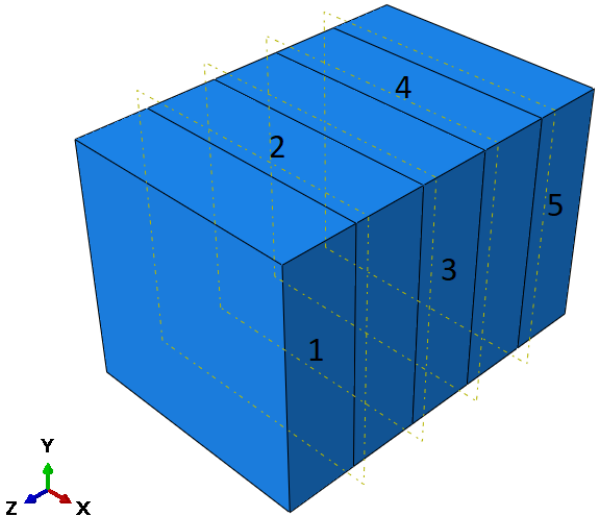

Figure 15. Numbering of the layers, with the first layer and gap located at one end and the rest numbered in order. The digits are written over its corresponding surface/edge.

Uniform drying

Gap widths are presented for each case and for each gap. Also, the ratio between gap width and the board width are presented, as well as the ratio between gap width and board thickness. Since the model is symmetric, only the gap width for three layers are presented for a five-layered element; Layer 4 and 5 equals 2 and 1. The ratio is presented with the unit of millimeters per meter. Note that the elements thickness is constant at 150 mm for every case except for when varying the board thickness.

Figure 16 shows what a deformed model looks like for uniform drying of the reference case.

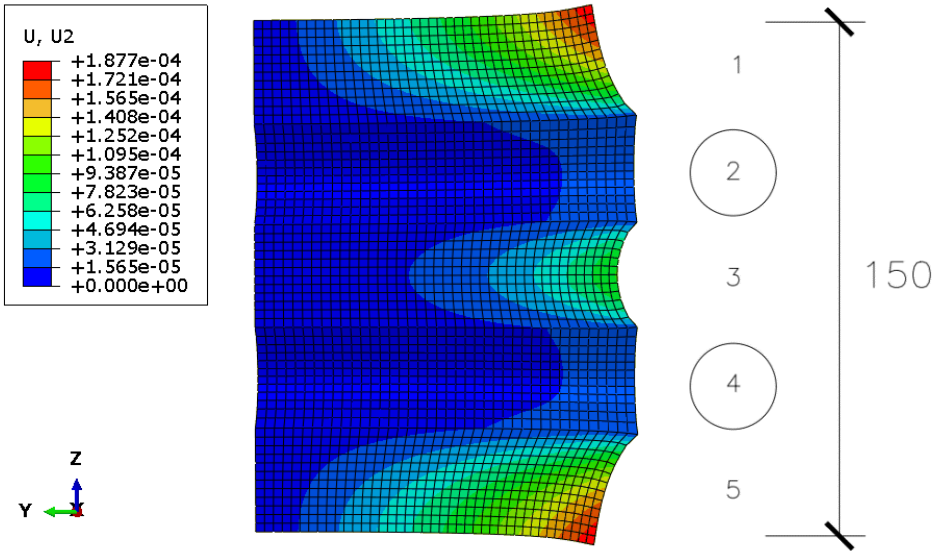

Figure 16. Showing how the element deforms after drying for layer 1, 3 and 5. Layer 2 and 4 are completely plane for the same surface but deforms similarly inwards. Note how the corners bends outwards. Figure of reference case.

Thickness

The study of varying thickness is the only one where the total thickness of the element varies, as every board within an element is given the same thickness.

Table 12. Showing the gap width for gap 1-3 for elements of different board thicknesses. Gap widths are given in millimeters.

Thickness			
[mm]	**Gap 1 Y [mm]**	**Gap 2 X [mm]**	**Gap 3 Y [mm]**
20	0.234	0.107	0.102
30	0.336	0.162	0.154
40	0.409	0.214	0.206
50	0.456	0.264	0.255
60	0.485	0.308	0.301

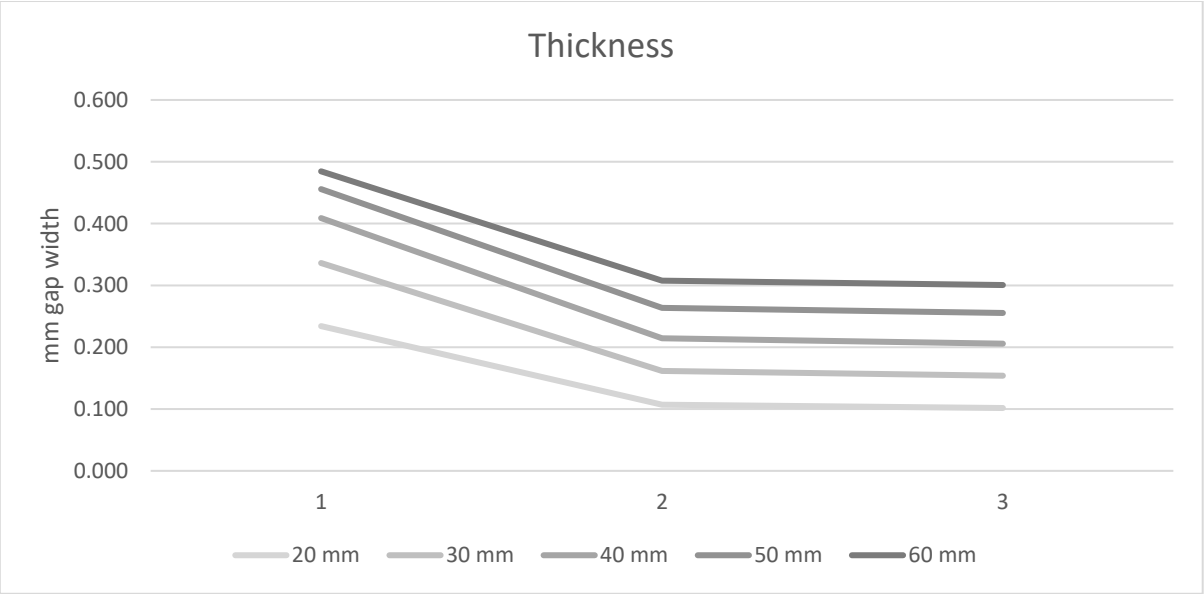

Figure 17. Gap widths for the arrangements given by variating the thickness.

Table 13. Showing the ratio between the gap width and the board width of 200 millimeters. The ratios are given in millimeters per meter.

Thickness (Gap width / board width)			
[mm]	**Gap 1 Y [mm/m]**	**Gap 2 X [mm/m]**	**Gap 3 Y [mm/m]**
20	1.17	0.535	0.508
30	1.68	0.808	0.770
40	2.04	1.07	1.03
50	2.28	1.32	1.28
60	2.42	1.54	1.50

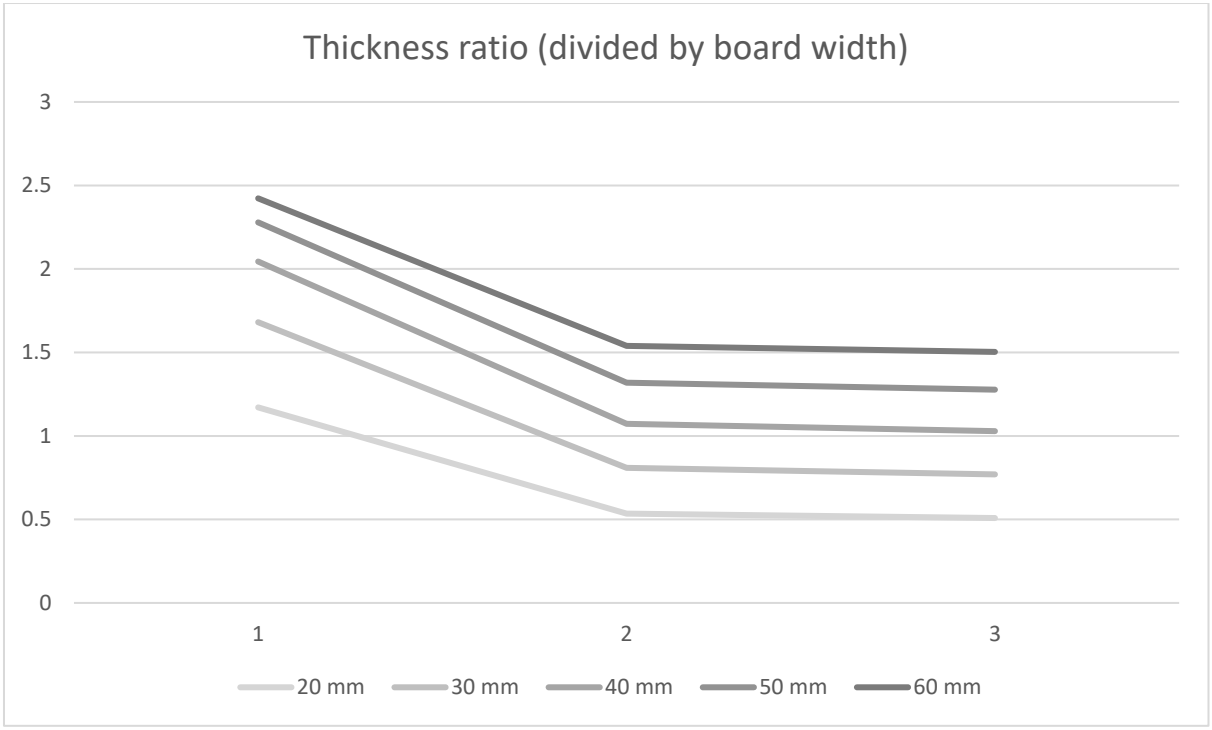

Figure 18. Ratio between gap width and board width for variating thickness.

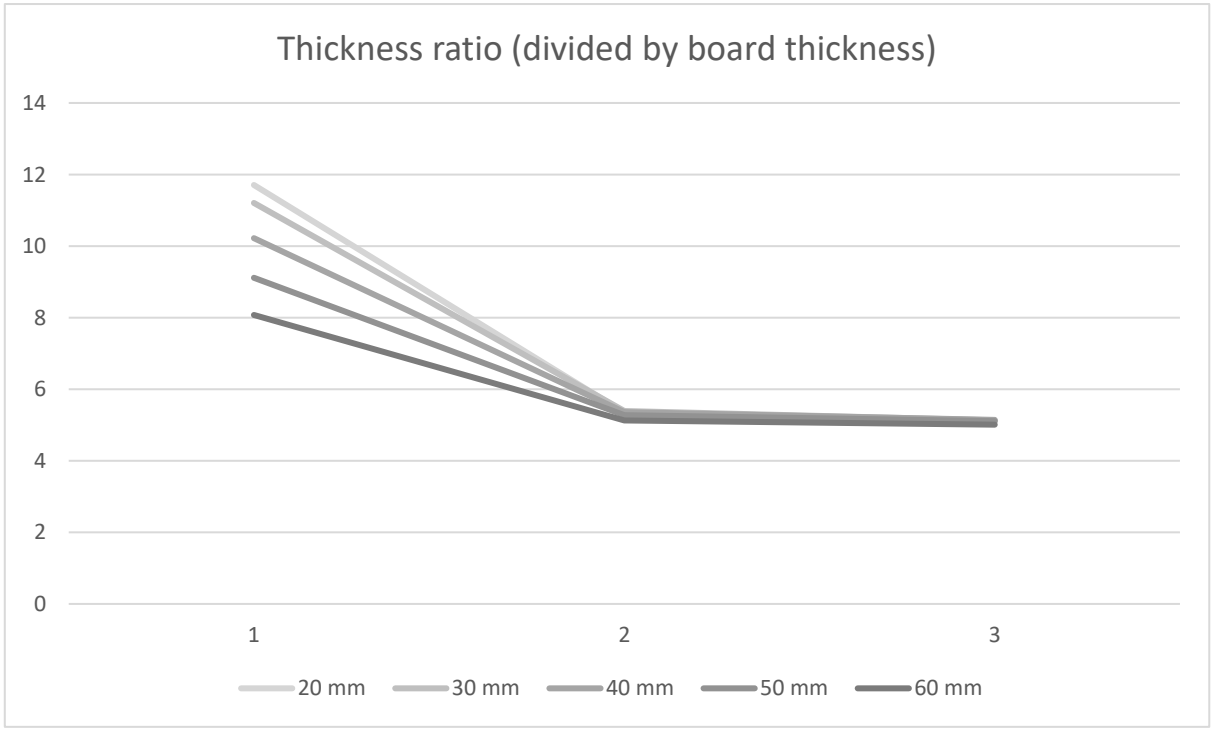

Figure 19. Ratio between gap width and board thickness for variating board thickness.

Table 14. Showing the gap width for gap 1-3 for elements of different board widths. Gap widths are given in millimeters.

Width			
[mm]	**Gap 1 Y [mm]**	**Gap 2 X [mm]**	**Gap 3 Y [mm]**
50	0.129	0.112	0.112
75	0.191	0.140	0.138
100	0.241	0.152	0.149
150	0.306	0.160	0.153
200	0.336	0.162	0.154
250	0.349	0.162	0.154
300	0.354	0.162	0.154

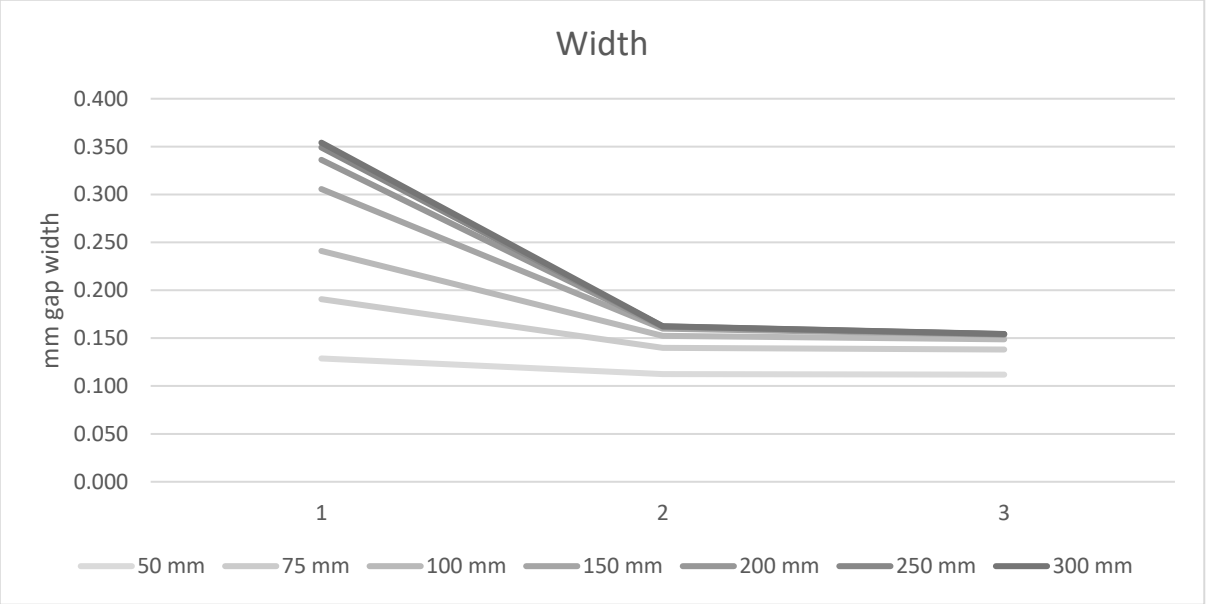

Figure 20. Gap widths for the arrangements given by variating the board width.

Table 15. Showing the ratio between the gap width and the board width. The ratios are given in millimeters per meter.

Width (Gap width / board width)			
[mm]	**Gap 1 Y [mm/m]**	**Gap 2 X [mm/m]**	**Gap 3 Y [mm/m]**
50	2.58	2.25	2.24
75	2.54	1.87	1.84
100	2.41	1.52	1.49
150	2.04	1.07	1.02
200	1.68	0.808	0.770
250	1.40	0.649	0.617
300	1.18	0.541	0.514

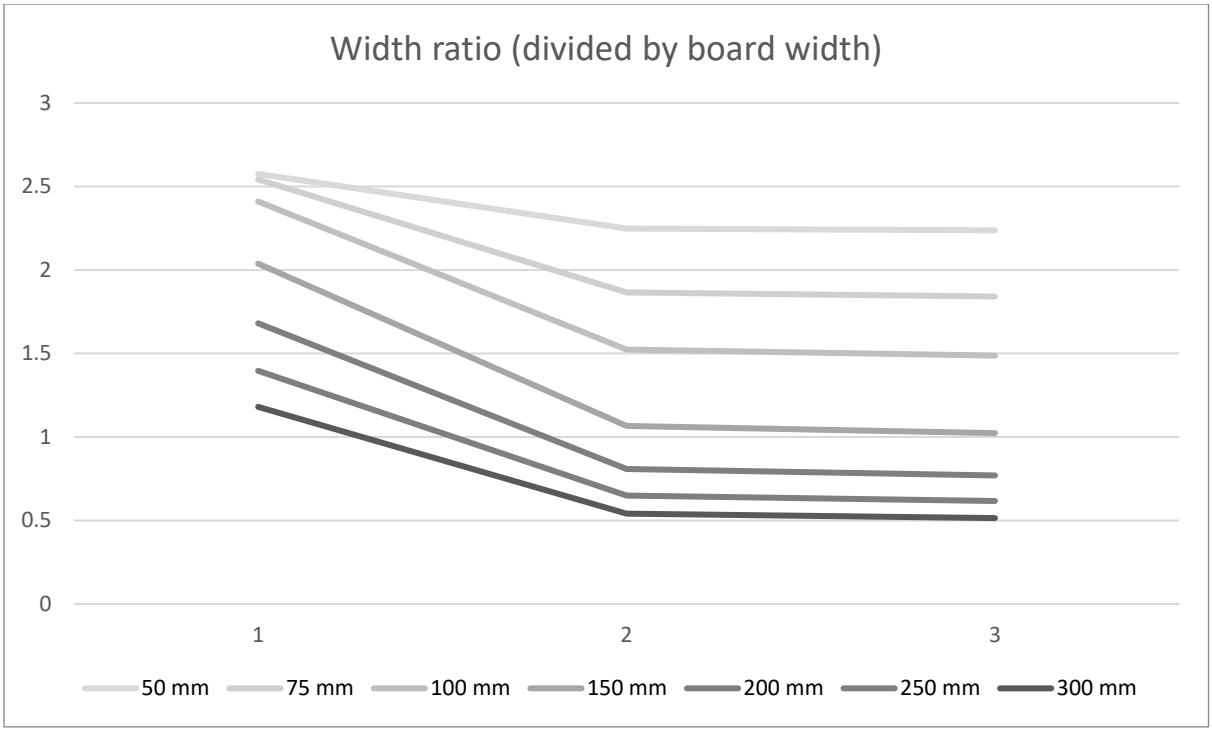

Figure 21. Ratio between gap width and board width for variating board width.

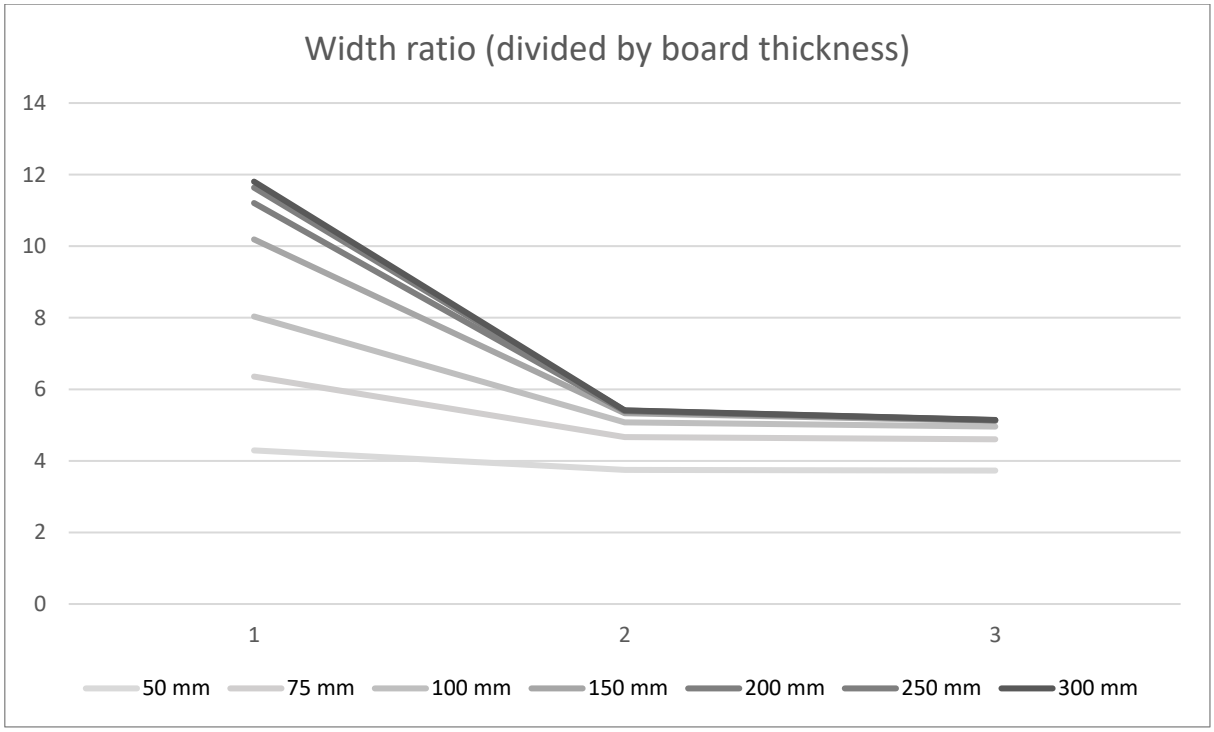

Figure 22. Ratio between gap width and board thickness for variating board width.

The relation between the different boards thicknesses are varied. For example, a factor of 1:2 gives layer 2 and 4 a thickness twice as large as the other layers. This means that every layer oriented in the same direction still has the same thickness.

Table 16. Showing the gap width for gap 1-3 for elements of different factor, meaning the relation between every second layer with the first value representing layer 2 and 4 while the other number is for layer 1, 3 and 5. Gap widths are given in millimeters.

Factor			
	Gap 1 Y [mm]	**Gap 2 X [mm]**	**Gap 3 Y [mm]**
1.5:1	0.292	0.198	0.130
1:1	0.366	0.162	0.154
1:1.5	0.368	0.126	0.175
1:2	0.384	0.105	0.187

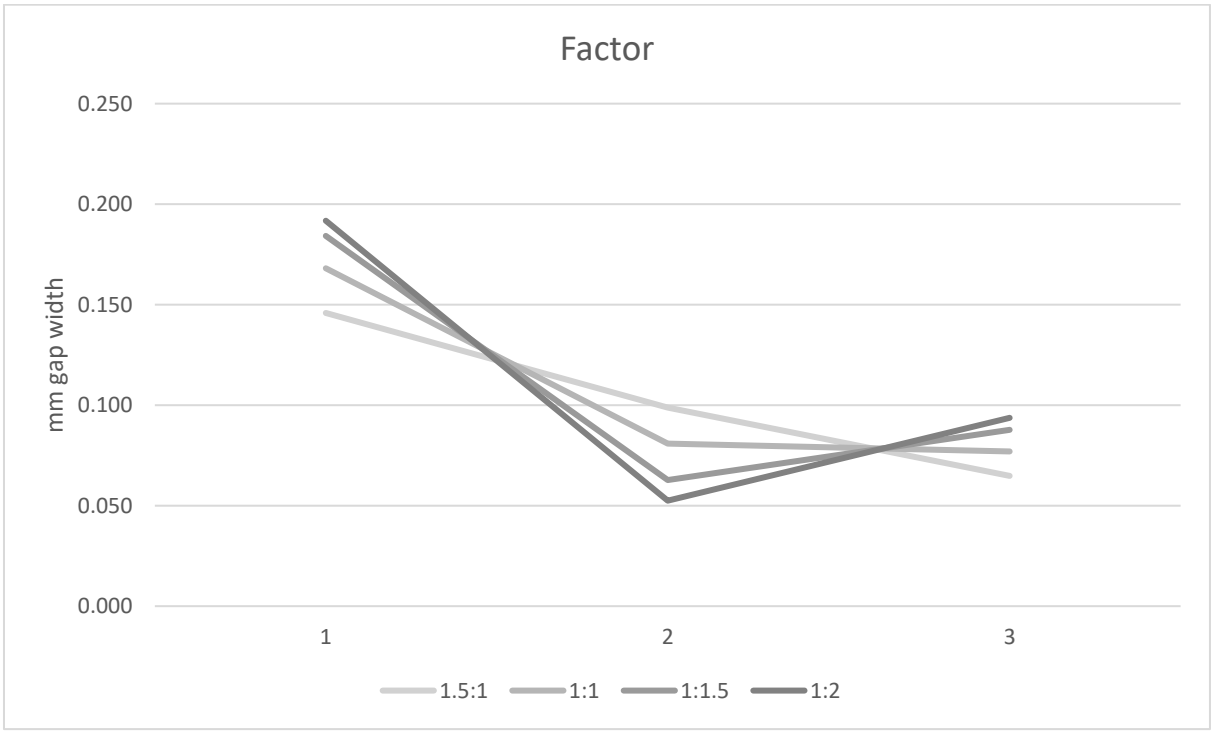

Figure 23. Gap widths for the arrangements given by variating the relation between board thickness.

Table 17. Showing the ratio between the gap width and the board width of 200 millimeters. The ratios are given in millimeters per meter.

Factor (Gap width / board width)			
	Gap 1 Y [mm/m]	**Gap 2 X [mm/m]**	**Gap 3 Y [mm/m]**
1.5:1	1.46	0.988	0.648
1:1	1.68	0.808	0.770
1:1.5	1.84	0.628	0.877
1:2	1.92	0.525	0.937

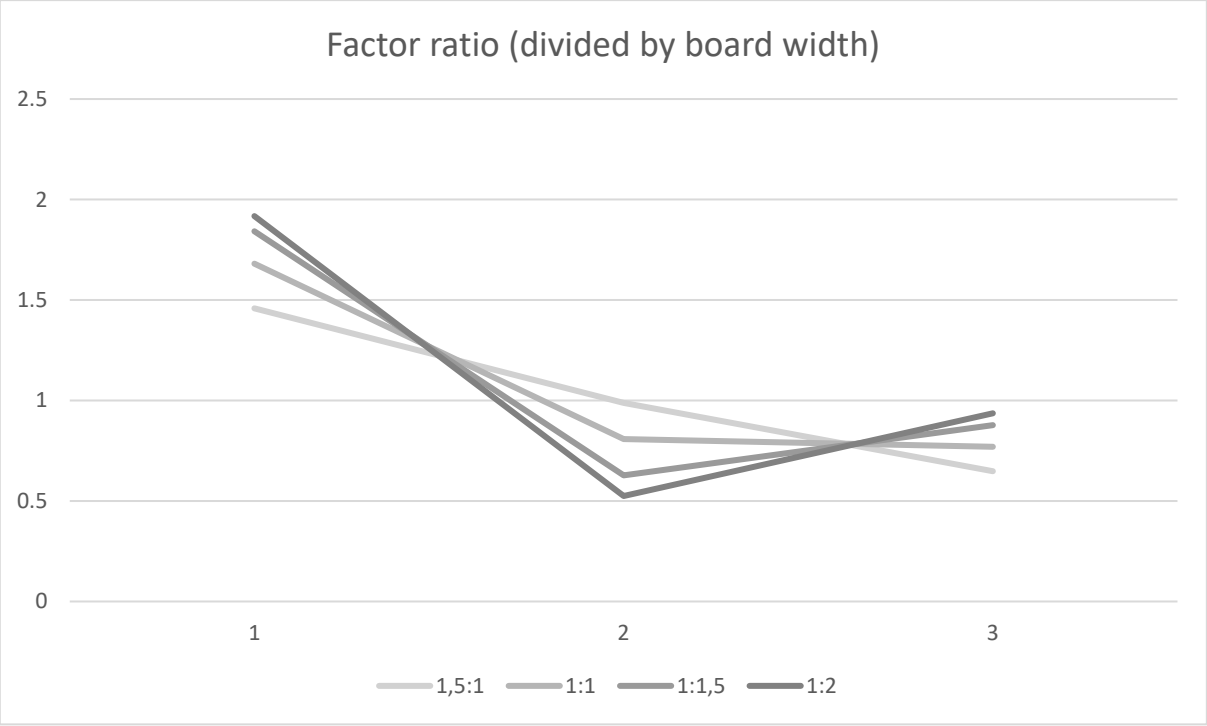

Figure 24. Ratio between gap width and board width for variating factor.

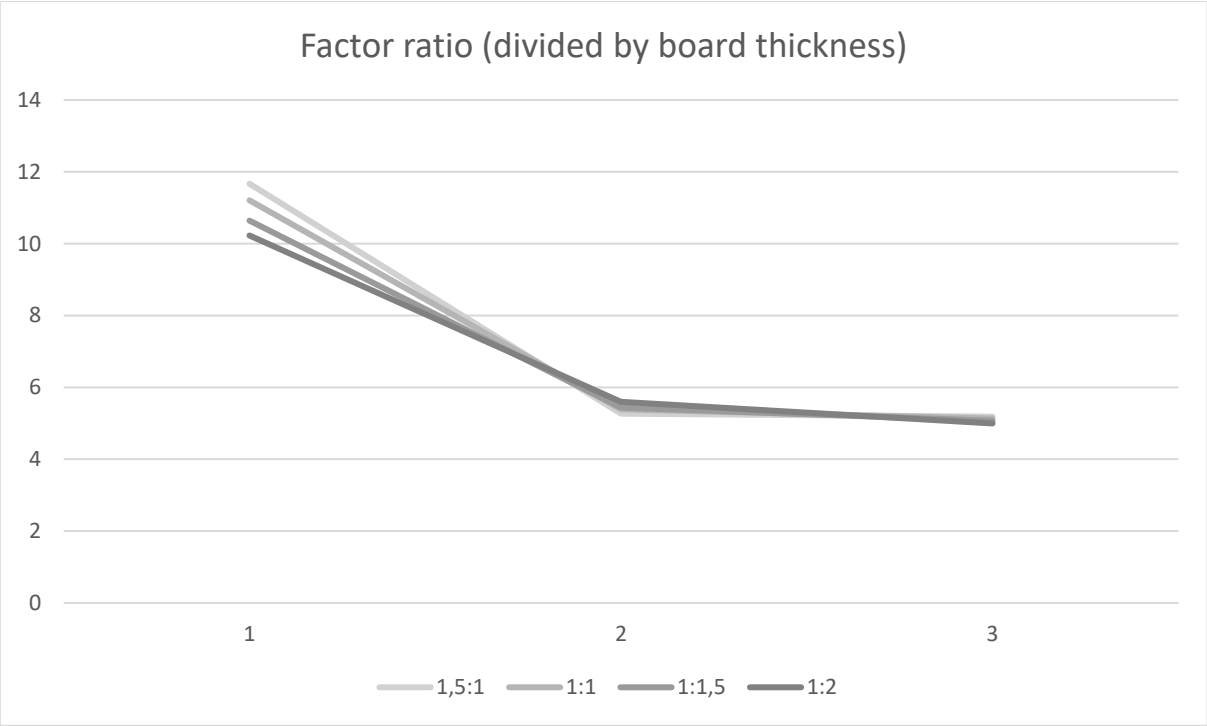

Figure 25. Ratio between gap width and board thickness for variating factor.

Number of layers

Three elements are studied with different number of layers: 3, 5 and 7 layers. All cases have the same total thickness of 150 mm for the entire element. Since the model is symmetric, only 2, 3 and 4 layers are presented for the three cases.

Table 18. Showing the gap widths for elements of different number of layers of boards. Gap widths are given in millimeters.

Number of layers				
Nr	**Gap 1 Y [mm]**	**Gap 2 X [mm]**	**Gap 3 Y [mm]**	**Gap 4 X [mm]**
3	0.451	0.269		
5	0.336	0.162	0.154	
7	0.254	0.114	0.108	0.110

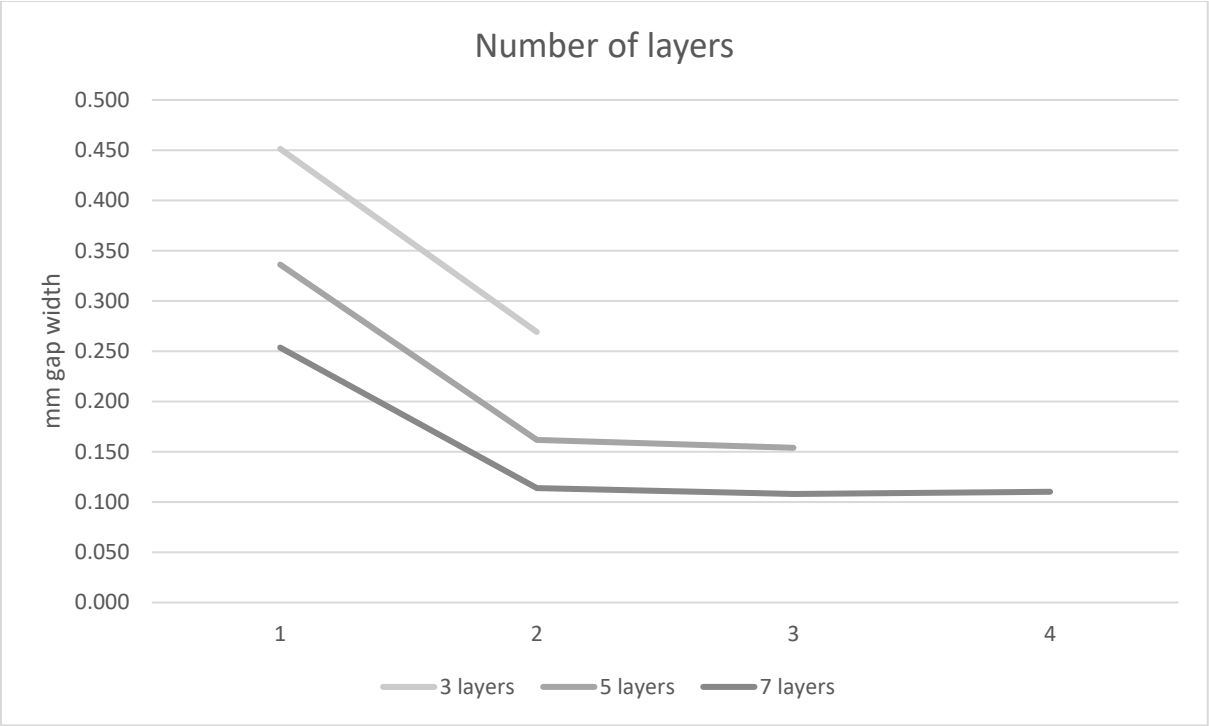

Figure 26. Gap widths for the arrangements given by variating the number of layers.

Table 19. Showing the ratio between the gap width and the board width of 200 millimeters. The ratios are given in millimeters per meter.

Number of layers (Gap width / board width)				
Nr	**Gap 1 Y [mm/m]**	**Gap 2 X [mm/m]**	**Gap 3 Y [mm/m]**	**Gap 4 X [mm/m]**
3	2.26	1.35		
5	1.68	0.808	0.770	
7	1.27	0.569	0.540	0.551

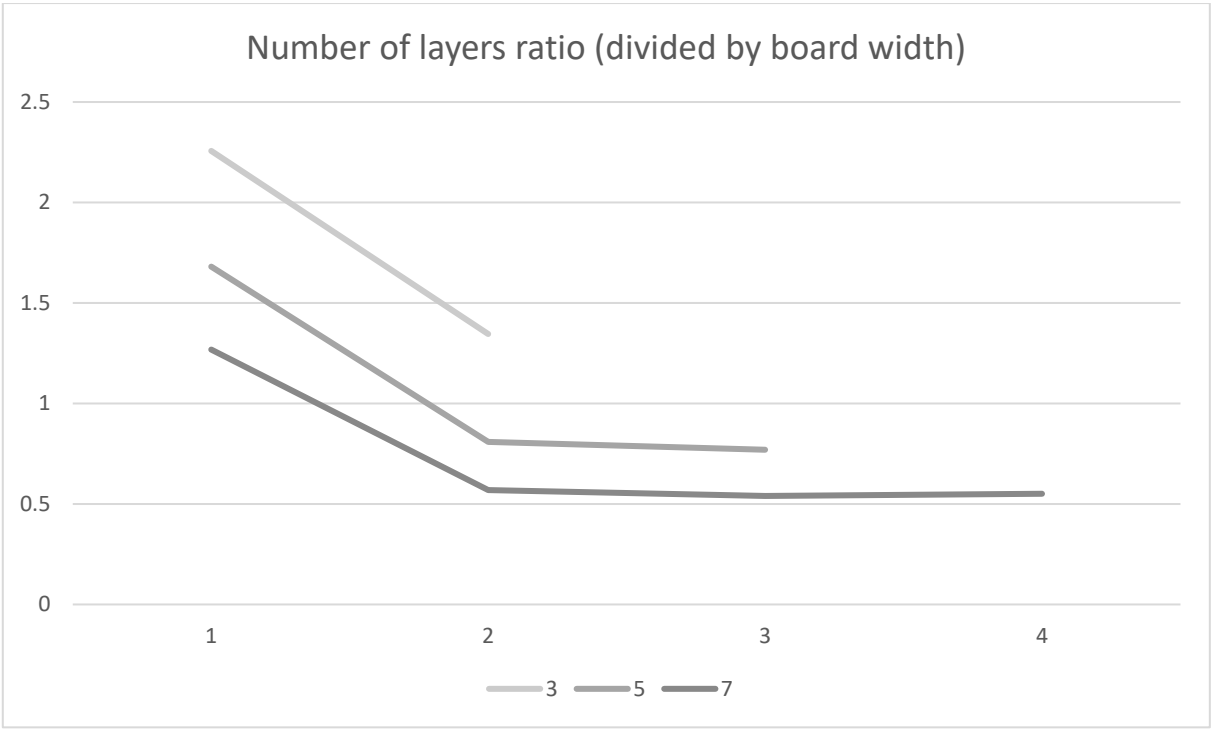

Figure 27. Ratio between gap width and board width for variating number of layers.

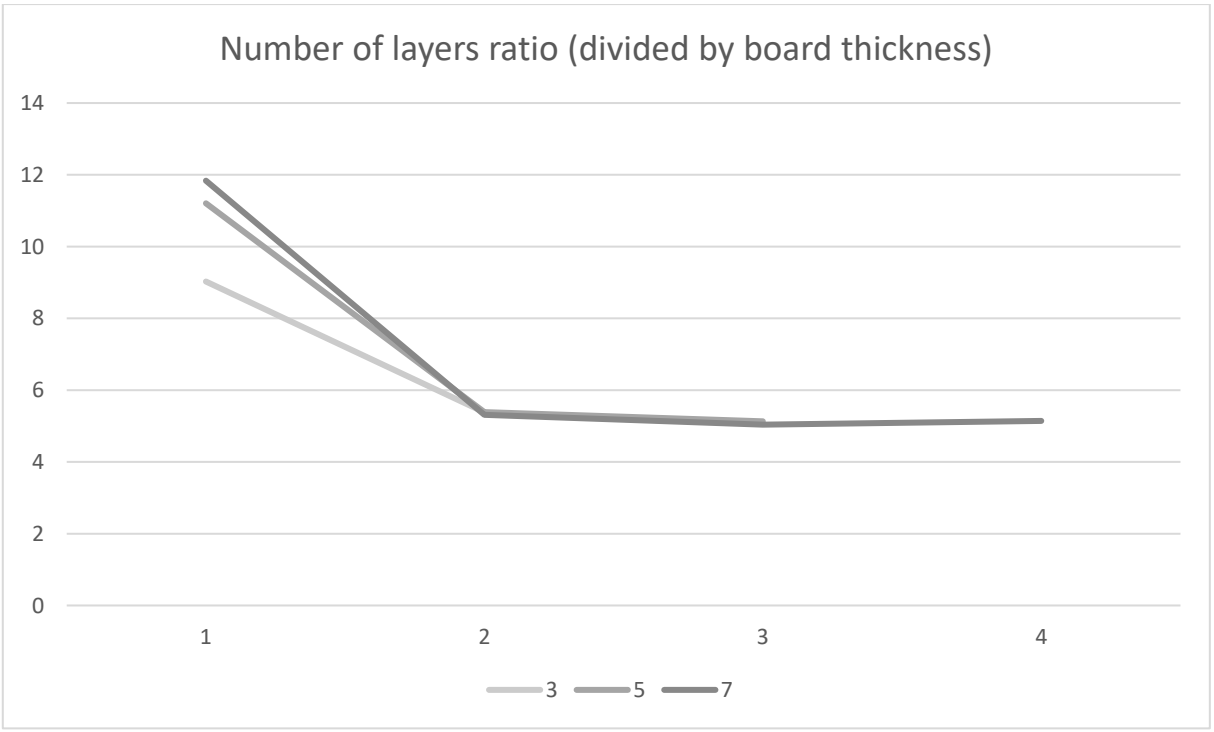

Figure 28. Ratio between gap width and board thickness for variating number of layers.

Elongation

The change in length measured for the reference case is presented in Table 20. The elongation in both x- and y-direction are presented as the elements cross-section differs for the two directions. The x-direction is the direction of the orientation of the boards in the outer layer, making a total of three layers of boards oriented in its direction.

Table 20. Elongation of element, reference case. Values in meters.

X (three layers)	1.630e-5
Y (two layers)	1.995e-5

The elongation according to the one-dimensional calculation gave an elongation of 2e-5.

Non-uniform drying

A model has been set up for the non-uniform load case. The non-uniform loading case will cause the slab to bend. The side which is drying will be the inside of the curvature, which means that this side will be shorter and thereby partly close the gap. One can therefore expect the gaps for the non-uniform load case to always be smaller than for uniform drying, if same dimensions and change in moisture content holds. Therefore, only the reference case has been studied.

The gap width given by uniform and non-uniform loading are compared in Table 21 and Figure 29. The gap widths in the figure for layer 4 and 5 are assumed to be precisely the same as for layer 2 and 1, for uniform drying.

Table 21. Comparison of gap widths for uniform and non-uniform drying.

Reference case					
[mm]	**Gap 1 Y**	**Gap 2 X**	**Gap 3 Y**	**Gap 4 X**	**Gap 5 Y**
Uniform drying	0.336	0.162	0.154	0.162	0.336
Non-uniform drying	0.225	0.139	0.080	0.061	0.014
Non-uniform drying	0.450	0.278	0.159	0.123	0.027

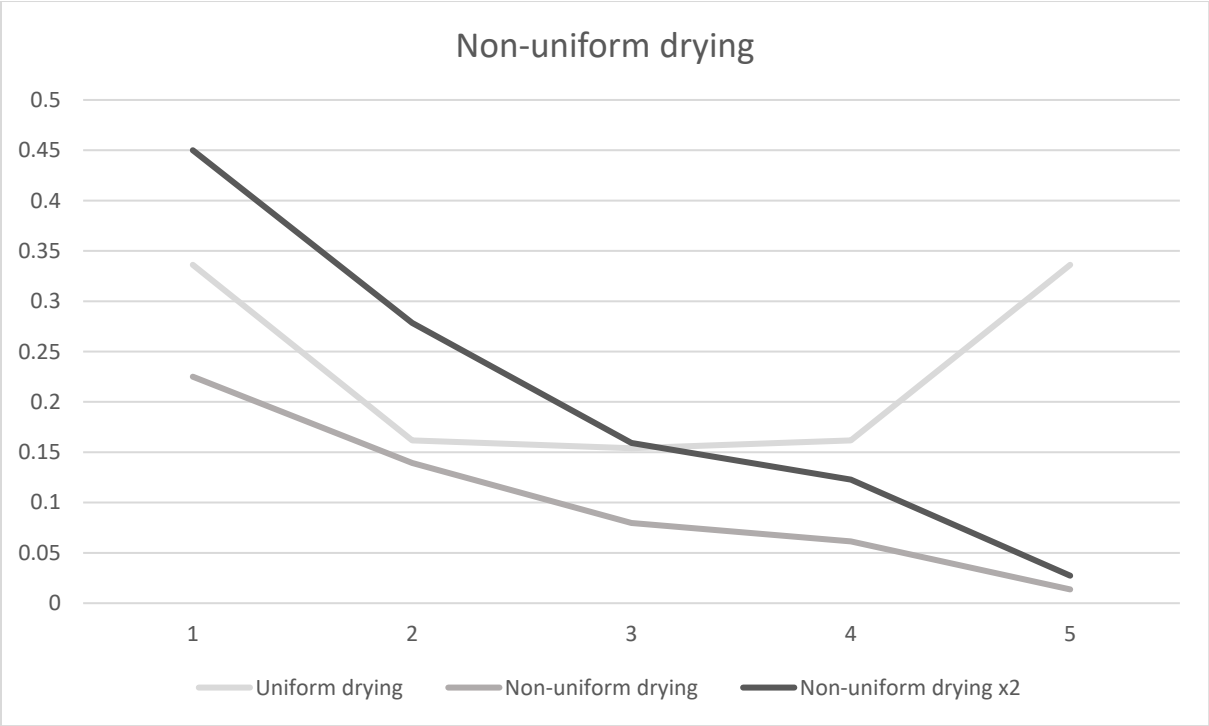

Figure 29. Comparison of gap widths for uniform and non-uniform drying.

For a non-uniform drying of one percent MC change at one end, the gap widths are always smaller than that of uniform drying. The gap width at the middle is also half the size. For a MC change with a mean value of one percent for the entire structure, i.e. two percent difference between both ends, the mid-gap is roughly the same, and the outer gap at the drying end is 34 percent larger than for uniform drying. As the expansion is assumed to vary linearly with moisture content, a two percent difference gives a result that is twice that of one percent MC change.

Bending

A model has been set up to use for studying the bending, which differs from the model calculating the gap widths for the non-uniform moisture distribution. The value for displacement are obtained from nodes along the neutral axis. The results are as follows, Table 22.

Table 22. Displacement at both ends. Values in meters.

Node at distance $y = 0.2$	$1.47583 \cdot 10^{-4}$
Node at distance $y = 0.0$	$1.11726 \cdot 10^{-4}$

The deformation caused by bending was given as the difference between the two nodal values.

$$\frac{1.47583 \cdot 10^{-4} - 1.11726 \cdot 10^{-4}}{0.2} = 17.929 \cdot 10^{-5} \frac{m}{m \cdot \%_{MC}} = 0.18 \frac{mm}{m \cdot \%_{MC}}$$

For this configuration, the slab will deform with 0.18 millimeter per meter and percentage-change in moisture content. That is considerably lower than the limit of 6.67 mm. As the deformation is small compared to the length, the displacement in length-direction caused by the bending can be neglected.

2D Composite

Relative humidity

Two set-ups are compared, one for each orientation of the boards, A and B. The results focus on the drying of concrete w/c 0.6. A comparison with the drying of w/c 0.38 follows.

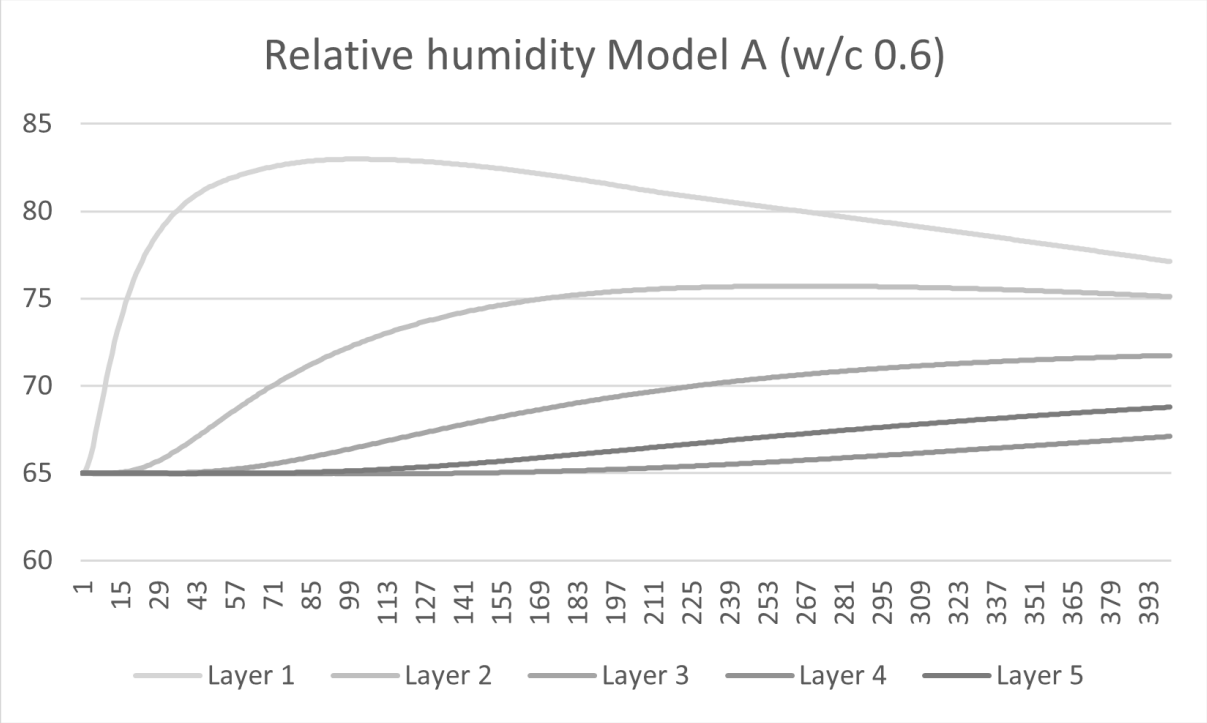

Figure 30. Relative humidity of layers as function of time for model A.

Figure 30 shows the relative humidity for the midpoint of the five layers as a function of time for model A. The humidity for the midpoint of the upper layer sees a distinct spike in the values, reaching 83 percent after 100 days. 76 percent is reached after 265 days for layer 2. No other layers sees a peak even after a year. Although the humidity had started to decrease for the second layer, it had not reached below 75 percent after 400 days. At that time, the concrete had

a relative humidity of 77 percent, in itself being very close to 75 percent. For layer 3, 4 and 5, relative humidity of 66 percent is reached as late as 87, 177 and 292 days.

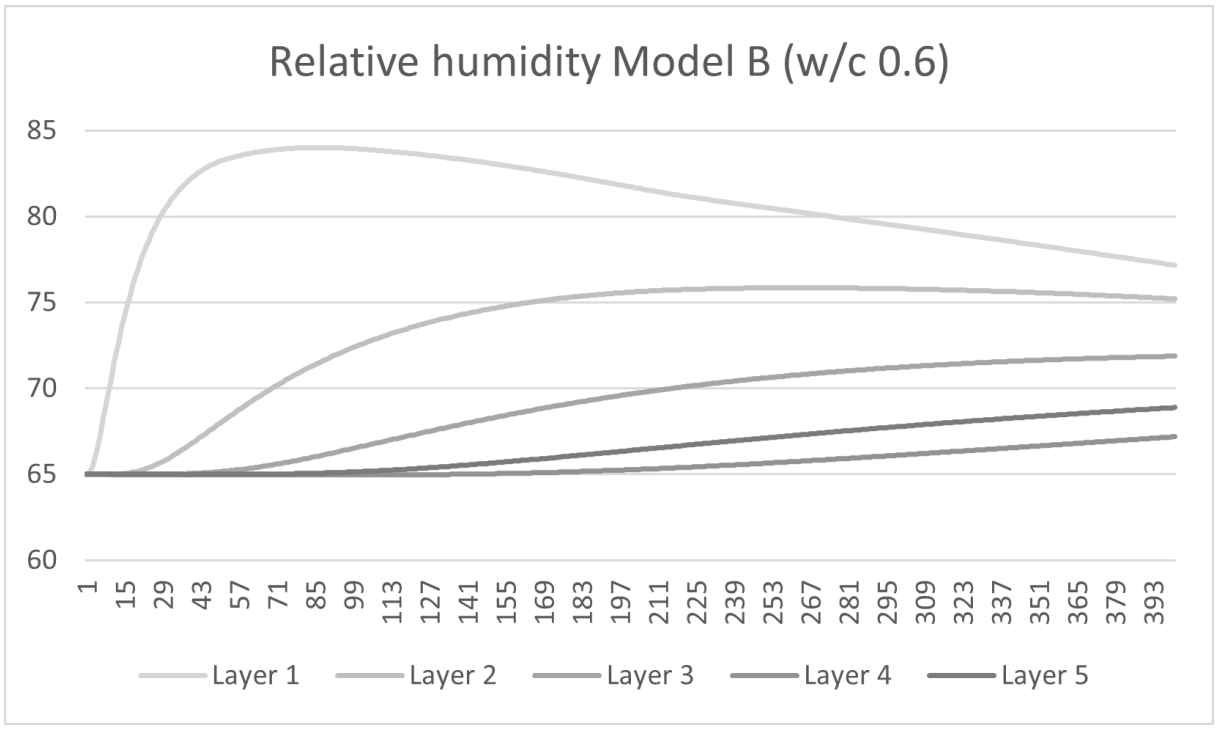

Figure 31. Relative humidity of layers as function of time for model B.

Figure 31 shows the relative humidity for the midpoint of the five layers as a function of time for model B. The humidity for the midpoint of the upper layer sees a distinct spice in the values, reaching 84 percent after 85 days. Layer 2 reaches a value of 76 percent, as for previous model, after 262 days. No other layers sees a peak even after a year. Although the humidity had started to decrease for the second layer, it had not reached below 75 percent after 400 days. At that time, the concrete has a relative humidity of 77 percent, in itself being very close to 75 percent. For layer 3, 4 and 5, relative humidity of 66 percent is reached as late as 84, 174 and 287 days.

The critical relative humidity of 75 percent was reached for the first layer of both model A and B. The second layer had a RH slightly above. The three other layers did not reach the critical value.

Two lowest layers does show values going below 65 percent, but barely. For both models. Likely that the film coefficient then had an impact.

Model B has 15 days earlier peak for layer 1 in relative humidity as compared to model A. Likely because of the higher diffusion coefficient, carrying moisture from the notch. The humidity for the node for the top layer gets a value slightly larger than for model A.

The exact max values for the top layer is presented in Table 23. The table shows a noticeable difference between the models.

Table 23. Maximal RH in the middle of top layer.

Top layer	RH [%]	Time [days]
Model A	82.99	101
Model B	84.01	85

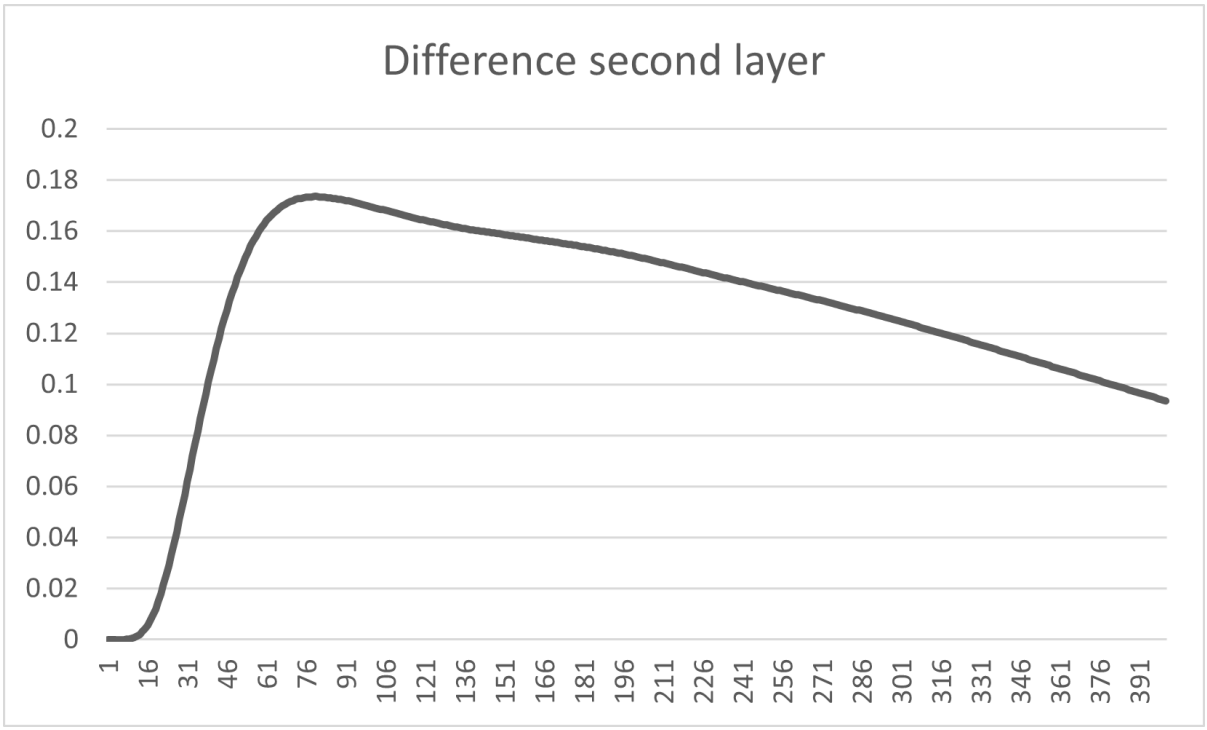

Figure 32. Difference between the RH for node at second layer for models A and B (one subtracted by the other).

The difference between both models for second layer is barely notable. One can however see a larger flow for model B in the second layer as more moisture is transferred from the notch to the rest of the layer.

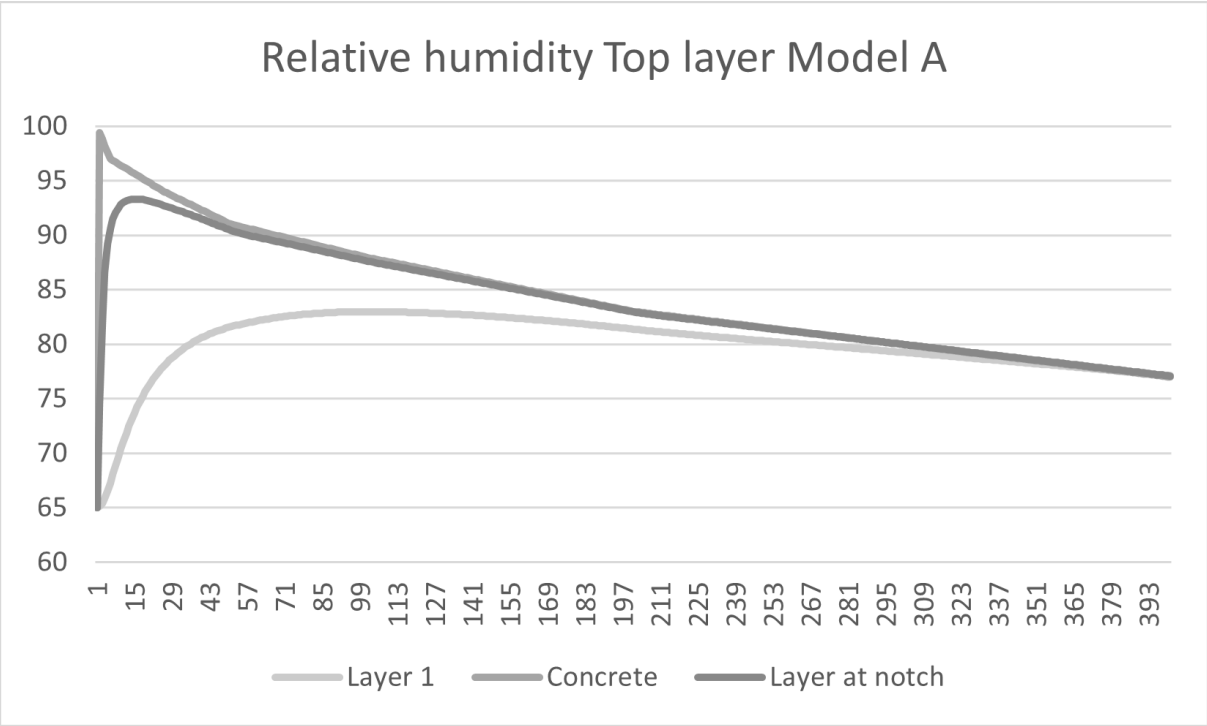

Figure 33. RH for concrete, node near concrete and node for first layer. Model A.

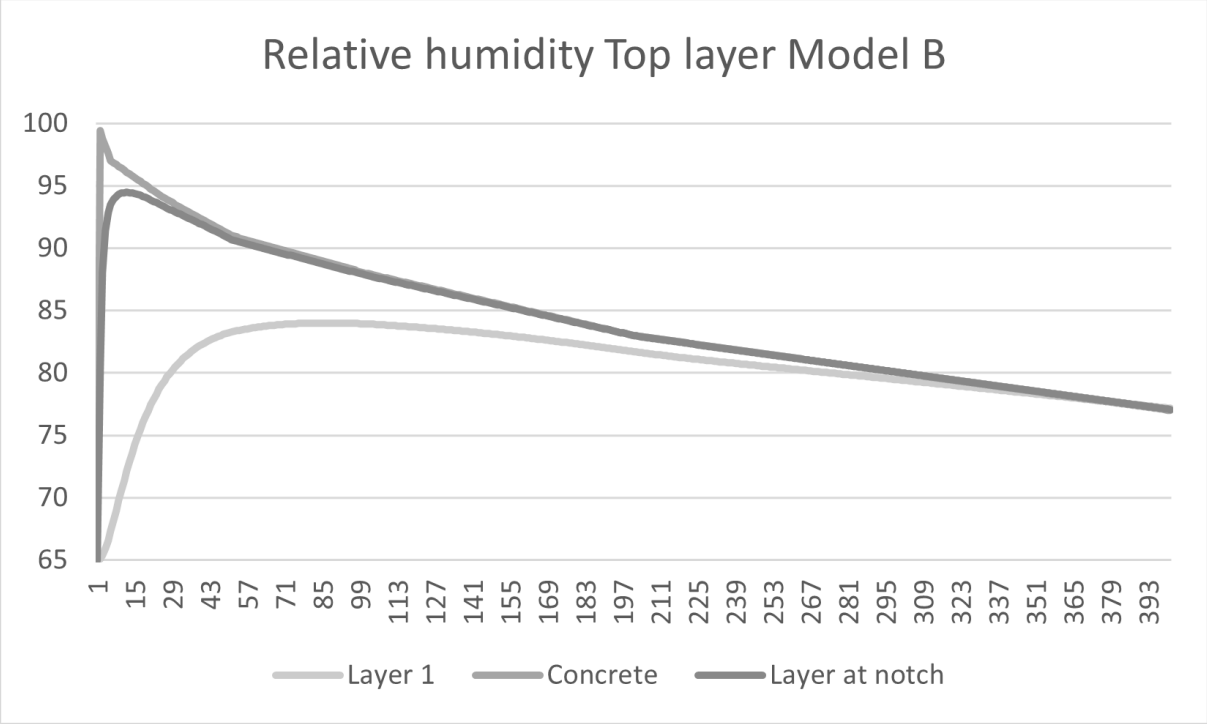

Figure 34. RH for concrete, node near concrete and node for first layer. Model B.

Top layer is seen to follow the humidity of the concrete layer after more than 300 days. The other node is located just 5 millimeters outwards from the inner corner. Here, the timber gets a humidity of almost 94.5 percent after just 10 days for model B and 93.3 after 15 days for model A, see Figure 33 and Figure 34. Then the graph follows the value for the concrete itself. The humidity of the inner node can after a certain time be seen having a relative humidity higher than that of the concrete, although its less than 0.1 percent.

The relative humidity right at the surface to the lower left-most position in the model is plotted in Figure 35. The RH reaches its lowest value after 107 days of a value of 64.9 percent. The decrease in relative humidity depends on the difference in RH between the node and the room, leading to the moisture flow decreasing with time, until the moisture from the concrete reaches the surface. Even though the relative humidity gets larger after 400 days, the value is relatively small. The RH for model B barely differs, having a value of just 0.07 percent larger after 400 days.

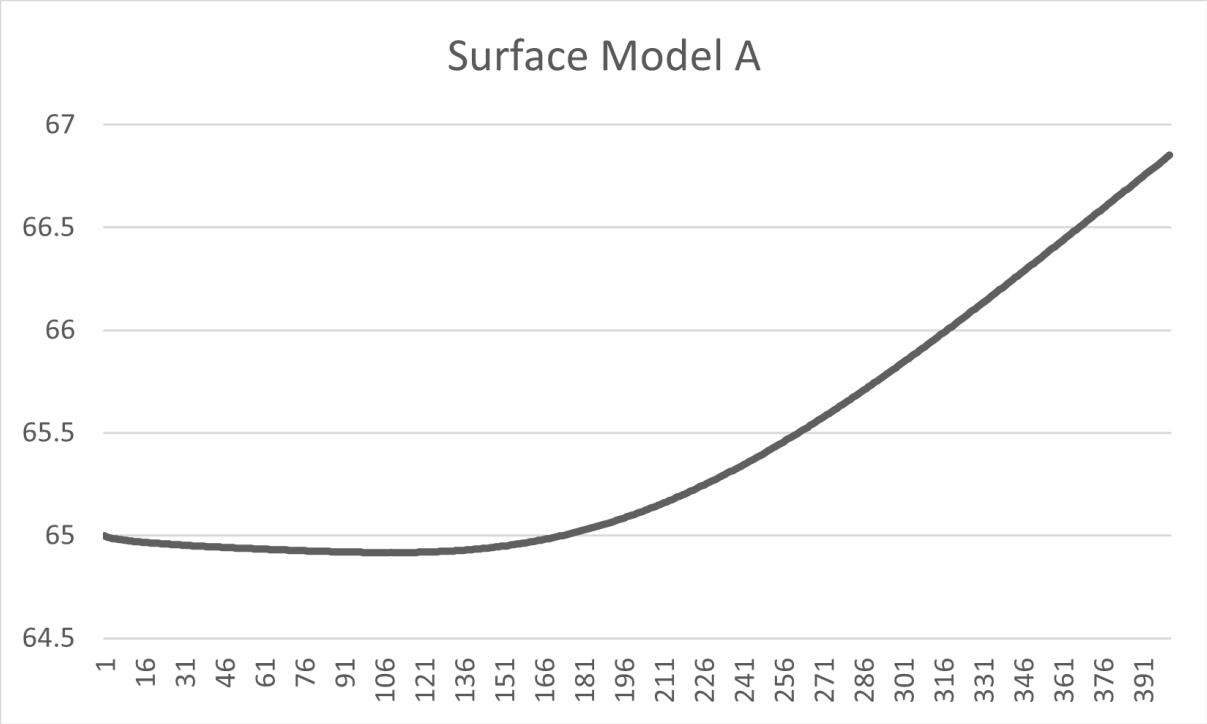

Figure 35. Model A. Relative humidity at surface.

The study by Autengruber, M. Lukacevic, M. and Füssl, J. (2020) shows a similar behavior. The lower half of the CLT element never reaches a MC above 15 percent, or RH of 80 percent. After some time, the drying of the entire element follows the same value with a slow decrease of the MC over a time period of multiple months. In the close vicinity of the concrete, the MC reaches above the FSP. They point out how Eurocode only account for a mean MC value for the climate class and not the variation within the element, like the one seen in the drying of the TCC element.

Figure 36 shows the relative humidity for each layer as function of time for water/cement ratio of 0.38. As the w/c 0.38 concrete goes towards a RH of 73 percent after 400 days, the w/c 0.6 is still above 75 percent for layer 1 and 2. This follows the RH of the concrete and the preset values for both types of concrete. The first layer of concrete with w/c 0.38 never shows a value above 80 percent, far below the w/c 0.6 RH of 83 percent.

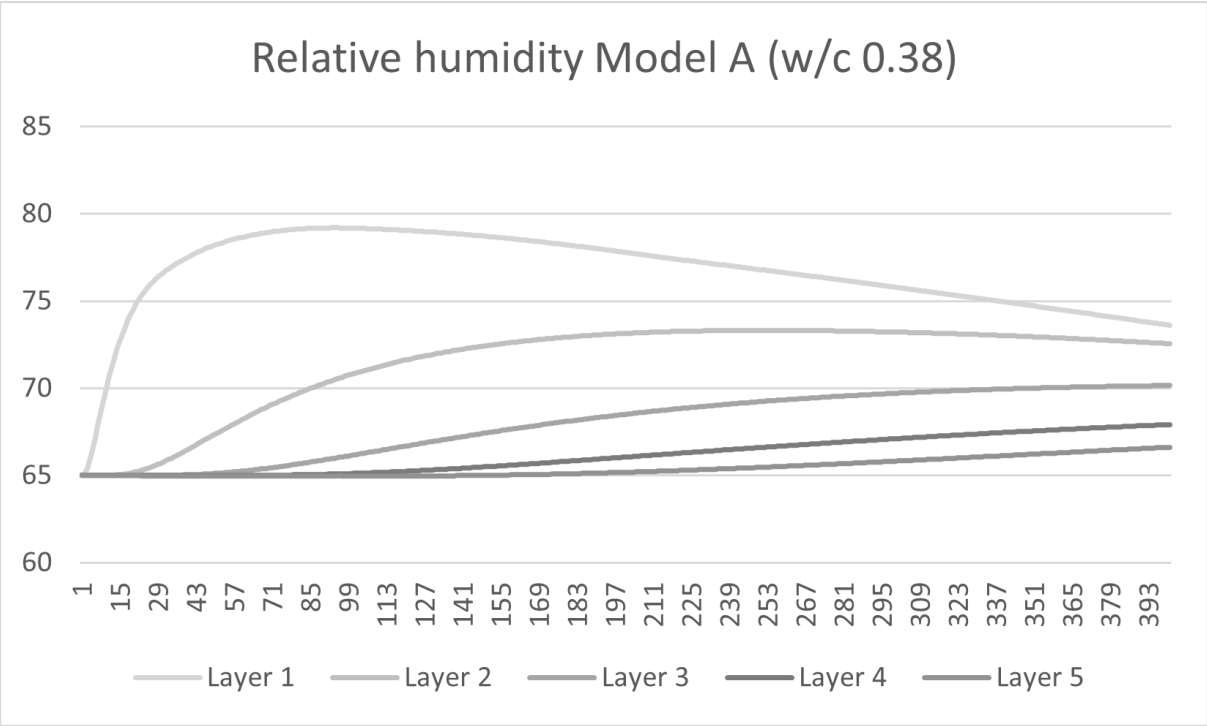

Figure 36. Relative humidity of layers as function of time for model A. Shows w/c 0.38.

Displacement

Displacement will be measured for the two lower corners of the TCC structure in y-direction, Y1 and Y2, and for the two right corners, X1 and X2, in x-direction, see Figure 13. The displacement along the right side is constrained to a linear distribution. The lower values are not, but the highest and lowest displacement values are expected to occur at the chosen nodes.

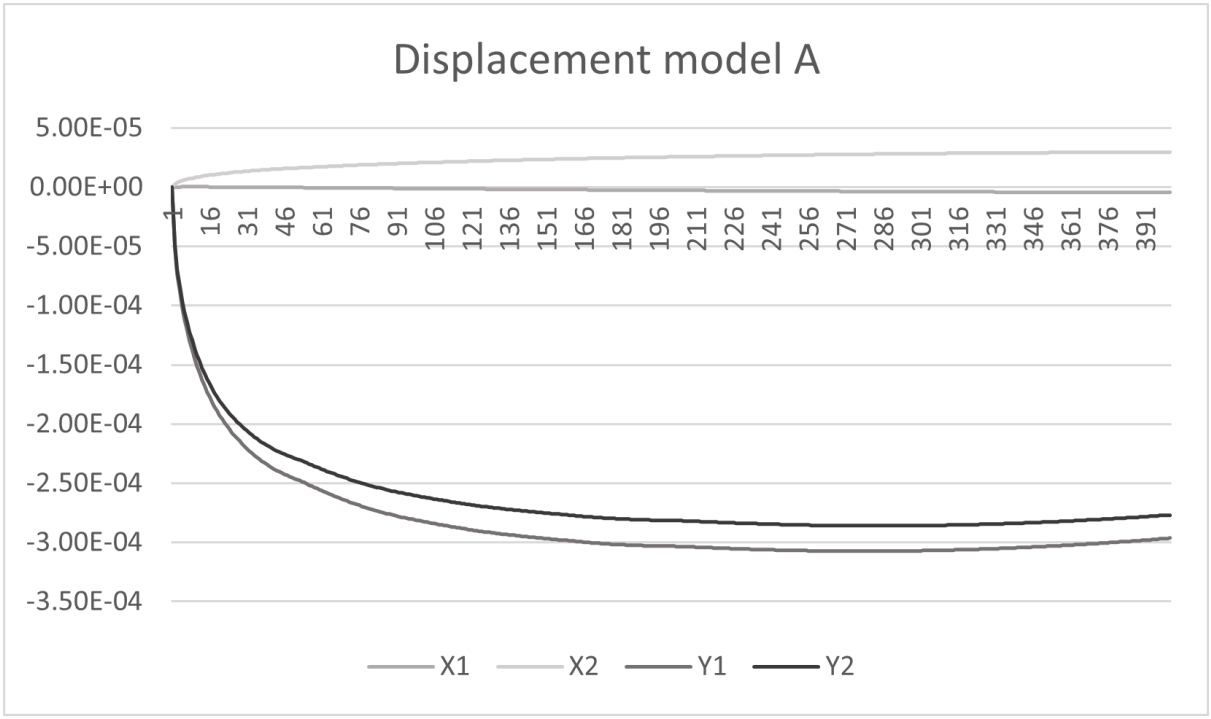

Figure 37. Displacement for model A.

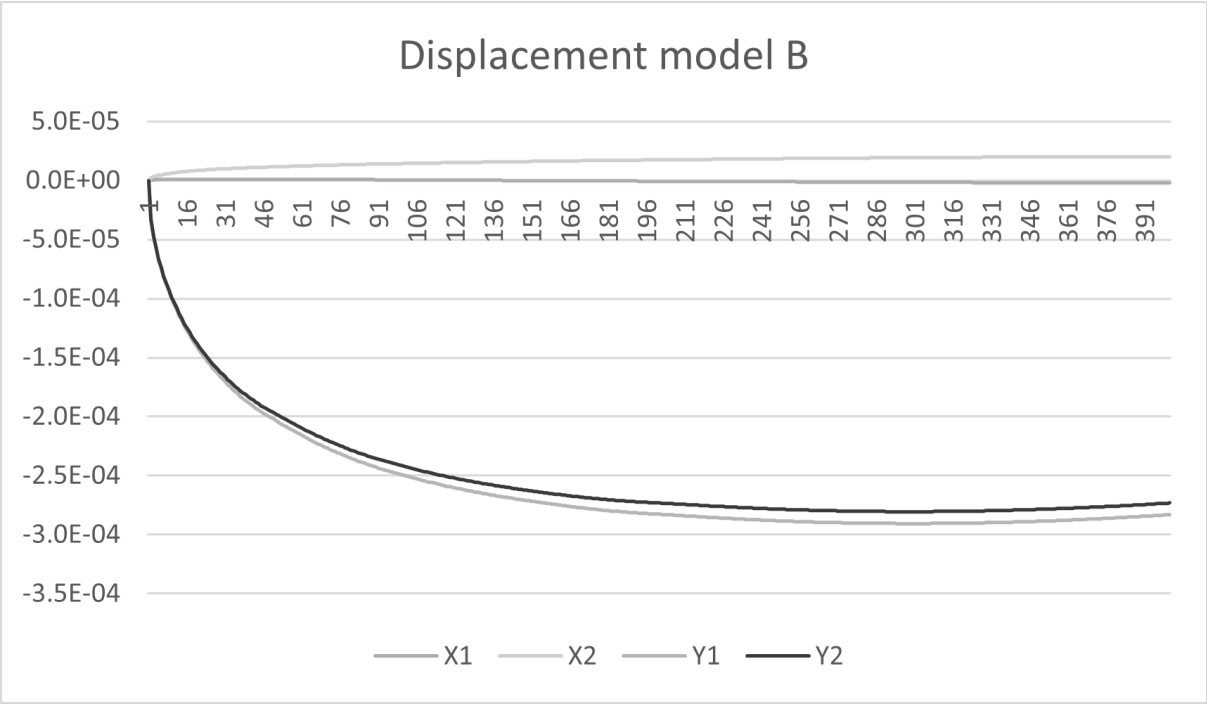

Figure 38. Displacement for model B.

The largest displacements and at what time it is reached is presented in Table 24. The nodes were presented in Figure 13.

Table 24. Largest values of displacements

		Time [days]	**Displacement [m]**
Model A	X1	9	3.17e-7
	X1	400	-4.59e-6
	X2	400	2.96e-5
	Y1	262	-3.07e-4
	Y2	246	-2.86e-4
Model B	X1	24	1.30e-6
	X1	400	-2.25e-6
	X2	400	2.03e-5
	Y1	299	-2.91e-4
	Y2	298	-2.81e-4

For both model A and B, one can see a peak for X1 after 9 and 24 days. Also, the elongation along the slabs thickness is at its peak after about 250 days, after which it starts to shrink again.

The elements total thickness increases and reaches a maximal increase of 0.3 mm after less than 300 days.

Bending

With the values for displacement in x-direction, the bending can be calculated. It is calculated as the difference in x-displacement divided by the structures height. It is presented as displacement in lateral direction per meter to be comparable to the bending of the 3D model.

Table 25. Bending of the TCC floor.

Model	Quota	Bending
Model A	1.37e-4 m/0.1m	1.37 mm/m
Model B	9.03e-5 m/0.1m	0.90 mm/m

The maximal bending for model A and B corresponds to 5-10 percent change in moisture content for the three-dimensional model, suggesting the TCC structure as stiffer.

Stresses

To know at what time steps the stresses might be expected to have a large value, the total internal strain energy for the model is looked at, see Figure 39 and Figure 40.

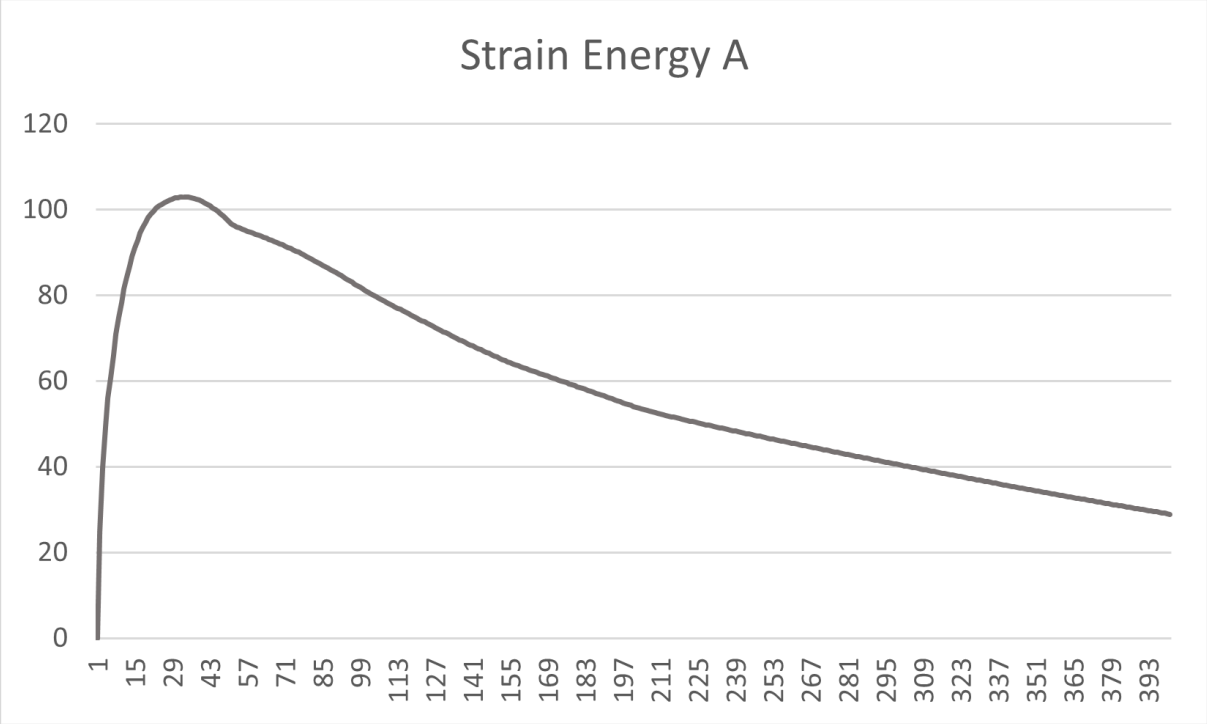

Figure 39. Total strain energy as function of time for model A.

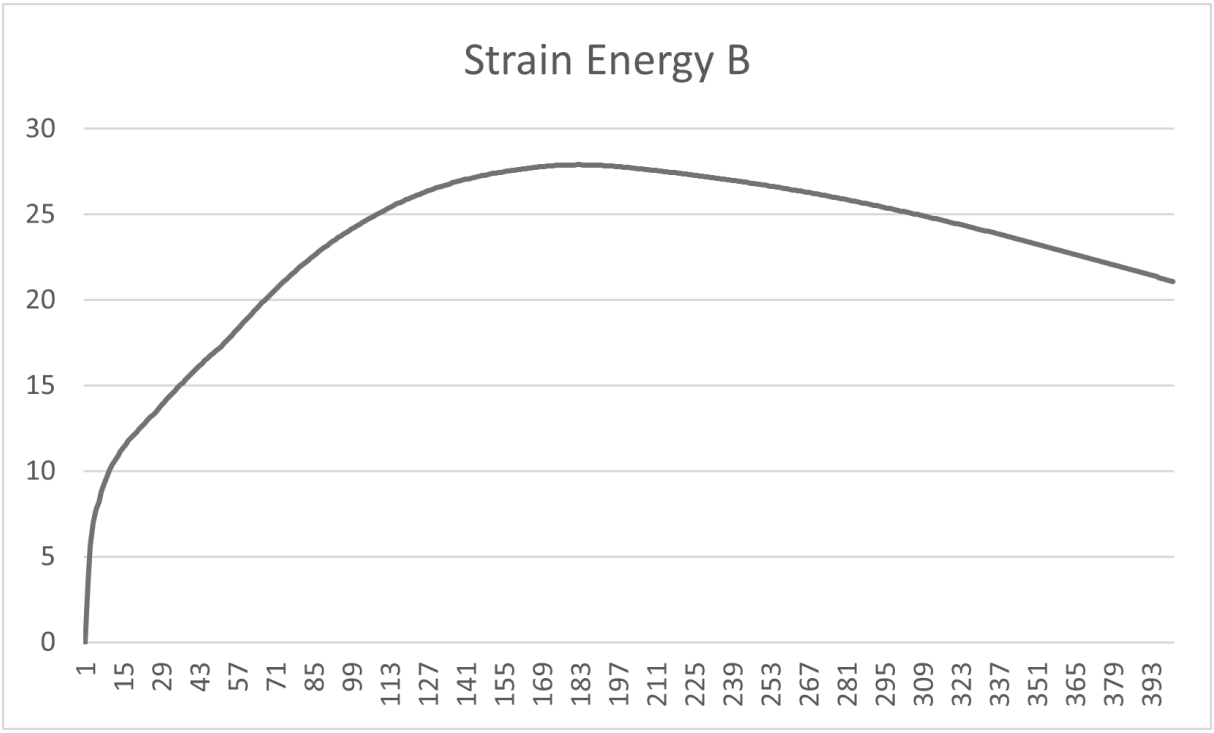

Figure 40. Total strain energy as function of time for model B.

A maximal strain energy for model A and B is achieved after 32 and 182 days, respectively. This is the time steps where the stresses will be studied for each model.

The stresses are overall seen as larger for the layers directed at 90 degrees as compared to the notches, being the second layer for model A and first layer for model B.

The stresses often most critical are the rolling shear stresses. The models are two-dimensional. The stresses of interest are therefore the shear stresses S_{12} in the layers having their fibre direction inwards in the model, parallel to the notches.

For model A, the largest shear stress S_{12} was for the first layer at its boundary to the notch at 2.14 MPa. At the first layers boundary towards the second layer, a rolling shear stress of -0.40 MPa was obtained. The model showed larger values for nodes around the notch and below it, while the nodes further out had a lower value and sometimes negative values.

For model B, the largest value is for the second layer at the interface to the first layer. The stress has a value of 140.2 kPa.

After reading the values, it was suspected that the largest values had not been acquired. By presuming that the correct node had been picked, the largest shear stress for that specific node was obtained. For model A, that value peaked at -475.8 kPa after just 16 days at the boundary to the next layer. For model B, a value of 264.1 kPa was reached after just 50 days.

Table 26. Max rolling shear at time step corresponding to maximum strain energy and time step for maximum stress at that node.

	Rolling shear	**Time [days]**	**Rolling shear**	**Time [days]**
Model A at notch	2.14 MPa	32	2.45 MPa	16
Model A at boundary	400.1 kPa	32	-475.8 kPa	16
Model B at boundary	140.2 kPa	182	264.1 kPa	50

The normal stresses are shown in Table 27. For model A, the maximal normal stress S_{11} is located in between at the inner corner of the notch, with generally high values at the boundary towards the concrete layer. For model B, the normal stress S_{11} is located below the notch. For both models, the S_{22} stress is located at the vertical boundary to the notch. The value being negative means that the element is being compressed. Over the entirety of the top layer, S_{11} stresses of 5 MPa are generally seen, while S_{22} (along the elements thickness) is just one tenth of that value. The values for the concrete are not considered.

Table 27. Stresses in x- (S_{11}) and y-direction (S_{22}).

Model	**Time [days]**	**S_{11} [MPa]**	**S_{22} [MPa]**
Model A	32	-11.3	-10.1
Model B	182	-6.6	-3.3

Discussion

Multiple models have been made for various configurations and numerous results have been obtained. Observations have been made as regards the results as well as the modeling itself. Thoughts have sprung up and ideas on how the modeling could have been made in a better way.

Uniform loading

An increase in thickness gives an increase in gap width due to a thicker board being more free to deform. The shrinkage could otherwise be expected to be independent of the board thickness. This could still be the case for even larger board widths, as the restriction from the connected adjacent layers will have a smaller effect. For the outer boards, the shrinkage across its thickness was larger in the middle of the boards as compared to its edges towards the gap, making the boards cup.

An overall larger board width gives a larger gap width. The gaps should be kept as small as possible. The ratio between gap widths and board widths does however become smaller for larger widths. So even though the gaps gets larger, the gaps takes up a smaller area. At very low widths the ratio is kept the same, as the shrinkage should be the same and leave as much open room no matter the dimensions. For larger board width (>150) the ratio gets lower. The gap width for inner gaps do not change for board widths over 150 millimeters, but the ratio does. The gaps for the outer most layers gets larger for a larger thickness. It would be interesting to check the widths for even thicker boards to see if the value ever reaches the value for the simple one-dimensional calculation, giving a value of 0.52 mm. This value is close to what was obtained for a board thickness of 60 mm, giving a gap width of 0.485 mm.

A CLT with fewer layers gives larger gap widths. The increase in gap width is likely linked to the larger board thickness, which is the result of fewer boards spanning the same thickness. The gap width for the variating thickness shows similar values as for varying number of layers. One difference between the configurations is the total thickness, where the total thickness is kept at 150 millimeters when changing the number of layers. The factor, or relation between the thickness of each board, does not seem to influence the results except the board thickness that is a result of the changing factor.

The gap widths gets an equal value no matter which layer it is located in, but with the outer most layers getting a gap width twice as large. That is seen as reasonable as the inner gaps are restrained at two ends, in contrast to the outer gaps that are restricted at one.

Overall, the gap width can be larger than 0.4 millimeters for change in one percentage moisture content. The value is in many cases larger than 0.3 millimeters for the outer gap. The inner gaps rarely gets larger than 0.2 millimeters. Even a change of ten percent MC gives less than 4 millimeters in most cases and 4.5 millimeters at most (three-layer CLT element or boards thicker than 50 mm). This is less than the max allowable width of 6 millimeters. A gap width of 2 millimeters is more difficult to not exceed. A board width has to be less than 100 millimeters for boards with a thickness of 30 millimeters to allow for a 10 percent MC increase. An increase of 6 percent will work in most cases. The modeling does however assume no initial gap width and no effect from for example mechanical loading.

The elongation for both directions of the element are similar. Even though the expansion coefficient differs greatly between the longitudinal and the radial direction, the shape robustness likely keeps the expansion about the same. A difference in values are expected as the number of layers for both directions will never be the same, but the direction with the most layers, of three for the reference case, results in a shrinkage just 22 percent larger. If the element is moistened the expansion ought to be larger at the gaps, making the gaps smaller the greater moisture content and eventually causing the edges of the gap to meet and cause stresses.

One could question how reasonable it is to only look at gap width and not also the ratio between gap width and board width when determining how large gaps that can be accepted.

Non-uniform loading

Non-uniform drying leads to bending. The shrinkage is by far the largest at the side subjected to drying, making the gaps the largest at the drying end. However, the bending of the elements does reduce it slightly as compared to the gap width for uniform drying. One could conclude that uniform drying is likely to always give larger gap widths than that of non-uniform drying in every situation, assuming the total difference in MC across the thickness is as in the uniform case.

For a non-uniform loading case with a mean MC change of one percent, the gaps are larger at the drying end than for the uniform loading case. The middle gap is about the same as for uniform loading. The outer most gap gets a width three times the width of the middle gap, though a difference by a factor of four could have been expected (twice the MC change and outer gaps twice as wide as inner for uniform drying).

Another model was made for the bending. The bending model differs from the model for the gap widths for non-uniform drying. The behavior of the model is expected to be the same. But with another model the boundary conditions could be placed so that obtaining the values of interest were the easiest for its corresponding case. The bending was considerably lower than the maximal limit. For longer boards, it might however still affect enough for it to be more difficult to fit at site.

For the max values for gap width and bending, one has to account for the addition from loading and deviations. Initial gap widths were also assumed to be non-existent. It is noted that many aspects can be looked at. The number of configurations are endless and the simplifications that are set can have an impact on the results, although they are seen as reasonable.

2D Composite

For the preset RH for concrete, one can see that even after one year, the concrete still has a high relative humidity. This will result in a high RH for the top layers of the CLT. It should be noted that the humidity varies within the element, i.e. that a mean value of the humidity or just the humidity at the CLT elements surface could underestimate the risks linked to a high moisture content. For example, the climate class for timber is set for the mean value of the element, which could be misleading.

The diffusion might behave very differently at very large relative humidities when capillary flow occurs. Now, a diffusion coefficient is set as constant as a simplification. That value did not differ much from that of concrete. A fibre saturation point at 100% RH was reached, at 27% MC. No expansion occurs beyond that. One might indeed expect a moisture content higher than 27% closest to the concrete. This will likely barely affect the timber element as a whole.

Diffusion coefficient of concrete is not considered in the model since the value of the relative humidity is preset in the concrete. One idea is that a too low diffusion coefficient for the concrete might hinder the concrete from supplying enough water to the timber. It seems however like the diffusion coefficients for timber and concrete are about the same, and probably even higher for wet, newly casted concrete.

Modeling the boundary conditions for the TCC as plane surfaces is a simplification, as in the beginning the deformation would mainly occur in the middle but not at the outer surfaces. However, since the model represents an infinitely large component the approach can still be seen as reasonable.

The TCC model shows displacements similar to the elongation of the 3D CLT elements, even though larger change in moisture content occurs. The moisture distribution is not evenly distributed, but it seems likely that the TCC model behaves stiffer than a floor element without the concrete. The bending of the TCC structure seems to be less severe than for the ordinary CLT element, considering that the ordinary element would reach an equal value of deformation if subjected to a MC change of less than 10 percent. The bending is most likely higher for the TCC structure after a longer time-period than 400 days, as the largest value was obtained for the last time step. A reason for a positive expansion for X1 and the concrete layer for the TCC models could be that expansion at the beginning mainly occurred above the slab's central axis. It is shown that both models reach a high RH for the top layer at an early stage.

Since the concrete still has a low/negligible hydration one might consider the material to not fully connect yet, even though the model states that, and that the stresses there probably are lower in reality. If that is the case, then the timber will instead move and expand. As the timber dries it wants to regain the shape it once had and could then be affected by tension. The results for bending of the TCC element might be false as the concrete might not be as stiff because of the low hydration the first days. It is also worth noting that the TCC element is thicker when accounting for the concrete, which in itself results in a smaller bending.

The assumption of plane strain elements is not precisely correct. We now assume no deformation in z-direction, but it should be able to expand a bit. Plane strain is however generally seen as the reasonable choice over plane stress for deep objects. Using a 2D-model will disregard the displacement in z-direction, as well as the normal stress. The shear stresses for surfaces parallel to the notch are also left out.

The concrete ought to create a lot of heat as well. This is not accounted for in the modeling. Since drying occurs during such a long time, the effect from temperature might not be as high. Hydration of concrete does however increase the temperature. The diffusion depends on vapor pressure, but the relative humidity is also affected by the temperature. Since the temperature is higher near the concrete, the relative humidity might in reality be lower.

Two-sided drying of concrete would dry out quicker. Two-sided drying generally gives a drying rate four times as large. This might not be the case for curing concrete. The drying of w/c 0.38

concrete could be a hint on the difference it would make for the wooden element if concrete of w/c 0.6 dried out from both ends, but no solid conclusions can be drawn.

Two-sided drying is not possible for the current model of the TCC structure since the relative humidity for the concrete are preset for every time step. In other words, the humidity for the concrete in the model will not change when drying occurs from more sides. Even membrane curing that was assumed is likely to under-estimate the drying as the drying is rather free at the surface against the timber.

The rolling shear stress between the layers could reach almost half of the maximal recommended value of 1.2 MPa set for glulam, reaching close to 0.5 MPa. The effect is likely not an issue if the mechanical loading are low during curing. Also, the higher shear stresses towards the boundary has more to do with the glue placed between. The value of over 2 MPa at the notch for model A could have been unreasonably high since the concrete is set as fully connected in the model.

The normal stresses can reach up to values of more than 10 MPa, located at the interface of the top layer. Even in the middle of the top layer, the timber were compressed at around 5 MPa. The constraints can be one reason for the higher values, as the constraint forces the element to expand along the entire thickness even when the largest change in RH mainly would occur in the middle of the TCC element.

Modeling

With the use of symmetry planes, smaller models have been used to replicate the behavior of a larger CLT element. No gaps have been explicitly modeled within the models as all gaps are located at the parts boundary. It is noted that for the uniform load case, yet another symmetry-plane could have been set and still get the same results. That symmetry plane would cut the part in half along the neutral axis. The non-uniform model, which consisted of two equal parts connected, can still give as good results with just one of the parts modeled.

With the use of the coupling constraint, the model used for the uniform loading case could likely have been used for the non-uniform case as well, which would make the model for non-uniform loading half as large. The constrained surface would then be set for two of the five layers, where the surfaces left out would correspond to the gaps.

Even though most of the modeling was made in the Abaqus modeling environment, the ability to edit the script was utilized. Editing and running as a script made it easier to do parametric studies, varying input variables. The script was kept as foreseeable as possible. When changing the script for one with another number of layers, Macro manager was of great help. However, changing the form of the parts and its dimensions led to problems. Every surface set was given reference numbers in the scripts that was counterintuitive and difficult to change in the script, especially without the Macro manager. Also, the Macro manager saved the script in a slightly different manner. The scripts that were assembled were not written from scratch as it was easier to take a script made from an existing model and alter it. The script will not be the most optimal as many rows that are not needed might be left in the script.

Using the total strain energy as an estimation on when the stresses could be the largest might be problematic. The method gives a time step to use, but it has been seen that this time step and

the time step with the largest stress value did not match. The total strain energy is calculated for the entirety of the model, and not just for nodes of interest. The singularities could also have an unreasonable large effect on the value. For the stresses, I could probably just have looked at the maximal and minimum value for each time step. The max values for shear stress and normal stress might occur at different time steps. It seems likely that the largest stresses would occur at about the same time.

For the reference case, boards with a width of 200 millimeters was used. This width does occur in reality, but 150 millimeters wide boards could be seen as more common and a better option.

Conclusion

Main purpose of this master thesis was to get an idea of the behavior of CLT elements under moisture loading. The emphasis has been on drying of CLT elements and timber-concrete composite floors. Gap widths have been viewed as a main issue. The TCC structure reaches a high humidity with stresses as a consequence.

To obtain as small gaps as possible one should have as small boards as possible, and rather more elements and layers than fewer. The ratio between gap width and board width is large for boards of smaller width, making the total exposed area larger for smaller width. Eurocode sets a limitation on crack width, not ratio. The ratio could likely be just as important for fire safety. As the outer gaps are larger, the outer layer could preferably be set as thinner than the inner boards.

The ratio between gap width and board thickness shows how important the thickness of the board is to estimate the gap width, even though the one-dimensional calculation does not indicate it. The outer boards cup in such a way that gap widths seems to get even larger for larger thickness. At the edge, the element is thicker than at the middle of the board.

For uniform drying, the outer gap widths are about twice as large as the others. This is reasonable as the gap is only attached at one end, unlike the other gaps being attached at both ends.

The gap widths for non-uniform drying is likely to always be smaller than that of uniform drying, if considering a difference of one percent MC change. The surface that got a reduced moisture content would shrink as for the uniform drying, however, the uneven moisture distribution causes the element to bend in such a way that the bending partly closes the gaps at the dried end. This also mean that the width of the gap does not vary linearly along the elements thickness.

It is concluded that both board width and thickness will influence the gap widths, but not the factor nor the number of layers. Gap widths are generally around 0.3 mm, but the values could reach above 0.45 mm per percentage MC change. Overall, the given gap widths are small enough for common dimensions and moisture variation.

The displacement of 0.18 millimeters obtained from bending and one percent MC change is considerably lower than the limit of 6.67 millimeter.

For the TCC floor, a relative humidity exceeding 75 percent can be expected for over a year. The higher humidity does however mostly affect the upper layers while the lower half is barely affected and only affected after a few months. The orientation of the boards has a noticeable difference for the maximal humidity and at what time it peaks for the top layer because of the diffusion from the notch. The results also indicates a higher stiffness for the composite structure. The rolling shear has a noticeable effect while normal stresses can reach up to values of more than 5 MPa of compression in the top layer. Between the layers, the rolling shear stress is expected to reach almost half of the maximum tolerated value.

Future work

As the properties of wood differs between specimens, more extreme values could be used to study the worst-case obtainable. More configurations could be tested. Especially other values for the concrete in the TCC model, for example two-sided drying. The heat from concrete hydration as well as the higher moisture content between the materials should be considered.

At MC above 98%, in the hygroscopic range, one might expect a higher moisture flow than considered. The moisture flow is in itself dependent on the moisture content. Diffusion has now been set as constant, even for the TCC model. Modeling of timber can be ever more meticulous, for example considering cylindrical coordinate system.

The non-uniform loading and TCC model did not account for different configurations. Conclusions were drawn for the non-uniform loading based solely on the reference case. More configurations could be needed to investigate.

The differences for drying of the TCC were compared for two principal orientations of the notch. Lower w/c ratio or faster drying scenarios where not compared when considering stresses.

The parametric studies could be made for more parameters. By using those results, a relation could be set up between the gap width and the studied parameter to apply when gap widths are to be estimated for a new configuration.

The stresses in the TCC model may give an indication of high stresses, but for actual values, one is referred to other studies where stresses have been a larger focus.

Lastly, the results should be compared to experimental results to know how well the model can replicate the reality, if a parameter is missing or how large deviation that can be expected from the results.

References

Alsayegh, G. (2012) *Hygrothermal properties of cross laminated timber and moisture response of wood at high relative humidity*. Ottawa: Carleton University.

Autengruber, M. Lukacevic, M. and Füssl, J. (2020). *Der Einfluss des Aufbringens von Frischbeton auf die Feuchtigheitsverteilung in Holz-Beton-Verbundkonstruktionen mit Kerven, untersucht mittels numerischer Simulationen*. Austria.

Borgström, E. (2016) *Design of timber structures.* Volume 1 & 2. Stockholm: Swedish forest industries federation

Borgström, E. Fröbel, J. (2019). *The CLT Handbook*. Stockholm: Swedish wood. https://www.swedishwood.com/siteassets/5-publikationer/pdfer/clt-handbook-2019-eng-m-svensk-standard-2019.pdf

Burström, P. (2014) *Byggnadsmaterial.* Lund: Studentlitteratur

Chiniforush, A.A. Akbarnezhad, A. Valipour, H. Malekmohammadi, S. (2019). *Moisture and temperature induced swelling/shrinkage of softwood and hardwood glulam and LVL: An experimental study.* Sydney, Australia. https://www.sciencedirect.com/science/article/abs/pii/S0950061819304106?via%3Dihub

Dahl, K. (2009) *Mechanical properties of clear wood from Norway spruce*. Trondheim: NTNU

Dassault Systèmes, (2015) *Abaqus 2016 HTML documentation*.

EOS, European organisation of the sawmill industry (2017). *Carbon efficient timber construction*. Brussels, Belgium. https://www.eos-oes.eu/en/topics.php?id=20 [04-08-20]

European commission (2020). *Global CO2 emissions continue to rise but EU bucks global trend*. Luxembourg: Office for Official Publications of the European Communities. https://ec.europa.eu/jrc/en/news/global-co2-emissions-continue-rise-eu-bucks-global-trend [08-04-21]

Fagerlund, G. (1999). *Bindemedelskemi*. Lund: Lunds tekniska högskola.

Falk, A. Dietsch, P. Schmid, J. (2016) *Cross laminated timber – a competitive wood product for visionary and fire safe buildings. Stockholm: USAB* https://www.cost.eu/wp-content/uploads/2018/07/57316.pdf (p. 107)

Fortino, S. Mirianon, F. Toratti, T. (2009). *A 3D moisture-stress FEM analysis for time dependent problems in timber structures.* VTT Technical Research Centre of Finland.

Greenspec (2020). *Crosslam timber / CLT-Fire resistance and rating.* https://www.greenspec.co.uk/building-design/crosslam-timber-fire-resistance-and-rating/

Mjörnell, K. (2003) *Uttorkning av byggfukt i självkompakterande betong*. Göteborg: SBUF, Report 10 041.

Naturvårdsverket (2019). *Underlag till regeringens klimatpolitiska handlingsplan*. Stockholm, Sweden. https://www.naturvardsverket.se/Documents/publikationer6400/978-91-620-6879-0.pdf?pid=24382 [04-08-20]

Nevander, L. & Elmarsson, B. (1981). *Fukthandbok*. Stockholm: AB Svensk Byggtjänst.

Nock (n.d.). *Om CLT*. Nock massiva trähus, Älvängen. https://www.nock.nu/om-clt/

Näringsdepartementet (2004). *Mer trä i byggandet: Underlag för en nationell strategi att främja användning av trä i byggandet*. Stockholm: Näringsdepartementet. https://www.regeringen.se/contentassets/622a4cddc02a4026a3bc3c4f5d5b94aa/mer-tra-i-byggandet---underlag-for-en-nationell-strategi-for-att-framja-tra-i-byggandet-ds-20041

Näringsdepartementet (2018). *Inriktning för träbyggande*. Stockholm: Näringsdepartementet. https://www.regeringen.se/49ee7f/contentassets/37f07802672c45078a20d3a375e82c25/20180626_inriktning-for-trabyggande.pdf

Ottosen, N. Petersson, H. (1992). *Introduction to the finite element method*.

Persson, K. (n.d.) *Transient heat flow*. Lund's University.

Scalet, T. (2015) *Cross laminated timber as sustainable construction technology for the future*. Helsinki: Helsinki Metropolia University of Applied Sciences.

Sjödin, J. & Serrano, E. (2006). *A numerical study of the effects of stresses induced by moisture gradients in steel-timber dowel joints.* Växjö.

SS-EN 16351:2015: Timber structures – Cross laminated timber – Requirements

SS:EN 92-1-1:2005: Eurocode 2: Design of concrete structures

SS-EN 95-1-1:2004: Eurocode 5: Design of timber structures

Stora Enso (n.d.) *CLT*. https://www.storaenso.com/en/products/wood-products/massive-wood-construction/clt [25-10-20]

Swedish wood (2017a) *Properties of softwood*. https://www.swedishwood.com/wood-facts/about-wood/from-log-to-plank/properties-of-softwood/ [23-07-20]

Swedish wood (2017b) https://www.swedishwood.com/wood-facts/about-wood/wood-and-the-environment/wood-is-a-sustainable-construction-material/ [04-08-20]

Swedish wood (2017c) *Samverkansbjälklag*. https://www.traguiden.se/konstruktion/kl-trakonstruktioner/bjalklag/5.1-bjalklag---oversikt/5.1.3-samverkansbjalklag/ [13-08-20]

Swedish wood (2017d) *Cellstruktur*. https://www.traguiden.se/om-tra/materialet-tra/traets-uppbyggnad/traets-uppbyggnad/cellstruktur/?previousState=1 [10-11-20]

Swedish wood (2017e) *KL-trä och brand*. https://www.traguiden.se/konstruktion/kl-trakonstruktioner/kl-tra-och-brand/ [10-11-20]

Swedish wood (2017f) *Moisture-related wood movement*. https://www.swedishwood.com/wood-facts/about-wood/wood-and-moisture/moisture-related-wood-movement/

Säll, H. (2002). *Spiral grain in Norway Spruce*. Växjö University, Sweden.

UNEP 2019, *Sand and sustainability: Finding new solutions for environmental governance of global sand resources*. GRID-Geneva, United Nations Environment Programme, Geneva, Switzerland.

Warfvinge, C. & Dahlblom, M. (2015), *Projektering av VVS-installationer.* Lund: Studentlitteratur AB